

Aus dem Institut für Neuroanatomie
der Medizinischen Fakultät Mannheim
(Direktor: Prof. Dr. med. C. Schultz)

Peroxisome isolation from mouse brain and cultured cells – development of two new isolation protocols

Inauguraldissertation
zur Erlangung des medizinischen Doktorgrades
der
Medizinischen Fakultät Mannheim
der Ruprecht-Karls-Universität
zu
Heidelberg

vorgelegt von
Andreas Felix Manner

aus
Mannheim
2021

Dekan: Prof. Dr. med. Sergij Goerd
Referent: Priv.-Doz. Dr. Markus Islinger

CONTENT

	Page
ABBREVIATIONS	1
1 INTRODUCTION	3
1.1 The peroxisomes – a versatile organelle.....	3
1.1.1 Peroxisome function	4
1.1.2 Peroxisome variability.....	6
1.1.3 Peroxisomal membrane.....	7
1.1.4 Interaction with ER and mitochondria	7
1.2 Peroxisomes in disease	8
1.2.1 Single enzyme deficiencies	8
1.2.2 Peroxisome biogenesis disorders.....	8
1.2.3 Peroxisome involvement in further neuronal diseases	9
1.3 Brain peroxisomes	9
1.3.1 Major brain peroxisomal functions and their link to disease	9
1.3.2 Peroxisomal populations in the brain.....	10
1.3.3 Alterations during aging.....	11
1.4 Difficulties of peroxisome purification from adult brain tissue.....	11
1.4.1 Peroxisome heterogeneity	11
1.4.2 Contaminating particles	13
1.4.3 Myelin	13
1.4.4 Peroxisome fragility	13
1.4.5 Previous protocols for the separation of PO from brain tissue.....	13
1.4.6 Strategies to overcome difficulties in brain peroxisome purification	14
1.5 Peroxisome isolation from cell culture.....	14
1.6 Goals	15

2	MATERIAL AND METHODS	16
2.1	Common materials and solutions	16
2.1.1	Chemicals.....	16
2.1.2	Solutions used in brain extraction, homogenisation and centrifugation.....	17
2.1.3	Density measurement.....	18
2.2	Peroxisome isolation from cultured cells	18
2.2.1	Cell line and cell culture.....	19
2.2.2	Transfection.....	19
2.2.3	Peroxisome isolation	20
2.3	Peroxisome isolation from murine brain.....	22
2.3.1	Animals.....	22
2.3.2	Brain preparation	23
2.3.3	Homogenisation	23
2.3.4	Protocol 1: examination of the different physical properties of adult and young mice's brain peroxisomes.....	24
2.3.5	Adaptations to protocol 1 aiming to improve peroxisome isolation capacity by differential and gradient centrifugation.....	26
2.3.6	Investigating the use of multiple re-homogenisations.....	26
2.3.7	Myelin removal: positioning and myelin removal gradient	26
2.3.8	Protocol 2: adaptations aiming to improve peroxisome isolation capacity by differential centrifugation	28
2.3.9	Differential centrifugation protocol	28
2.3.10	Further purification via density gradient centrifugation using different gradient media.....	29
2.3.11	Protocol 3: Addressing brain peroxisome purification by serial gradient centrifugation	30
2.3.11.1	Protocol layout.....	31
2.3.11.2	Organelle separation gradient (OSG).....	32
2.3.11.3	Separation of the bottom fraction of gradient for further peroxisomal subpopulations.....	33
2.3.11.4	Combination of 2 organelle separation gradients	34
2.3.12	Final separation via Nycodenz gradients.....	34
2.3.12.1	Continuous Nycodenz gradient	35
2.3.12.2	Nycodenz-step gradient	35
2.3.12.3	Testing for peroxisomal "ghosts"	35

2.4	Methods for post separation analysis	36
2.4.1	Bradford protein assay	36
2.4.2	Immunoblotting.....	36
2.4.2.1	Preparation of SDS-PAGE gels.....	36
2.4.2.2	Sample preparation for Western blot.....	36
2.4.2.3	Electrophoresis.....	37
2.4.2.4	Western blotting	38
2.4.3	Immunodetection	38
2.4.3.1	Peroxisomal marker	39
2.4.3.2	Mitochondrial marker.....	39
2.4.3.3	ER marker	40
2.4.3.4	Synaptosomal marker	40
2.4.3.5	Myelin marker.....	40
2.4.3.6	Transfected protein	40
2.4.3.7	Secondary antibodies.....	40
2.4.4	Image acquisition	41
2.4.5	Semi-quantitative analysis of western blot results	41

3 RESULTS.....	42
3.1 Peroxisome isolation from cultured cells	42
3.1.1 Differential centrifugation for pre-purification	42
3.1.2 Organelle distribution on Nycodenz and Optiprep density gradients.....	43
3.1.3 Organelle shift due to ACBD5 and VAPB overexpression.....	45
3.2 Peroxisome isolation from murine brain.....	46
3.2.1 Protocol 1: Analysis of the physical properties of adult brain peroxisomes using a protocol designed for peroxisome separation from juvenile mouse brain	46
3.2.1.1 Peroxisome pre-purification.....	46
3.2.1.2 Nycodenz density gradient	47
3.2.2 Influence of re-homogenisation on myelin content/organelle preservation	48
3.2.3 Myelin removal and by sucrose step-gradients	49
3.2.3.1 Gradient composition	49
3.2.3.2 Positioning of the myelin removal step.....	49
3.2.4 Optimization the differential centrifugation procedure	50
3.2.5 Protocol 2: adaptations aiming to improve peroxisome isolation capacity by differential and gradient centrifugation.....	52
3.2.6 Analysis of different gradient media in the final purification steps ..	52
3.2.6.1 Optiprep	52
3.2.6.2 Sucrose	55
3.2.6.3 Nycodenz	56
3.2.6.4 Comparison among the gradient media	57
3.2.6.5 Transfer of the continuous sucrose gradient to a step-gradient	58
3.2.7 Protocol 3: improvement of the isolation protocol by serial step gradient centrifugation.....	59
3.2.7.1 Organelle separation gradient (sucrose)	59
3.2.7.2 Optimised organelle separation gradient.....	61
3.2.7.3 Separation of the bottom fraction of gradient for further peroxisomal subpopulations.....	63
3.2.7.4 Combination of two serial sucrose organelle separation gradients (OSG)	64
3.2.8 Further purification on Nycodenz gradients	66
3.2.8.1 Testing for peroxisomal “ghosts”	67

4 DISCUSSION	69
4.1 Peroxisome isolation from cultured cells	69
4.1.1 Resulting marker and organelle pattern in Nycodenz and Optiprep gradients	69
4.1.2 Peroxisome-ER interaction – application of the new developed protocol	69
4.1.3 Function of interaction	71
4.2 Peroxisome isolation from murine brain	71
4.2.1 Comparison of peroxisome isolation from adult mice with those published for young mice	72
4.2.2 Differences in physical properties of peroxisomes	74
4.2.3 Other alteration in aging	75
4.2.4 The issue of different antibodies	76
4.2.5 Peroxisome separation from adult mice’s brain tissue	77
4.2.5.1 Homogenisation	77
4.2.5.2 Myelin removal	77
4.2.5.3 Addressing the issue of peroxisome isolation by differential centrifugation	78
4.2.6 Density gradient centrifugation in adult mice’s brain peroxisome isolation - differences among the gradient media	78
4.2.6.1 Sucrose	79
4.2.6.2 Optiprep	80
4.2.6.3 Nycodenz	80
4.2.6.4 Differences among the gradient media due to medium uptake	81
4.2.7 Peroxisome pre-purification using a series of sucrose density-gradients	82
4.3 Peroxisomal subpopulations derived	82
4.3.1 Assessing for peroxisomal “ghosts”	82
4.3.2 peroxisomal subpopulations	83
5 SUMMARY	84
6 LITERATURE	85
7 LEBENSLAUF	97
8 DANKSAGUNG	98

ABBREVIATIONS

ABC-transporter	ATP-binding-cassette-transporter
ACBD4	Acyl-CoA Binding Domain Containing 4
ACBD5	Acyl-CoA Binding Domain Containing 5
ACAD11	Acyl-CoA Dehydrogenase Family Member 11
ACOX	Acyl-CoA oxidase
ACOX1	Acyl-CoA oxidase 1
ALS	Amyotrophic lateral sclerosis
APS	Ammonium persulfate
ATP	Adenosine triphosphate
BSA	Bovine serum albumin
CNS	Central nerve system
DAAO	D-amino acid oxidase
D-BP	D-bifunctional protein
DHA	Docosahexaenoic acid
DMEM	Dulbecco's Modified Eagle Medium
DNA	Deoxyribonucleic acid
EDTA	Ethylenediaminetetraacetic acid
ER	Endoplasmic Reticulum
FA	Fatty acid
FADH ₂	Flavin adenine dinucleotide
GPI	Glycosylphosphatidylinositol
H ₂ O ₂	Hydrogen peroxide
HB	Homogenisation buffer
HEPES	2-(4-(2-Hydroxyethyl)piperazin-1-yl)ethane sulfonic acid
HepG2	Name of a human liver cancer cell line
ICH	Immunohistochemistry
MAVS	Mitochondrial antiviral signaling adaptor
MOPS	3-(N-Morpholino)propane sulfonic acid
mPTS	Peroxisomal membrane targeting signal
mRNA	Messenger ribonucleic acid
NAPDH	Nicotinamide adenine dinucleotide phosphate
NMDA-receptor	N-methyl-D-aspartate receptor
OSG	Organelle separation gradient
PBD	Peroxisome biogenesis disorder
PEI	Polyethyleneimine 25K
PEX5	Peroxine 5
PEX7	Peroxine 7
PEX11	Peroxine 11
PEX13	Peroxine 13
PEX14	Peroxine 14
PEX19	Peroxine 19
PMSF	Phenylmethylsulfonyl fluoride
PMP	Peroxisomal membrane protein
PMP22/Pxmp2	Peroxisomal membrane protein 2

Abbreviations

pmts	peroxisomal membrane targeting signal
PO	Peroxisome
POMC	Pro-opiomelanocortin
PPAR	Peroxisome proliferator-activated receptor
PPAR α	Peroxisome proliferator-activated receptor alpha
PT	3-ketoacyl-CoA thiolase
PTS1	Peroxisome targeting signal 1
PTS2	Peroxisome targeting signal 2
ROS	Reactive oxygen species
TWEEN 20	Polysorbate 20
ULCFA	Ultra long chain fatty acid (>C ₃₂)
VAPB	Vesicle-associated membrane protein-associated protein B
VLCFA	Very long chain fatty acid (>C ₂₂)

1 INTRODUCTION

1.1 The peroxisomes – a versatile organelle

Peroxisomes are ubiquitous organelles (Schrader and Fahimi, 2008) located in the cytosol (De Duve and Baudhuin, 1966). They consist of a single lipid bilayer and often contain a crystal-like core (De Duve and Baudhuin, 1966). Peroxisomes are abundant in nearly all eukaryotic specimens ranging from unicellular organisms via fungi and plants to mammals (Subramani, 2004). In mammals, peroxisomes have been demonstrated in all tissues except erythrocytes and mature spermatozoa (Dastig et al., 2011; Islinger et al., 2012b; Schrader and Fahimi, 2008). Peroxisomes serve as a compartment for hazardous reactions separated from cytosol. For this purpose, peroxisomes contain different sets of enzymes in their matrix - partially in a crystal-like core (De Duve and Baudhuin, 1966). Several membrane-bound proteins regulate protein and substrate import as well as product export (Islinger et al., 2012b; Schrader and Fahimi, 2008). Further enzymes are also membrane-bound. Peroxisomes contain neither DNA nor translation machinery (Schrader and Fahimi, 2008). All peroxisomal proteins are encoded in nuclear DNA and translated usually on free or, in case of pre-import into the ER, membrane-bound ribosomes (Schrader and Fahimi, 2008). These latter proteins are subsequently imported into peroxisomes via vesicle-based import mechanisms.

The imported enzymes are responsible for the peroxisomal metabolic functions. Peroxisomes distinguish themselves by the high variability of enzyme content and are able to adapt rapidly to metabolic stimuli and required functions (Islinger et al., 2012b). Enzyme content differs among tissues, cell types and nutritional status (Islinger et al., 2012b).

In contrast to the variable matrix enzymes, several of the membrane-bound proteins, which are responsible for peroxisome biogenesis and maintenance, are located ubiquitously on peroxisomes (Gabaldon, 2010; Schrader and Fahimi, 2008). This highly conserved subgroup of membrane bound proteins is called peroxins (Gabaldon, 2010; Schrader and Fahimi, 2008).

Moreover, peroxisomes do not act as isolated entities but are integrated into a complex metabolic network with other organelles in particular mitochondria (Schrader et al., 2015), endosomes (Guimaraes et al., 2015), lipid droplets (Cui et al., 2016; Joshi and Cohen, 2019; Kilwein and Welte, 2019), lysosomes (Chu et al., 2015) and ER (Costello et al., 2017a; Costello et al., 2017b; Hua et al., 2017), cytosolic and membrane-bound enzymes (*figure 1*).

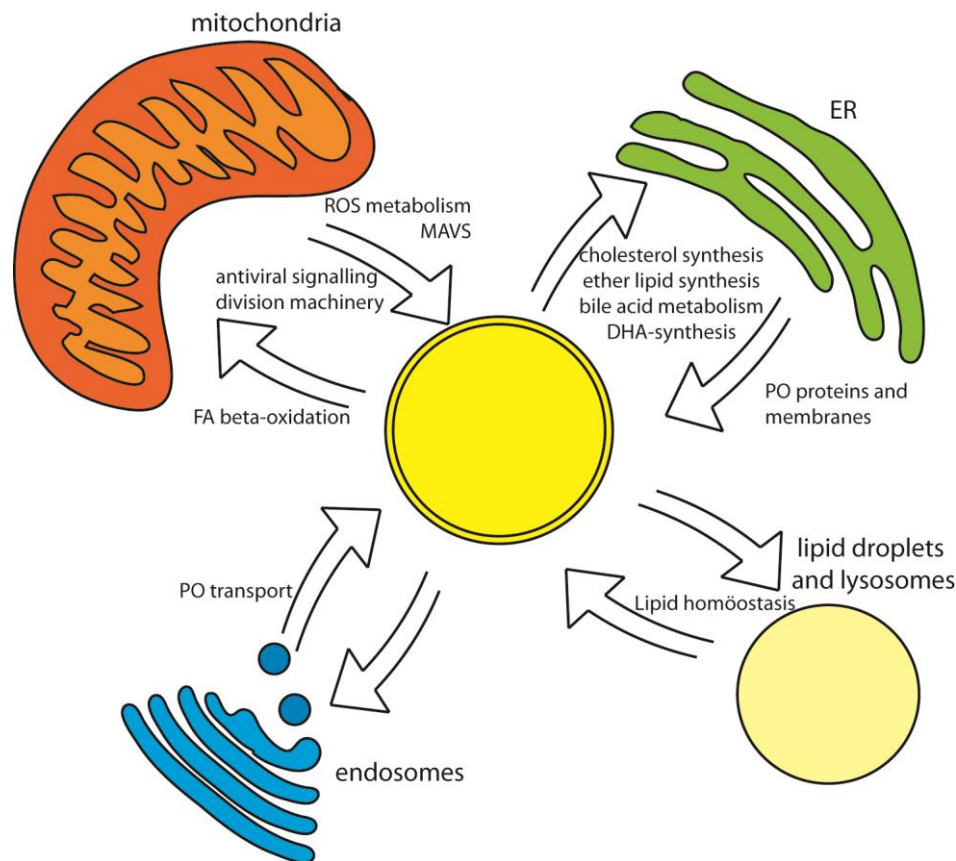


Figure 1: Peroxisome - organelle interaction:

So far, interaction of peroxisomes with mitochondria, ER, lipid droplets, lysosomes and endosomes are reported, of which most metabolic links have been reported in interaction with mitochondria and ER. Interactions with both these organelles are addressed in paragraph 1.1.4.

1.1.1 Peroxisome function

Peroxisomes are an inherent component of various metabolic pathways. Their enzyme content and metabolic functions exhibit tissue- and cell-type dependent differences (De Duve and Baudhuin, 1966; Islinger et al., 2012b); e.g. liver peroxisomes differ from kidney peroxisomes (De Duve and Baudhuin, 1966); the peroxisomal proteome of lung tissue and testis differs from both (Islinger et al., 2012b).

Reactive oxygen species (ROS) metabolism is eponymous for peroxisomes. H_2O_2 and other ROS are produced as byproducts e.g. in peroxisomal β -oxidation, as peroxisomes lack the capacity of NADPH reduction and proton transfer from endogenous to unbound $FADH_2$ (Kim and Miura, 2004). Reactive nitrogen species are also partially produced in peroxisomes. Apart from these endogenously produced ROS, those from other origins are likely also degraded in peroxisomes, i.e. by catalase, hereby protecting the cell from oxidative stress. With this double role, peroxisomes play an important role in oxidative stress homeostasis. Apart from their role in oxidative stress, ROS also act as signaling molecules. E.g. in hypothalamic neurons, ROS serve as signaling molecules regulating pro-opiomelanocortin (POMC) tone (Diano et al., 2011). Peroxisomes regulate the ROS concentration in these neurons with their ROS-scavenging enzymes (Angermüller et al., 2009; Islinger et al., 2012b). In accordance with the important role in ROS detoxification, several peroxisomal enzymes are sensible to oxidative switches modulating their enzymatic properties (Islinger et al.,

2012b). A dysregulation of ROS-scavenging function of peroxisomes appears to be associated with various diseases, i.a. possibly to hypervulnerability to sound (Delmaghani et al., 2015), diabetes associated lipotoxicity in pancreatic beta cells, and aging (Baboota et al., 2019; Islinger et al., 2012b). Furthermore, ROS homeostasis is required for normal respiratory capacity of mitochondria (Islinger et al., 2012b).

A second major metabolic function of peroxisomes is the beta-oxidation of fatty acids (Trompier et al., 2014). While mitochondrial beta-oxidation metabolizes preferentially medium-long chain fatty acids, peroxisomal beta-oxidation focusses on very long-chain fatty acids (VLCFAs), eicosanoids and docosanoids, poly- and monounsaturated fatty acids and branched-chain fatty acids (Trompier et al., 2014). VLCFAs are important components of membrane lipids (sphingolipids and glycerophospholipids), which are involved in skin barrier formation, liver homeostasis, myelin maintenance, spermatogenesis, retinal function and anti-inflammatory pathways (Kihara, 2012). Contained mainly in the outer leaflet of plasma membranes, especially in the brain, VLCFA containing sphingolipids affect membrane functions by influencing lipid microdomain formation, altering membrane fluidity and stabilizing highly curved membranes (Kihara, 2012). VLCFA also act as precursors of anti-inflammatory compounds (Kihara, 2012). An accumulation of VLCFA – especially in the brain – is potentially toxic (Darwisch et al., 2020; Trompier et al., 2014). Highly elevated concentrations of VLCFA are deleterious for energy-dependent mitochondrial functions and are capable to induce cell death (Schonfeld and Reiser, 2016).

Eicosanoids and docosanoids are signaling molecules made from polyunsaturated long-chain fatty acids. Subtypes of eicosanoids are inter alia involved in vasoconstriction and -dilatation, vaso-permeability, bronchodilatation and -constriction, coagulation and anticoagulation, and inflammation (Biringier, 2020; Calder, 2020). They act via autocrine and paracrine signaling (Calder, 2020). The involvement in these vital functions indicates the importance of the eicosanoid equilibrium. Peroxisomal enzymes also break down dicarboxylic acids (Islinger et al., 2012b; Nguyen et al., 2008; Trompier et al., 2014) and are involved in the alpha-oxidation of phytanic acid (Trompier et al., 2014), which is an agonist of PPAR-alpha. Elevated levels of phytanic acid, a metabolite of chlorophyll, which is ingested via dairy products and meat, are neurotoxic (Nagai, 2015; Schonfeld and Reiser, 2016).

Ether lipid biosynthesis is a further peroxisomal function: The pre-squalene segment of the pathway of isoprenoid/cholesterol biosynthesis, i.e. first two steps in plasmalogen synthesis is also located in peroxisomes (Hogenboom et al., 2004a; Hogenboom et al., 2004b; Islinger et al., 2012b; Kovacs et al., 2002; Kovacs et al., 2007; Trompier et al., 2014; Wanders and Waterham, 2006). The formed ether lipids serve as a second messenger reservoir, buffer oxidative stress and contribute to membrane fluidity (Dean and Lodhi, 2018; Trompier et al., 2014). Here they play a crucial role in organization and stability of lipid raft microdomains, which form the basis of many membrane regions involved in cellular signaling (Dean and Lodhi, 2018; Lohner, 1996; Paltauf, 1994). In brain tissue ether lipids exhibit especially high abundance in myelin membranes (Pieringer et al., 1977).

Involvement of peroxisomes in bile acid metabolism and polyamine catabolism has also been observed in liver tissue (Ferdinandusse et al., 2009; Kovacs et al., 2009; Nishikawa et al., 2000; Schrader and Fahimi, 2008; Vujcic et al., 2003). The peroxisomal ether lipid pathway is necessary for producing the alkyl chain for glycosylphosphatidylinositol (GPI) anchor synthesis (Islinger et al., 2012b; Kanzawa et al., 2009; Kanzawa et al., 2012). GPI-anchors attach several membrane-bound proteins to the lipid bilayer membranes (Islinger et al., 2012b). GPI-anchored proteins

are involved in cell–cell and cell–environment interactions and contribute to lipid microdomains (Islinger et al., 2012b).

Apart from these metabolic functions, peroxisomes appear to play an important role in antiviral defense in cooperation with mitochondria (Dixit et al., 2010; Islinger et al., 2012b). Peroxisomes transmit a rapid interferon-independent response mediated by mitochondrial antiviral signaling adaptor (MAVS), which alters peroxisome morphology (Islinger et al., 2012b).

1.1.2 Peroxisome variability

The abundance of peroxisomes and peroxisomal enzymes varies among tissues and cells. Peroxisomes show a high variety of and variability in number, shape and size (De Duve, 1960; Schrader et al., 2000). Peroxisomes and peroxisomal enzymes are known to rapidly adapt to metabolic stimuli by increase or decrease in peroxisome content or alteration in the peroxisomal proteome or even change of shape (Lazarow and De Duve, 1976; Schrader et al., 2012; Schrader et al., 2000; Schrader et al., 1998). Peroxisomes can form by growth and division (fission) from pre-existing organelles and by de novo synthesis through vesicle formation from the ER (Costello and Schrader, 2018; Islinger et al., 2012b) or mitochondria (McBride, 2018; Mohanty and McBride, 2013; Speijer, 2014) (*figure 2*).

A recent hypothesis interprets mitochondrial targeting of several peroxins to mitochondria in the absence of peroxisomes as hint for a hybrid mitochondrial and ER origin of de novo synthesized peroxisomes (Sugiura et al., 2017). The highly conserved peroxisomal proteins, the peroxins, initiate and perform peroxisome formation, division and enzyme import into peroxisomes (Islinger et al., 2018; Li and Gould, 2002). Apart from the above-mentioned modulation of existing enzymes' function by ROS-sensitive switches, peroxisomal enzymes and peroxisomal proliferation can be induced by peroxisome proliferator-activated receptors (PPARs) (Diano et al., 2011; Issemann and Green, 1990; Lodhi and Semenkovich, 2014; Reddy and Hashimoto, 2001). PPARs are nuclear transcription factors, which are activated by a variety of peroxisomal metabolites (Lodhi and Semenkovich, 2014; Wang, 2010). These transcription factors do not only induce peroxisome formation but also multiple peroxisomal and other cellular metabolic pathways (Lodhi and Semenkovich, 2014; Reddy and Hashimoto, 2001).

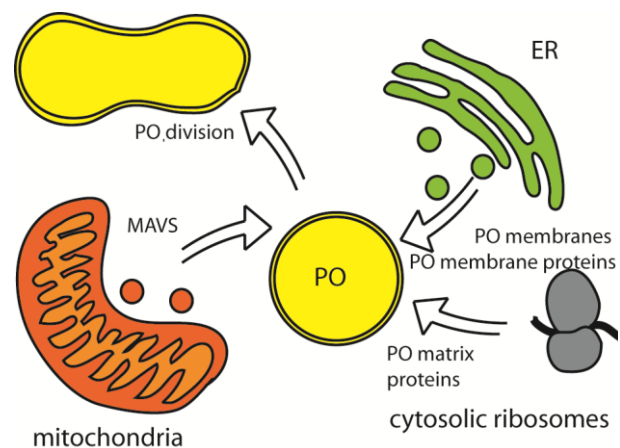


Figure 2: Peroxisome biogenesis

Overview on peroxisome formation. Peroxisomes can either form from preexisting peroxisomes via division and fission or be de novo synthesized deriving vesicles from ER and mitochondria. Matrix proteins can be derived from cytosolic ribosomes. After recognition of the peroxisome targeting signal they are imported via pore formation which is further described in paragraph 1.1.3.

Reddy and Hashimoto, 2001). PPARs are nuclear transcription factors, which are activated by a variety of peroxisomal metabolites (Lodhi and Semenkovich, 2014; Wang, 2010). These transcription factors do not only induce peroxisome formation but also multiple peroxisomal and other cellular metabolic pathways (Lodhi and Semenkovich, 2014; Reddy and Hashimoto, 2001).

1.1.3 Peroxisomal membrane

The peroxisomal membrane consists of a single lipid bilayer. To permit substrate import and product export, the peroxisomal membrane has two distinct systems. The membrane forms an unselective barrier, which is freely permeable for small molecules up to a molecular weight of 300 to 400 Da (Antonenkov et al., 2004b). This permeability derives from a homotrimeric unselective channel constituted of peroxisomal membrane protein 2 (Pmp2/PMP22) (Rokka et al., 2009) and potentially a second pore formed by PEX11 (Mindthoff et al., 2016), which is responsible for the substantial channel-forming activity in Pmp2 knockout mice (Islinger et al., 2012b). However, several peroxisomal metabolites exceed this exclusion limit. For the import of molecules larger than 300 Da specific transporters exist: fatty acids (FAs) and cofactors are imported via specific transporters, i.a. ATP-binding-cassette-transporters (ABC-transporters) (Antonenkov and Hiltunen, 2012; Kemp et al., 2011; Visser, 2002). Matrix protein import is performed by a complex machinery of peroxins, of which several have so far been identified. Remarkably, the proteins are imported in a folded and even oligomerized state (Rucktaschel et al., 2011). For correct import, peroxisomal matrix proteins possess a peroxisomal targeting sequence (PTS), which is either recognized by PEX5 (PTS1) or PEX7 (PTS2) (Ma and Reumann, 2008; Ma et al., 2009; Maynard et al., 2004; Montilla-Martinez et al., 2015; Rucktaschel et al., 2011). After interaction of this cargo-peroxin-complex with PEX13/14, a pore is formed, through which proteins are imported (Chan et al., 2016).

The peroxisomal membrane is derived from the ER by vesicle fusion or direct transfer of phospholipids (Raychaudhuri and Prinz, 2008). The peroxisomal membrane proteins (PMPs) bear a specific targeting signal (peroxisomal membrane targeting signal (mPTS)). While most PMPs are recognized by and imported via interaction with the import receptor Pex19, several other PMPs lack PEX19 binding sites and are supposed to be transported to the peroxisome via vesicles budding from the ER (Costello and Schrader, 2018; Geuze et al., 2003).

1.1.4 Interaction with ER and mitochondria

As peroxisome function and protein composition indicate, peroxisomal enzymes are involved in numerous metabolic pathways. However, often only a part of these pathways takes place in peroxisomes, while they are completed in other organelles requiring efficient metabolite exchange between organelles. The absence of peroxisomes induces functional disturbances of mitochondria compromising ATP production (Peeters et al., 2011). This suggests a close link among peroxisomes and mitochondria. Peroxisomal catalase deficiency, resulting in a decreased redox capacity of peroxisomes, has a similarly impairing effect on mitochondria (Islinger et al., 2012b; Peeters et al., 2011). Apart from ROS metabolism, both organelles also cooperate in other metabolic pathways (Fransen et al., 2017; Wanders et al., 2015). A cooperation in FA beta-oxidation is known: Peroxisomal beta-oxidation acts as a pre-processing unit – it oxidizes and shortens FAs until they are of medium length (Demarquoy and Le Borgne, 2015; Le Borgne et al., 2011). Then mitochondrial beta-oxidation takes over, as more energy can be generated by this pathway (Demarquoy and Le Borgne, 2015; Le Borgne et al., 2011). Carnitine octanoyl transferase and carnitine-octanoyl transport link peroxisomal β -oxidation to mitochondrial Krebs cycle (Demarquoy and Le Borgne, 2015; Le Borgne et al., 2011; Trompier et al., 2014). A further exchange may exist via mitochondria derived vesicles, which are supposed to be involved in transport from mitochondria to peroxisomes (Camoës et al., 2009; Fransen et al., 2017; Islinger et al., 2012b; Neuspiel et al., 2008). In antiviral signaling and defense,

mitochondria and peroxisomes also appear to cooperate (Islinger et al., 2012b; Ivashchenko et al., 2011). Beside this metabolic and functional link, peroxisomes and mitochondria also share key components of their division machinery, which in turn might serve a coordinated adaptation on metabolic needs of both organelle numbers (Fransen et al., 2017; Schrader, 2006). Further indicating the close link among mitochondria and peroxisomes an at least partly mitochondrial origin of peroxisomal de novo synthesis is hypothesized (Fransen et al., 2017; McBride, 2018; Mohanty and McBride, 2013; Speijer, 2014; Sugiura et al., 2017).

With the ER, peroxisomes also maintain a close relationship (*figure 1*): Peroxisomal membranes lipids are ER-derived (Baumgart et al., 1989). Several PMPs are integrated into the peroxisomal membrane via ER-derived vesicles (Giannopoulou et al., 2016). Furthermore at least one way of peroxisome de-novo-synthesis starts from the ER (Costello and Schrader, 2018; Islinger et al., 2012b; Sugiura et al., 2017). Besides, metabolic interactions, i.e. in squalene and cholesterol synthesis exist (Wanders et al., 2015). Further links among peroxisomes and ER exist in ether lipid synthesis, docosahexaenoic acid (DHA)-synthesis and bile acid metabolism (Ferdinandusse et al., 2009; Wanders et al., 2015).

1.2 Peroxisomes in disease

Peroxisomes are involved in a broad spectrum of diseases ranging from hereditary peroxisome biogenesis disorders (PBDs) over single enzyme deficiencies to a potential involvement in carcinogenesis (Delille et al., 2006), as well as situations related to oxidative stress such as inflammation, ischemia-reperfusion, diabetes (Delille et al., 2006) and neurodegenerative diseases (Delille et al., 2006; Santos et al., 2005; Uzor et al., 2020).

1.2.1 Single enzyme deficiencies

Hereditary peroxisomal disorders subdivide into single enzyme deficiencies and peroxisomal biogenesis disorders (PBD). In single enzyme deficiencies, clinical symptoms depend upon the specific protein defect and derive either from accumulation of peroxisomal substrates or lack of products. X-linked adrenoleukodystrophy is the most common single enzyme deficiency (Delille et al., 2006): An accumulation of VLCFA leads to progressive demyelination and neurodegeneration in the CNS (Steinberg et al., 2006), adrenal gland insufficiency and finally premature death (Delille et al., 2006). Beta-oxidation disorders additionally induce steatosis or steatohepatitis (Delille et al., 2006). Alanine-glyoxylate aminotransferase deficiency manifests clinically as hyperoxaluria and concomitant renal failure (Delille et al., 2006).

1.2.2 Peroxisome biogenesis disorders

Peroxisome biogenesis disorders (PBDs) are caused by an inherited defect in peroxin genes. Protein import into peroxisomes is disturbed, which results in lack of a part of peroxisomal matrix proteins, empty organelles or even the complete absence of peroxisomes (Delille et al., 2006). PBDs are made up of Zellweger spectrum disorders, Zellweger syndrome, neonatal adrenoleukodystrophy and Refsum disease and rhizomelic chondrodysplasia type 1 (Wanders, 2014). While some of these peroxisomal biogenesis abnormalities are incompatible with life, others go along with severe multi-organ dysfunction or brain diseases, exhibiting demyelination, abnormal myelination (Baes and Aubourg, 2009), axonal degeneration and neuronal migration defects (Faust et al., 2005; Power and Moser, 1998; Waterham et al., 2016).

1.2.3 Peroxisome involvement in further neuronal diseases

Apart from these hereditary peroxisomal disorders, several hints for the involvement of peroxisomes in further neuronal diseases exist. A mouse model of amyotrophic lateral sclerosis (ALS) exhibits reduced activity of peroxisomal D-amino acid oxidase (DAAO), an enzyme, whose impairing mutation causes an ALS-like phenotype (Sasabe et al., 2012). Excess D-serine, which is degraded by peroxisomal DAAO, is a risk factor for schizophrenia (Errico et al., 2008; Islinger et al., 2012b; Kirov et al., 2005). Models of PBD show elevated levels of oligomerized and phosphorylated alpha-synuclein, which is an inherent component of Parkinson's disease (Assayag et al., 2007). The neurodegenerative Alzheimer's disease goes along with altered plasmalogen-, VLCFA- and docosahexaenoic acid-levels, which suggests a peroxisomal contribution (Assayag et al., 2007; Jo et al., 2020; Kou et al., 2011).

Brain pathology in PBDs and peroxisomal substrate accumulation in several neurological diseases point to/imply a profound role of peroxisomes in both brain formation and function.

A further link between peroxisomes and disease exists in cancer. The nuclear transcription factor peroxisome proliferator-activated receptor alpha (PPAR α) is a non-genotoxic carcinogen, which is capable of inducing mainly liver tumors when chronically activated (Delille et al., 2006; Gonzalez et al., 1998). The resilience of PPAR α knockout mice to hepatic carcinogenesis support this hypothesis though this connection could not be transferred to primates (Delille et al., 2006; Gonzalez et al., 1998). Beside this pathogenetic role, PPAR α is an important regulator of inflammation (Delille et al., 2006; Devchand et al., 1996),

1.3 Brain peroxisomes

Peroxisomes play an important role in brain development and function. This is most obvious regarding the severe loss of brain functionality due to neural symptoms in peroxisomal disorders (Moser, 1999). Hereditary peroxisomal disorders, all subtypes of X-linked adrenoleukodystrophia and Zellweger syndrome, are characterized by profound structural and functional brain alterations. The existence of hereditary diseases with both late and early onset, indicates that peroxisomes play an important role in formation and maintenance of neural and glial structures. Many inflammatory and degenerative diseases of the brain also go along with alterations in peroxisomes. This hints at an important role of peroxisomes in brain function.

1.3.1 Major brain peroxisomal functions and their link to disease

Peroxisomes are present in all neural cell types (Trompier et al., 2014). In both, adult and adolescent mice, glial peroxisomes predominate (Trompier et al., 2014). As selective peroxisome knockouts in neurons and astrocytes resulted in less impaired phenotypes than oligodendrocyte knockouts (Bottelbergs et al., 2010; Hulshagen et al., 2008; Islinger et al., 2012b), the impairment seems especially due to compromised functions in the latter cell type. Oligodendrocytes are responsible for the formation of myelin sheets. An indispensable constituent of myelin sheets are ether phospholipids as well as plasmalogens, squalene and its derivatives (Morell and Quarles, 1999). Therefore, it is probable, that the impairments derive from loss of myelination by oligodendrocytes. Without the isolation provided by the myelin sheet, axonal conduction is hindered, which leads to the observed axonal degeneration (Bottelbergs et al., 2010). This central function in myelin metabolism makes brain peroxisomes an

important agent in demyelinating diseases. Apart from this role in myelination and maintenance of myelin sheets, brain peroxisomes carry out further tasks.

Another well-known and important role of peroxisomes is the metabolism of reactive oxygen species (ROS), described above. As an excess of ROS is potentially toxic for cells, ROS homeostasis is of high importance. Apart from the prevention of oxidative stress, ROS generated by peroxisomes serve as cellular signals, e.g. in hypothalamic neurons. The peroxisomal ROS metabolism appears to be involved in neurodegenerative diseases, as disturbed peroxisomal function in Alzheimer mouse models indicates, as well as in neuroinflammatory diseases and ischemia-reperfusion. A third important task of peroxisomes in brain is the beta-oxidation of very long-chain fatty acids (VLCFA), whose accumulation would otherwise disturb cellular homeostasis and lead to functional impairments. Peroxisomes also perform the last step of docosahexaenoic acid (DHA) synthesis. DHA is a major component of phospholipids of neuronal cell membrane. 40% of all polyunsaturated fatty acids in brain are DHA. DHA or a variety of its bioactive derivatives play an important role in intracellular signaling (Berger et al., 2016).

The degradation enzymes of certain potentially toxic neuromodulatory metabolites, e.g. phytanic acid and of several D-amino acids are also located within peroxisomes (Errico et al., 2008; Nagai, 2015; Sasabe et al., 2012; Schonfeld and Reiser, 2016; Wolosker et al., 2008). Especially D-serine, which is a physiological co-agonist of NMDA-receptors and necessary for their activation and hereby capable to influence synaptic plasticity (Wolosker et al., 2008), is of interest in physiology and pathology: D-serine imbalance is discussed as a cause of schizophrenia (Errico et al., 2008). Peroxisomes as D-amino acid degradation site might therefor be involved its pathogenesis.

1.3.2 Peroxisomal populations in the brain

The differing phenotypes in selective peroxisomal knockouts indicate the presence of cell-type specific subtypes of peroxisomes, which is verified by immunofluorescence imaging (Ahlemeyer et al., 2007). Apart from several peroxins involved in peroxisome biogenesis and protein import, metabolic peroxisomal membrane and matrix proteins are expressed at considerably different levels in neurons and astrocytes (Ahlemeyer et al., 2007). Neuronal peroxisomes are usually smaller and contain less catalase than glial ones (Ahlemeyer et al., 2007; Holtzman, 1982). Differences in selective knockouts (*paragraph 1.3.1*) support the hypothesis of cell-type specific peroxisomal functions. A further differentiation among sub-types exists: Though both are neurons, Golgi cells contain more, and more intensely PEX14-stained peroxisomes than granule cells in the cerebellum (Grant et al., 2013). Peroxisomes in Purkinje cells, however, seem to contain only little acyl-CoA oxidase (ACOX), Catalase, D-bifunctional protein (D-BP), and 3-ketoacyl-CoA thiolase (PT) (Nagase et al., 2004). Knockout of Purkinje-cell specific peroxisomes causes motor-phenotype and loss of axonal integrity revealing cell-type specific functions independent of glial function (De Munter et al., 2018). Catecholaminergic neurons seem to incorporate a higher catalase-positive peroxisomal population than other neurons (Arnold and Holtzman, 1978; Holtzman, 1982).

In addition to these cell-type specific differences, considerable variance exists among different brain regions. Periventricular zone of neocortex, plexus and ependyma of lateral and 4th ventricle, the external and internal germinative layers of the cerebellum, the cerebellar nuclei and the whole cornu ammonis exhibit high levels of peroxisomes in newborn mice (Ahlemeyer et al., 2007). Dentate gyrus exhibits moderate, marginal zone and zona intermedia of neocortex low levels (Ahlemeyer et al., 2007). Even within

the same neuronal subtype, peroxisomal abundance varies. For example, pyramidal cells of motor cortex contain more peroxisomes than those in parietal cortex (Ahlemeyer et al., 2007).

Independently of peroxisomal abundance, variance in immunofluorescence signal among brain regions is known for numerous peroxisomal enzymes: So far, diverging patterns are known for D-amino acid oxidase (DAAO) (Holtzman, 1982), catalase (Ahlemeyer et al., 2007; Arnold and Holtzman, 1978; Holtzman, 1982; Houdou et al., 1991; Nagase et al., 2004), acyl-CoA oxidases (ACOX) (Ahlemeyer et al., 2007), (Nagase et al., 2004), D-bifunctional protein (D-BP) (Nagase et al., 2004) and peroxisomal 3ketoacyl-CoA thiolase (PT) (Ahlemeyer et al., 2007; Nagase et al., 2004). The ciprofibrate-driven peroxisomal proliferation without catalase amplification in cerebral neuron supports the hypothesis of a function-specific peroxisomal proteome (Grant et al., 2013).

These differences in peroxisomal proteome are also reflected by the size, i.e. Catalase-positive peroxisomes are comparatively large (Holtzman, 1982).

1.3.3 Alterations during aging

The differential onset and symptoms of peroxisomal diseases indicate a change in peroxisomal function during aging. This goes along with an alteration in peroxisome number in most cell types and brain regions between youth and adolescence (Ahlemeyer et al., 2007). Overall, abundance of peroxisomes in cortex decreases during postnatal development, but with variation among the brain regions (Ahlemeyer et al., 2007). While peroxisome number significantly decreases in cortical plate to the corresponding layer 3 of cortex and in hippocampal pyramidal cells (Ahlemeyer et al., 2007), the number in cerebellar nuclei, ependyma and plexus of the lateral ventricle remains at a similar level (Ahlemeyer et al., 2007). Purkinje cells even contain more peroxisomes than their precursors (Ahlemeyer et al., 2007).

Peroxisomal enzyme pattern exhibits a different development, i.a. catalase level peaks during myelination and decreases afterwards (Tsay et al., 2000). Enzyme expression does not necessarily follow the abundance of peroxisomes. I.e. while peroxisome number increases in the stratum moleculare of neocortex, abundance of catalase, PT and ACOX1 remains at a similar level (Ahlemeyer et al., 2007).

The fact, that peroxisomes from adult mouse brain (Singh et al., 1989) enrich at a different density than those from infant brain (Cimini et al., 1993; Kovacs et al., 2001; Lazo et al., 1991), supports the idea of a change in peroxisomal proteome making them interesting for further research.

1.4 Difficulties of peroxisome purification from adult brain tissue

Multiple obstacles impede peroxisome isolation from brain tissue: The comparatively low abundance of peroxisomes, the complex tissue structure with highly specialized cell types and liposomal particles forming during tissue homogenisation.

1.4.1 Peroxisome heterogeneity

Brain tissue is a complex structure. It consists of astrocytes, oligodendrocytes, neurons, microglia and other less abundant cell types. With this diversity in respect to contained cells, each with its specific tasks, brain tissue is by far more inhomogeneous than other tissues, from which peroxisomes have been isolated so far. Peroxisomes are expressed in all these cell types (Trompier et al., 2014). Because each of these cell types has specific functions and a different pattern of metabolic pathways,

peroxisomes are likely an inhomogeneous group, as they adapt to the specific metabolic needs (Islinger et al., 2012b). Cultured neurons and astrocytes from newborn mice exhibit a comparable abundance of peroxisomes but show heterogeneity in peroxisomal protein content (Ahlemeyer et al., 2007). Whereas the immunoreactivity of peroxins and peroxisomal-targeting signal is similar in both cell types (Ahlemeyer et al., 2007), the signal of imported enzymes and proteins, such as catalase and PMP70, is significantly stronger in cultured astrocytes than in neurons (Ahlemeyer et al., 2007). Independent of culture origin, catalase-positive peroxisomes in astrocytes are more intensely stained and larger than in neurons (Ahlemeyer et al., 2007). In immunohistochemistry of newborn mice, astrocytes and oligodendrocytes exhibited a similar abundance of catalase positive peroxisomes (Arnold and Holtzman, 1978). Whereas most glial peroxisomes exhibit a similar protein pattern, neuronal peroxisomes of differently specialized brain areas differ in pattern of expressed proteins in IHC, which might be due to the different functions of the single neurons. In contrast to the majority of neurons, catecholaminic brain region neurons and sympathetic ganglia contain appreciable numbers of catalase-positive peroxisomes (Arnold and Holtzman, 1978).

Apart from the heterogeneity in peroxisomes derived from different cell types within a specific brain area/layer, peroxin staining reveals inhomogeneity among brain regions and even areas / layers within these brain regions (Ahlemeyer et al., 2007): This variability in abundance of peroxisomal enzymes has been published concerning D-amino acid oxidase (DAAO) (Holtzman, 1982), Catalase (Ahlemeyer et al., 2007; Arnold and Holtzman, 1978; Holtzman, 1982; Houdou et al., 1991; Nagase et al., 2004), acyl-CoA oxidase (ACOX1) (Ahlemeyer et al., 2007; Nagase et al., 2004), D-bifunctional protein (D-BP) (Nagase et al., 2004), peroxisomal 3-ketoacyl-CoA thiolase (PT) (Ahlemeyer et al., 2007; Nagase et al., 2004). Even peroxisomes, defined by the presence PEX14, with neither ACOX1 nor catalase IHC-signal detectable are known (Nagase et al., 2004).

This complex pattern of peroxisomes increases in complexity during maturation of the brain. From birth on, the peroxisomal heterogeneity concerning differences among brain regions, areas and layers within a specific region and the different cell types within a specific area / layer increases (Ahlemeyer et al., 2007; Arnold and Holtzman, 1978)

Additionally, other mechanisms are at play: e.g. the neurotrophic growth factors (NGF) trigger high levels of catalase at birth and its strong decrease during postnatal brain development. This perinatal catalase upregulation may aim at the protection of neurons from oxidative injury (Ahlemeyer et al., 2007; Nikolaou et al., 2006). Coinciding with the catalase peak (Ahlemeyer et al., 2007), NGF, which stabilizes catalase mRNA level in neural processor cells (Sampath and Perez-Polo, 1997) and which induces peroxisomal proliferation (Schrader et al., 1998), is highly upregulated around birth (Nikolaou et al., 2006).

Furthermore, metabolism induced alterations in peroxisome size and shape have been demonstrated (Schrader et al., 1998).

All these features influence the physical properties of peroxisomes, which is demonstrated by the differing densities at which peroxisomes enrich in density gradient centrifugation:

Peroxisomal subpopulations defined by DAAO and catalase have different equilibrium densities (Gaunt and de Duve, 1976). The effect of the differences among areas on equilibrium density of peroxisomes is demonstrated by the shift from 1.152 - 1.162 g/ml for PO isolated from the brain stem to higher values (1.177 g/ml) through the inclusion of cerebellar tissue (Cimini et al., 1993).

1.4.2 Contaminating particles

In contrast to other tissues, the cellular surface in CNS is comparatively high. Neurons have large dendritic and axonal extensions, oligodendrocytes form isolators of membrane bundles and the star-shaped astrocytes extend their appendices in between the other cells. Therefore, the percentage of cellular membranes in the homogenate is higher than in other tissue, which affects separation.

To release peroxisomes, the brain tissue must be broken up by homogenisation. Brains are mechanically homogenised, as this procedure outperforms chemicals in intact tissue (Burden, 2008). While cytosolic corpuscular components are released, cellular membranes are broken into pieces of different size, which shape liposomes. ER particles of various sizes are converted into microsomes. Synaptosomes are generated from disrupted, resealing synapses during homogenisation of brain tissue (Islinger et al., 2011). Myelin and other membranes are broken down into fragments of different size and density, which end up in various subcellular fractions (Lazo et al., 1991). All these particles can be found at a wide range of sizes and densities impeding separation.

1.4.3 Myelin

With myelin a further contaminant lacking in other tissues is present in brain. The presence of large amounts of myelin is even regarded as major difficulty in brain peroxisome purification (Lazo et al., 1991). Myelin is fragmented into vesicles of various densities during homogenisation (Singh et al., 2000). These fragmented myelin particles become a source of contamination in almost all the organelles isolated from brain (Singh et al., 2000). They are even reported to be capable of impairing organelle separation in Nycodenz gradient (Kovacs et al., 2001). This impairing effect is due to the myelin vesicles formed by homogenisation trapping organelles, hereby altering their physical properties (Larocca and Norton, 2007). To enable organelle separation, myelin must be removed before separating the organelles.

1.4.4 Peroxisome fragility

Peroxisomes are highly fragile organelles. A spontaneous release of the peroxisomal core enzymes has been reported even in isoosmolar solutions (Antonenkov et al., 2004a). Together with the so far only partially known peroxisomal proteome and peroxisome heterogeneity including non-membrane-bound proteins and enzymes (*paragraph 1.4.1.*), release of “core” proteins has to be avoided and results have to be checked for peroxisomal membranes, so called “ghosts”.

1.4.5 Previous protocols for the separation of PO from brain tissue

The valuable tool of immunohistochemistry, which has been mainly used to investigate peroxisomes in brain (*paragraph 1.4.1.*), is limited to known proteins with pre-existing antibodies and thus to a comparatively low number of target proteins due to the overlapping spectra of the secondary antibodies. A further obstacle is the presence of lipofuscin granules, structures of clustered oxidized lipids and proteins, which have strong auto-fluorescence and hinder appropriate imaging especially in humans (Terman and Brunk, 2004). Lipofuscin granules accumulate with aging and are highly abundant in neuronal tissue (Terman and Brunk, 2004).

As peroxisomal proteins might also locate to other organelles in brain like ACAD11 (He et al., 2011), an isolation procedure of subpopulations might be necessary to better characterize brain peroxisomes, subpopulations and their proteome.

Previous organelle separation protocols circumvent the problems of myelin and peroxisomal heterogeneity mainly by using nascent animals (Cimini et al., 1993; Kovacs et al., 2001; Lazo et al., 1991), which have a comparatively low myelin content. As brain myelination is on its maximum in this phase, a high need for peroxisomal lipid production exists. This gives rise to a comparatively high concentration of a peroxisomal population specialized on e.g. squalene production, which can be extracted (Kovacs et al., 2001). Immunohistochemistry studies reveal various alterations in brain peroxisomes with aging (Ahlemeyer et al., 2007). This circumvention limits the significance of peroxisomal isolation to their role in myelin production, as the isolated catalase-positive glia are thought to be closely related to myelinogenesis in the developing brain (Houdou et al., 1991).

Existing studies with adult animals have so far focused on single peroxisomal subpopulations defined by core enzymes, such as catalase or DAAO, and achieved only low degrees of purification (Gaunt and de Duve, 1976; Singh et al., 1989). Though some protocols provide a certain degree of peroxisome purification (Gaunt and de Duve, 1976; Singh et al., 1989) or immunohistochemical insights (Ahlemeyer et al., 2007; Arnold and Holtzman, 1978; Grant et al., 2013; Holtzman, 1982; Houdou et al., 1991; Nagase et al., 2004), little is known about adult brain peroxisomes.

The valuable characterization of peroxisomes from adult brain is so far compromised by the lack of appropriate isolation protocols

1.4.6 Strategies to overcome difficulties in brain peroxisome purification

As peroxisomes are known to shift in density dependent on the surrounding medium (Antonenkov et al., 2004a) and a correlation among peroxisome size and certain peroxisomal enzymes has been observed (Arnold and Holtzman, 1978; Holtzman, 1982), separation by physical properties seems promising. To overcome the above-mentioned problems, we designed a complex purification protocol based on the reports from previous experiments. All these previous studies dealt with myelin with a single sucrose step gradient centrifugation (Cimini et al., 1993; Kovacs et al., 2001; Lazo et al., 1991; Singh et al., 1989), a procedure, which has to be adapted on the larger amounts of myelin in adult brain.

1.5 Peroxisome isolation from cell culture

Cell culture is a well-established tool to study the effect of enzymes or organelles on a specific cell type. Compared to whole organisms, single cells are easier to target and manipulate e.g. by overexpression or knockout of genes (Ahlemeyer et al., 2014) or by nutritional stimuli (Ponce-Ruiz et al., 2015).

Isolation of organelles from cell culture broadens the spectrum of investigations possible with cultured cells. It enables the investigation of a specific organelle proteome and permits the quantification of an organelle's metabolism, whereas the number of proteins that can be investigated using immunofluorescence imaging is limited. Density-shift-assays are a special type of isolation procedure, which provides evidence for the interaction of two proteins or molecules. Transferred to the field of organelle isolation, density-shift-assays prove the existence of bonds between two organelles. In combination with manipulations in protein expression, specific mediators of these bonds between two organelles can be assessed.

As effects of other surrounding cell types and the organism itself are neglected, cell culture experiments are unable to replace organelle preparation from whole organism. These tissue effects are especially relevant in neuronal tissue, where neurons and glia cooperate in metabolic pathways, i.e. transmitter degradation and nutrition. In the study of peroxisomes, peroxisome isolation from cultured cells and from tissue complement one another. As in tissues, protocols must be adapted according to the specific needs. Apart from the usual precautions taken in cell culture, organelle isolation from cells bears some inherent difficulties: harvest of the cells and especially homogenisation must be particularly gentle to avoid disruption of the organelles (Burden, 2008). Especially organelles surrounded by a single lipid bilayer are jeopardized. As hardly any extracellular matrix is existent compared to tissue, lower homogenisation forces can be applied (Burden, 2008).

To utilize the full potential of cultured cells, the protocol must be capable of dealing with altered physical properties of cellular organelles due to manipulations of protein expression. In density-shift-assays this gains further importance. To allow organelle isolation also under such changing conditions, special care must be taken with each purification step. The pre-processing steps with removal of debris, nuclei and insufficiently homogenised or contaminating particles must be carefully adapted. A final centrifugation by a continuous gradient might provide an adequate solution for this problem, as instabilities in density carry less weight and the results of a pull-down-assay appear as a position shift in this gradient.

Our new cell purification protocol is developed for the purpose of investigations on organelle interaction, i.e. the ER-peroxisome interplay, more specifically the the investigation of the interaction of ACBD5 and VAPB (Costello et al., 2017a; Manner and Islinger, 2017).

1.6 Goals

This study aims to provide tools for the investigation of peroxisomes in adult brain tissue and in cell culture, to enable closer investigation of the altered composition and functionality of peroxisomes during e.g. aging.

The purification protocols shall enable to analyse the protein composition of peroxisomes from the brain (e.g. in subsequent proteomics studies) to identify potential brain-specific functions of the organelle. To avoid a lack of sample size and to guarantee functionality with all brain tissues, experiments were carried out on whole mice brain. In a first step a pre-existing protocol for peroxisome isolation in growing mice (Kovacs et al., 2001) was tested in adult mice. This protocol was subsequently optimized by implementing knowledge about peroxisome isolation from other tissues and about organelle isolation from brain tissue. Further variations of the protocol were performed based on obtained results. Additionally, different gradient media were tested. In all applied procedures special care was taken to avoid osmotic damage and disruption of the peroxisomes.

To assess peroxisomes in single cell lines, a protocol to isolate peroxisomes from cultured cells, i.a. HepG2, which can be easily used for knockdown or overexpression experiments, was developed. The protocol is intended to deal with manipulations in organelle proteome by knockdown or overexpression and shall be usable in density-shift-assays for organelle interaction analysis (Costello et al., 2017a; Manner and Islinger, 2017).

2 MATERIAL AND METHODS

2.1 Common materials and solutions

2.1.1 Chemicals

Chemical	Supplier
Acetic acid	Roth, Germany
Aminocaproic acid	AppliChem, Germany
Ammonium persulfate (APS)	Roth, Germany
Benzamidine hydrochloride	Roth, Germany
Bovine serum albumin	Roth, Germany
Bromophenol blue	Sigma Aldrich, Germany
Coomassie Brilliant Blue R-250	Roth, Germany
di-Sodium hydrogen phosphate dihydrate	Roth, Germany
Dulbecco's Modified Eagle Medium (DMEM)	Roth, Germany
Ethylenediaminetetraacetic acid (EDTA)	Roth, Germany
Ethanol	Roth, Germany
Fetal calf serum (FCS)	Thermo Fisher, USA
Glycerine	Roth, Germany
Glycine	Roth, Germany
2-(4-(2-Hydroxyethyl)piperazin-1-yl)ethane sulfonic acid (HEPES)	AppliChem, Germany
Isopropanol	Roth, Germany
Methanol	Roth, Germany
3-(N-Morpholino)propane sulfonic acid (MOPS)	Roth, Germany
ROTI Nanoquant	Roth, Germany Cat. No. K880.1
Nycodenz	Axis shield, Norway Cat.No. 1992424
Optiprep (Iodixanol)	Axis shield, Norway Cat.No. 1114542
PageRuler Prestained Protein Ladder	Thermo Fisher, USA Cat No. 26616
PageRuler Plus Prestained Protein Ladder	Thermo Fisher, USA Cat No. 26619
Penicillin	Roth, Germany
Peqlab Midi-prep kit (now XChange Plasmid Midi Kit)	Peqlab, Germany Cat No. 12-7401-02
Phenylmethylsulfonyl fluoride (PMSF)	Roth, Germany
Polyethyleneimine 25K (PEI)	Polysciences, Germany Cat. No 23966-1
Polysorbate 20 (Tween 20)	Roth, Germany
Potassium chloride	Roth, Germany
Potassium dihydrogen phosphate	Roth, Germany
Powdered milk blotting grade	Roth, Germany
Sucrose	Roth, Germany
Sodium acetate anhydrous	Roth, Germany
Sodium bicarbonate	Roth, Germany
Sodium chloride	Roth, Germany
Sodium dodecyl sulfate (SDS)	Roth, Germany

Chemical	Supplier
Sodium hydroxide	Roth, Germany
Streptomycin	
Sulfuric acid	Roth, Germany
N,N,N',N'-Tetramethylethylenediamine (TEMED)	Roth, Germany
Tris(Hydroxymethyl)aminomethane (Tris Pufferan)	Roth, Germany
N-[Tris(hydroxymethyl)methyl]-3-aminopropanesulfonic acid (TAPS)	Roth, Germany
Triton X-100	Roth, Germany
Trypsine/EDTA-solution	Thermo Fisher, USA Cat.No. R001100

Table 1: Chemicals

2.1.2 Solutions used in brain extraction, homogenisation and centrifugation

All solutions used for brain extraction, homogenisation and centrifugation are based on a buffer system (gradient buffer), in which the gradient generation constituents, sucrose, Nycodenz or Optiprep (iodixanol), are dissolved.

The purpose of this gradient buffer is to avoid proteolysis and to balance pH in order to avoid effects introduced by change in the buffer solutions in the experiments, gradient buffer composition is kept constant.

The gradient buffer contains 1 mM aminocaproic acid, 5 mM benzamidine-hydrochloride for protease inhibition, 0.1%(v/v) ethanol, 1mM EDTA and 5mM MOPS or HEPES (table 2). The use of two different buffer systems derives from the implementation of different pre-existing peroxisome purification protocols, which were used as a basis for the development of this peroxisome purification procedure. Both buffers work at the physiological pH level of brain tissue: Peak buffer capacity of HEPES ranges from a pH value of 7.2 to 7.6, MOPS has its maximum buffer capacity from pH 6.5 to 7.9. Physiological intracellular pH of neurons in preparation ranges among 7.03 – 7.46 (Ruffin et al., 2014) Older papers working on tissue slices, define optimum pH range for neuronal tissue at 7.0 – 7.5 (Elliott and Birmingham, 1949).

To avoid osmotic damage to the cellular organelles, differential centrifugations are carried out in gradient buffer containing 250mM or 320mM sucrose. Density gradients are formed of different concentrations of sucrose, Nycodenz or Optiprep in the gradient buffer. Whereas sucrose and Nycodenz directly solubilized in gradient buffer, Optiprep is diluted from a commercial 60% stock solution. The concentrations of the respective media of which gradients are constituted are described in the respective paragraphs.

Gradient buffer	
Substance	Concentration
HEPES/MOPS	5mM
Ethanol	1%(w/w)
EDTA	1mM
Benzamidine hydrochloride	5mM
Aminocaproic acid	1mM
Solvent:	Distilled water

Table 2: Gradient buffer recipe

Directly before the experiment 1ml phenylmethylsulfonylfluoride (PMSF) dissolved in isopropanol is added per 100ml of each used solution. This corresponds to a final concentration of 1mM PMSF. Protease activity was inhibited by PMSF, aminocaproic acid, benzamidine and EDTA.

2.1.3 Density measurement

Abbé refractometer	
Digital-Refraktometer DR 301-95	A.Krüss Optronic, Hamburg, Germany

Table 3: Refractometer

The density of gradient solutions is measured with an Abbé refractometer or an electronic refractometer device (Digital-Refraktometer DR 301-95 (A.Krüss Optronic, Hamburg, Germany)). Before each use the refractometer is calibrated with distilled water. Each measurement is repeated twice, in the case of incongruent results more often.

Refractive index of Nycodenz behaves linearly to its concentration (Rickwood et al., 1982). Hence, the density of Nycodenz solutions in gradient buffer is calculated according to the equation $d[g/ml]=3.242 \cdot \eta - 3.323$ derived from Nycodenz product data sheet, where d denotes for the density of the solution and η for the measured refractive index. Due to comparatively low content of other chemicals in gradient buffer, these are neglected in this calculation. The calculation of the density of sucrose solutions is performed according to the equation $d[g/ml]=(\eta - 0.96)/0.3733$. For Optiprep the formula $d[g/ml]=3.2441 \cdot \eta - 3.4584$ is used.

2.2 Peroxisome isolation from cultured cells

Cell culture provides a useful tool in peroxisomal proteomic studies: It can be used to study localization of potential peroxisomal proteins (Zhou et al., 2015), the investigation of formation of peroxisomes (Dimitrov et al., 2013) and the effects of knockout or overexpression of peroxisomal proteins on the single cell (Ahlemeyer et al., 2014). Furthermore, cell culture provides a valuable tool in the investigation of single external, e.g. nutritional stimuli on protein expression and localization on the single cell (Ponce-Ruiz et al., 2015). A more specialized application is the study of interactions among organelles (Costello et al., 2017a; Costello et al., 2017b; Costello and Schrader, 2018; Schrader et al., 2015). Besides immunofluorescence microscopy, the isolation of single organelles from cultured cells followed by the evaluation of their content is a potent technique to investigate an organelle's proteome. Organelle separation from cultured cells and successive proteomic examinations exceed immunofluorescence microscopy in the measurement of quantifiable effects.

Interaction-assays can prove physical interaction between two organelles. When carefully extracted from cells and isolated from other organelles, the physical interaction between two organelles can be shown by co-localisation of the two organelles involved in density gradient centrifugation. To highlight this effect and to distinguish the co-localisation from unspecific signals, overexpression of the proteins involved in interaction and comparison to wild-type is required.

Our new cell purification protocol is developed for the purpose of investigations on organelle interaction, i.e. the ER-peroxisome interplay. In this context, overexpression of proteins of interest, i.a. the mediators of this interaction is required. This overexpression is performed by transfection of the cells with plasmids (GFP-ACBD5 and myc-VAPB) bearing the respective genes (details in Costello et al. 2017 (Costello et al., 2017a)). We focused on the investigation of the interaction of ACBD5 and VAPB (Costello et al., 2017a).

2.2.1 Cell line and cell culture

For the experiments, the well-characterized cell line HepG2 is used. This immortalized, human hepatoblastoma carcinoma cell line is epithelial and well-differentiated (Lopez-Terrada et al., 2009). They are adherent, grow in monolayers and small aggregates. The cell line is described to be stable and suitable as transfection host.

Deriving from hepatic tissue, the HepG2 cells contain a considerable number of peroxisomes. The cell line has been used for characterization studies of peroxisomal proteins before (Ahlemeyer et al., 2014; Dimitrov et al., 2013; Hosoi et al., 2017; Petroni et al., 2019; Zhou et al., 2015). The peroxisome isolation protocols from these studies served as hallmarks for the development of this specific protocol.

As recommended, HepG2 cells are cultivated in Dulbecco's modified Eagle's medium (DMEM) with low glucose, 10% FCS with addition of Penicillin/Streptomycin at 37°C, 5% CO₂. All operations are carried out under aseptic conditions.

When the cultured cells exhibit 80% confluence, i.e. about 6.5×10^6 cells, cells are harvested or split for further propagation. For this purpose, medium is aspirated, the cells are washed once with 10ml pre-heated phosphate-buffered saline (PBS) per T75cm² flask. The cells are detached by incubation with 1ml trypsin solution per flask for 2 minutes. Success of the detachment is checked via microscopy. When successful, trypsin reaction is stopped through addition of the 10ml cell culture medium supplemented with 10% FCS, the solution is retrieved and pelleted at 1000 x g for 5 minutes. The cell-containing pellet is resuspended and then either further processed or sowed at about 2.1×10^6 cells per T75cm² flask. To this end, cells are counted with a Neubauer improved Hemocytometer.

2.2.2 Transfection

For the investigation of peroxisome-ER interactions, cells are transfected with plasmids encoding the ER fusion protein Myc-VAPB and the peroxisomal fusion protein EGFP-rACBD5. The plasmids are propagated in E.coli bacterial culture and purified via Peqlab Midi-prep kit. Plasmid content is quantified via photometric measurement.

As transfection method, transfection with 25kDa polyethylenimine (PEI; Polysciences) was used. The transfection solution is mixed for 10 seconds according to *table 4*, and then incubated at room temperature. The solution is applied on the cells, which were previously washed for 3 times with PBS, After transfection the cells were incubated for 24 hours at 37°C. Control cells were mock transfected with PEI only for comparison. Transfection efficiency was determined by immunofluorescence analysis of additionally incubated coverslips.

Transfection solution (per T75cm ² flask)	
Plasmid	66,66µg DNA
PEI in Aqua dest (1µg/µl)	333µl
DMEM	3000µl

Table 4: Recipe transfection solution

2.2.3 Peroxisome isolation

Centrifuges and rotors		
Rotina 420R centrifuge	Hettich Zentrifugen, Tuttlingen, Germany	Centrifugation 1-3
Sorvall WX Ultra 100 centrifuge	Thermo Fisher Scientific, Waltham, USA	Centrifugation 4-6
Sorvall Surespin 360 swinging bucket ultracentrifuge rotor	Thermo Fisher Scientific, Waltham, USA	Centrifugation 4 and 6
Beckman VT150 fixed angle rotor	Beckman Coulter, Brea, USA	Gradient centrifugation (centrifugation 5)

Table 5: Centrifuges and rotors used in peroxisome isolation from HepG cells

Peroxisomes were isolated from transfected HepG2 cells by this protocol (*figure 3*), To be capable to deal with density shifts by transfection, a continuous gradient is chosen as final purification step, which can deal with organelles of different density. For comparability and examination of the effects of the transfection,

Per experiment and gradient, 10 to 12 T75cm² cell culture bottles were grown. After a washing step with PBS containing protease inhibitors, HepG2 cells are abraded via a cell scraper and solved in PBS, which is removed by centrifugation at 500 x g for 5min and replaced by homogenisation buffer. After homogenisation, cells are disrupted with shear stress, which is applied by 5ml syringe and 27G needle. After shearing, cellular debris and nuclei are pelleted at 600 x g for 10 minutes. The supernatant (**sup1**) is further centrifuged at 2000 x g, 10min. The resulting supernatant (**sup2**) undergoes a further centrifugation, whose pellet (**P3**) is suspended in homogenisation buffer and applied on top of a continuous Nycodenz gradient ranging from 1.14g/ml to 1.19g/ml. After centrifugation for 45 minutes at 100.000 x g, the gradient is ml-wise harvested. The derived 12 fractions are measured concerning density and protein content and concentrated by centrifugation. The samples are analyzed by immunoblotting.

To determine the best purification procedure, several approaches were tested. As the centrifugation steps 1 to 4 have proved their value, they remained unchanged. For the final gradient, both Optiprep and Nycodenz are tested for their separation capability. The gradient length is adapted for best separation capacity, which is capable to image both transfected and not transfected organelles.

Phosphate buffered saline (per 1l)	
di-Sodium hydrogen phosphate dihydrate	1.78 g
Potassium dihydrogen phosphate	0.2 g
NaCl	8 g
KCl	0.2g
Distilled water	ad 1l

Table 6: Recipe Phosphate buffered saline (PBS)

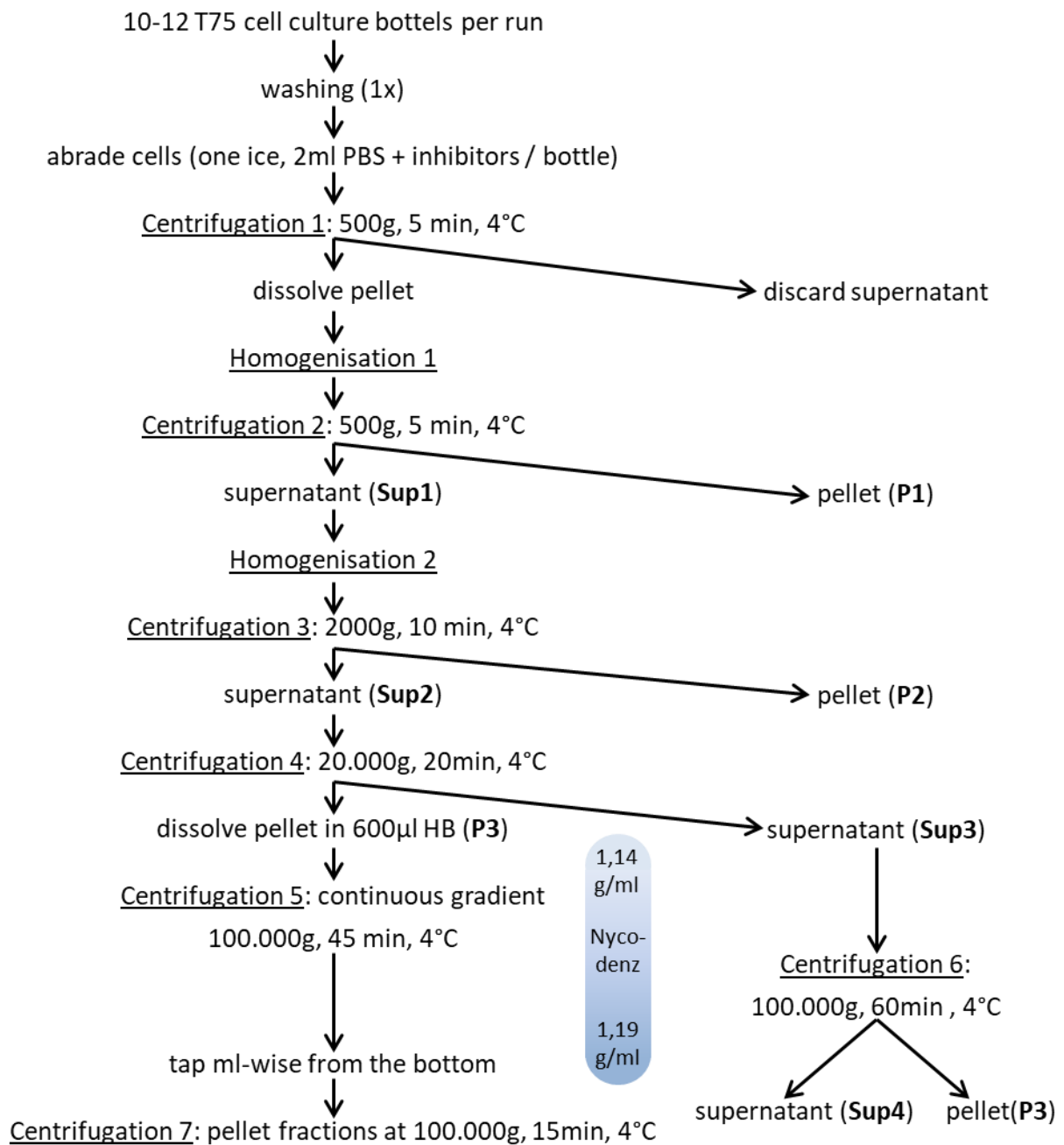


Figure 3: Peroxisome isolation protocol optimized on ER-PO-interaction

Centrifugations 2 to 4 serve to elevate peroxisome and ER concentration and to remove debris, mitochondria and cytosol. The purified organelles are further split up on a continuous gradient in centrifugation 5. Split up of supernatant **Sup3** in centrifugation 6 acts as control of organelle purification in centrifugation 4. All pellets were dissolved in homogenisation buffer containing 250mM sucrose (table 7).

2.3 Peroxisome isolation from murine brain

Besides cell culture studies, studies on organelles isolated from tissues grant valuable knowledge on organelle function. While cultured cells are best suited for experiments involving a single or few cell types, organelles isolated from tissue can be used to examine the organelles' role in the interaction with various cell types forming the tissue. Brain tissue consists of various cell types and subtypes with specific distinct functions: Metabolic pathways of glial cells and neuronal cells are intertwined with each other. An example for this link is the removal and degradation of neuronal transmitters and thus termination of synaptic signal. Astrocytes surrounding the synapses degrade neuronal transmitters produced by neurons. Cell-type specific functions include among others myelin formation, D-serine degradation (Wolosker et al., 2008), ULCFA formation and metabolism (Deak et al., 2019).

Due to their common use as models for diseases and in brain research, brain peroxisome isolation protocol was developed in mice.

To investigate the peroxisomes in adult brain tissue, a new protocol had to be developed. Preexisting protocols solely address nascent or newborn mice's or rat's brain (Cimini et al., 1993; Gaunt and de Duve, 1976; Kovacs et al., 2001; Lazo et al., 1991; Posset et al., 2015; Singh et al., 1989; Singh et al., 1993).

Based on pre-existing protocols of peroxisome isolation from different tissues and cell culture, as well as on isolation procedures for different organelles, several approaches for the isolation of peroxisomes from murine brain were performed. The protocols were extended and adapted in several steps. Multiple gradient and centrifugation parameters were altered and tested, taking pre-existing knowledge on peroxisomes into account: Among others, a peroxisome purification protocol working in young mice from 0 to 25 days of age by Kovacs et al (Kovacs et al., 2001) was tested for effectivity in adult mice and the differences of physical properties of adult and nascent mice's brain peroxisomes were examined (*paragraph 2.3.4*). Further purification procedures incorporated, are peroxisome isolation protocols from rat liver and cell culture (Schrader et al., 1994) and protocols dealing with peroxisome isolation from infant rat brain (Lazo et al., 1991; Singh et al., 1989; Singh et al., 1993) and infant mouse brain (Posset et al., 2015).

2.3.1 Animals

For all experiments the Balb-c inbred strain was used. Balb-c strain is used as general multipurpose model in cancer, cardiovascular autoimmunity, sensineural and neurobiological research.

For experimental comparability, female mice aged 6 weeks were used for all experiments. Animals were bred by Janvier labs (Le Genest-Saint-Isle, France). The animals were kept in animal stable for one week with food ad libitum with 12h light-darkness cycle. These conditions were followed strictly because peroxisomes alter by nutrition and external stimuli.

Maintenance and all experiments were conducted in accordance with the German guidelines for humane care and use of laboratory animals.

2.3.2 Brain preparation

Homogenisation buffer (HB) / 250mM sucrose solution	
MOPS / HEPES	5mM
EDTA	1mM
Ethanol	0.1%(v/v)
Aminocaproic acid	1mM
Benzamidinium-HCl	5mM
Sucrose	250mM
PMSF (added directly before use)	2mM
Solvent: distilled water.	

Table 7: Recipe Homogenisation buffer

For all isolation experiments, the mice were killed by cervical dislocation. Afterwards, the corpses were decapitated directly at the skull's base. In order to avoid contamination by fur, it was moistened with ethanol. Before the skull could be cracked, skin and tissue underneath were removed by two cuts from skull base towards the eyes. Skin and galea were then removed. With two cuts through the foramen magnum in latero-nasal direction, the cranium was opened with anatomical forceps. The brain was removed in total and transferred into buffered sucrose-solutions.

The concentration of these sucrose-solutions depended on the following processing steps. The molarity of these sucrose solutions was either 0.25M or 0.88M depending on the subsequent isolation protocol (*paragraph 2.3.3*). Hypoosmolar solutions were avoided, to prevent osmotic lysis of the tissue.

2.3.3 Homogenisation

Motor-driven Potter-Elvehjem Homogeniser	
Homgen plus	Schuett-biotec, Göttingen, Germany

Table 8: Homogenising device

The brains were mechanically homogenised by shearing with a motor-driven Potter-Elvehjem Homogeniser of type Homgen plus (Schuett-biotec, Göttingen, Germany). This mechanical homogenisation procedure was chosen because intact tissue can only be homogenised insufficiently using chemicals (Burden, 2008). Similar homogenisation devices had also been used in preceding peroxisome isolation procedures (Lazo et al., 1991; Singh et al., 1993). In each experiment, the extracted brains were homogenised in 250mM or 0.88 M homogenisation buffer (*paragraph 2.3.2*) for 2 minutes at about 4°C. The pistil was three times slowly moved up and down during this time. Homogenisation was performed at 600 rpm (*protocol 1*) or 900 rpm (*protocol 2 and 3*). The homogenisation speed in protocol 1 was applied to achieve accordance to the original protocol by Kovacs and colleagues (Kovacs et al., 2001)

2.3.4 Protocol 1: examination of the different physical properties of adult and young mice's brain peroxisomes

Centrifuges and rotors		
Rotina 420R centrifuge	Hettich Zentrifugen, Tuttlingen, Germany	Centrifugation 1-3
Sorvall RC6 plus centrifuge	Thermo Fisher Scientific, Waltham, USA	Centrifugation 4- 6
Sorvall WX Ultra 100 centrifuge	Thermo Fisher Scientific, Waltham, USA	Centrifugation 7, 8 and gradient centrifugation
Sorvall Surespin 360 swinging bucket ultracentrifuge rotor	Thermo Fisher Scientific, Waltham, USA	Centrifugation 7 and 8
Beckman VTI50 fixed angle rotor	Beckman Coulter, Brea, USA	Gradient centrifugation

Table 9: Centrifuges and rotors used in protocol 1

To compare the physical properties of adult and adolescent mice's brain peroxisomes, adult mice's brain peroxisomes were purified according to a purification procedure published to work with the brains of 0 to 25 day old mice (Kovacs et al., 2001).

As brain alters in composition with age this protocol was investigated with respect to whether it works with adult mice. The major change is the postnatal increase in myelin content, which is known to highly affect the fractionation of cellular organelles (Kovacs et al., 2001).

Protocol 1 (*figure 4*) involves a combination of differential and step gradient centrifugation in sucrose solution followed by Nycodenz density gradient centrifugation. The extracted brains were homogenised with 600 rpm. Large corpuscular components, such as nuclei and large cellular debris, of this homogenate were removed via the first centrifugation step at 1000 x g for 10 minutes at 4°C producing the Post-Nuclear Supernatant (**PNS**). To increase the yield in peroxisomes, the correspondent pellet was re-homogenised and centrifuged twice applying the same parameters. All supernatant from these centrifugation (1-3) steps were pooled with the initial **PNS**.

In two successive centrifugation steps of 5,500 x g, 10 minutes, large mitochondria were removed. The supernatant of these steps, which was used for further processing, is called the post-mitochondrial supernatant (**PMS**). The pellet contained the heavy mitochondrial fraction (**M**). **PMS** was subsequently centrifuged at 18,000 x g for 30 minutes (centrifugation 6). Organelles remaining in the supernatant (**SN**) were then pelleted by centrifugation with 106,400 x g for 60min with swinging bucket rotor (centrifugation 7). As a result of a high peroxisome content in both supernatant (**SN**) and pellet of this 7th centrifugation (**P**), the 6th centrifugation was henceforth performed with 37,000 x g - hereby diverging from the original protocol published by Kovacs et al (Kovacs et al., 2001). The centrifugation speed chosen derives from a protocol used for mitochondria removal in liver peroxisome purification (Islinger et al., 2012a). The pellet derived by centrifugation 6, **L1**, the light mitochondrial fraction, which is described to contain the majority of peroxisomes by Kovacs et al (Kovacs et al., 2001), and the pellet **P** of centrifugation 7 were then centrifuged on a sucrose step gradient (*figure 5*) for myelin removal (centrifugation 8).

Fraction **L2** was finally separated using a continuous Nycodenz-gradient ranging from pure gradient buffer (*paragraph 2.1.2*) to 40% Nycodenz, as published by Kovacs et al

(Kovacs et al., 2001). Centrifugation applied was 85 minutes at a force of 142.000g in a vertical-type VTi50 rotor (Beckman-Coulter) (Kovacs et al., 2001). As pure gradient buffer is hypoosmolar, an adapted continuous Nycodenz-gradient (10-40%) was used in a second trial.

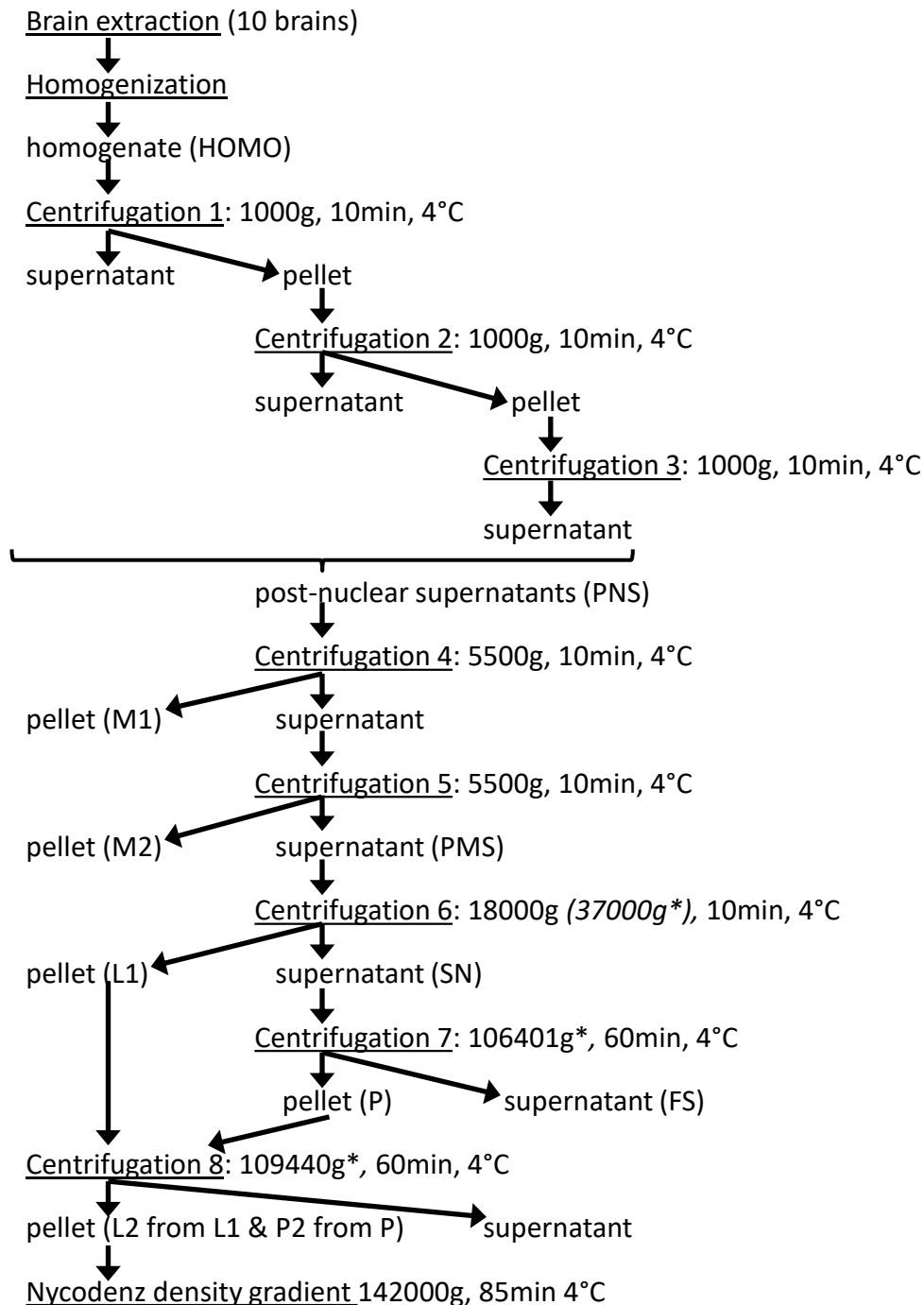


Figure 4: Protocol 1 adapted from Kovacs et al (Kovacs et al., 2001)

Homogenate was further processed via centrifugation 1-3 to the post nuclear supernatant (PNS). After this initial depletion of debris and nuclei, heavy mitochondria were removed (centrifugation 4 and 5) and subsequently light-peroxisomal fraction (L1) and peroxisomal fraction (P1) isolated (centrifugation 6 and 7). These fractions were then further processed (centrifugation 8) via a sucrose step gradient for myelin removal (I2 and P2). Deviations from the original protocol are marked with *. The differences in centrifugation 7 and 8 derive from the use of different centrifuges but identical rotors as in the original protocol.

2.3.5 Adaptations to protocol 1 aiming to improve peroxisome isolation capacity by differential and gradient centrifugation

In the preceding experiments the procedure developed by Kovacs et al (Kovacs et al., 2001) was tested for use in adult mice's brain. A sufficient purification was not achieved as differences in the starting material most probably impair purification process (*paragraph 3.2.1*). To overcome these difficulties the single steps of the purification procedure and their order were evaluated, then additional purification steps were introduced and tested. To improve the effect generated through the continuous gradient used by Kovacs et al. (Kovacs et al., 2001), experiment concerning gradient generating medium, gradient length and constitution were adapted.

As both differential and step gradients were tested, tests were performed according to two major protocol layouts. In the first protocol differential centrifugation was examined, in the second serial gradient centrifugation. Results were combined according to the issues they address. Homogenisation method remained unchanged as it proved to produce intact organelles (Kovacs et al., 2001). However, the re-homogenisation process described by Kovacs et al (Kovacs et al., 2001) was reassessed in a first step. A crucial step of the isolation procedure is the elimination of myelin using a sucrose gradient (Cimini et al., 1993; Kovacs et al., 2001), which was therefore incorporated in our protocol. To avoid that the hydrophobic myelin interacts with organelle membranes during in the pellets produced by differential centrifugation, this step was transferred to the beginning of the isolation procedure.

2.3.6 Investigating the use of multiple re-homogenisations

The sample for differential centrifugation in preparation in protocol 1 was derived by 3 cycles of homogenisation, centrifugation at 1,000 x g and resuspending the pellets with a glass pistil (centrifugation 1-3; *figure 4*). The sample (**PNS**) was derived by pooling the resulting supernatants (*figure 4*).

By comparing the derived supernatants the usefulness of this procedure in respect to the composition of the sample was assessed.

As tissue fractionation with motor-driven Potter-Elvehjem homogeniser produced intact peroxisomes in brain tissue derived samples (Kovacs et al., 2001), we used the identical method and forces in tissue fractionation (*paragraph 2.3.3*).

2.3.7 Myelin removal: positioning and myelin removal gradient

As the myelin highly affects the purification results (Kovacs et al., 2001), it has to be removed. The myelin removal gradient used in protocol 1 proofed its capability to reduce myelin content in the sample (*paragraph 3.2.1*). However, no complete myelin removal could be achieved.

To improve myelin removal procedure and test its limits, different positions and compositions of the myelin gradient were tested.

Myelin removal gradient consisted of a less dense sucrose layer, which was layered above the density adjusted sample. This basic layout was positioned above a 2M sucrose layer to avoid pelleting (*figure 5*). So far published myelin removal gradients consisted of 250mM or 320mM sucrose and a sample adjusted to the density among 800mM to 880mM sucrose (Cimini et al., 1993; Kovacs et al., 2001; Lazo et al., 1991; Posset et al., 2015; Singh et al., 1993).

The initial myelin removal gradient consisted of two layers of 320mM, and 250mM sucrose solution in gradient buffer, respectively. The fraction **PNS** was adjusted to the density of 850mM sucrose using a 2 M sucrose solution and placed at the bottom of the step gradient. The gradient was centrifuged for 90min at 106,000 x g (in protocol 1 and serial gradient centrifugation). Similar results were also achieved by centrifugation for 30 min at 75,000 x g in differential centrifugation protocol (*paragraph 2.3.8*).

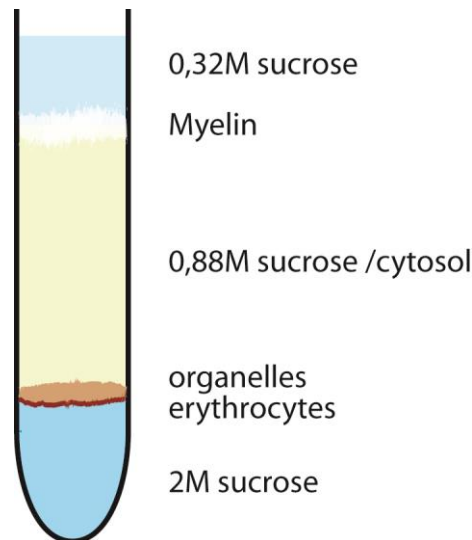


Figure 5: Myelin removal gradient and intended position of myelin, organelles and cytosol

Myelin was enriched as fluffy-white layer at the border of 320mM to 850mM sucrose solution. Myelin layer and supernatant above were discarded. When used without 2M sucrose cushion, the pellet was resuspended with the yellowish-brown layer below the fluffy myelin layer, otherwise it was mixed with the fraction bordering to the 2M sucrose and re-homogenised with it. Subsequently, it was adjusted to the density needed for the organelle separation gradient (OSG) (*paragraph 2.3.11*) or dissolved in 250mM sucrose for differential centrifugation (*paragraph 2.3.9*).

In order to simplify the isolation procedure, in protocol 3 step gradients for myelin removal and organelle separation (*paragraph 2.3.11.2*) were combined in a single gradient: For this purpose, gradients with 250mM, 320mM or 500mM sucrose solution as top layer and 850mM or 700mM sucrose as application site of the sample were tested. The derived myelin removal step among 320mM/500mM and 700mM sucrose solution in GP was incorporated in OSG. In further experiments, the capability of myelin removal gradient and OSG concerning demyelination and organelle separation was examined (*figure 30*).

In the majority of published isolation protocols for brain peroxisomes, myelin removal was performed after an initial mitochondria removal (Cimini et al., 1993; Kovacs et al., 2001; Posset et al., 2015; Singh et al., 1993) but its use as an initial centrifugation step was also described (Lazo et al., 1991). To prevent an aggregation of myelin with organelle membranes in a pellet, we assessed whether a myelin removal before or after differential centrifugation is advantageous. To assess gradient position we compared homogenate after debris removal (**PNS**) and mitochondria depleted samples (**PMS**) before and after myelin removal (**PNSZ** and **PMSZ** respectively) concerning myelin and organelle content.

2.3.8 Protocol 2: adaptations aiming to improve peroxisome isolation capacity by differential centrifugation

Differential centrifugation is used in multiple peroxisome isolation protocols from cells (*paragraph 2.2.3*) (Volkl and Fahimi, 1985) and organelles (Islinger et al., 2012a). As myelin removal is crucial for the isolation of peroxisomes (Cimini et al., 1993; Kovacs et al., 2001), a sucrose gradient for myelin removal is incorporated (Cimini et al., 1993). All differential centrifugation protocols followed a similar layout: After an initial gradient for myelin removal, the sample was fractionated by differential centrifugation. The peroxisome-enriched sample from the differential centrifugation procedure was further separated by a density gradient, for which different gradient media were tested and compared (*figure 6*).

2.3.9 Differential centrifugation protocol

Centrifuges and rotors		
Rotina 420R centrifuge	Hettich Zentrifugen, Tuttlingen, Germany	Centrifugation 2
Sorvall RC6 plus centrifuge	Thermo Fisher Scientific, Waltham, USA	Centrifugation 3
Sorvall WX Ultra 100 centrifuge	Thermo Fisher Scientific, Waltham, USA	Centrifugation 1, 4, 5 and gradient centrifugation
Sorvall Surespin 360 swinging bucket ultracentrifuge rotor	Thermo Fisher Scientific, Waltham, USA	Centrifugation 1, 4, 5 and gradient centrifugation

Table 10: Centrifuges and rotors used in protocol 2

After homogenisation in 0.88M sucrose solution (*paragraph 2.3.3*), myelin was instantaneously removed via an established 3-step gradient (*paragraph 2.3.7*) (Cimini et al., 1993; Kovacs et al., 2001; Singh et al., 1993). For this purpose, the homogenate (0.88 M sucrose) was layered between a 0.25M/0.32 M solution a 2M sucrose cushion (*recipe paragraph 2.1.2*). This 3-step gradient was centrifuged at 75,000 x g for 30 min (*figure 6*). After centrifugation, myelin accumulated at the boundary of the 0.88M and 0.32M/0.25M sucrose solution (*figure 5*). It formed a fluffy, white layer. This myelin layer and soluble cytosolic components were discarded, whereas the brownish “organelle fraction” concentrating at the border of 0.88M and 2M sucrose was removed, pelleted, and resuspended in 320mM sucrose for further purification. Remaining cell detritus was removed by centrifugation at 600xg, 10 min, 4°C. The resulting supernatant corresponded to fraction **A**. Subsequently “heavy mitochondrial” (**B**) and “light mitochondrial” pellets (**D**) containing the bulk of peroxisomes and synaptosomes were prepared in two successive centrifugation steps. “Heavy mitochondria” elimination was performed at 11.000 x g/12.000 x g for 15 min, fraction **D** (light mitochondria) was pelleted at 60.000 x g/70.000 x g for 30min. In a last differential centrifugation step, microsomes (**G**) remaining in fraction **E** (supernatant of **D**) were separated from cytosolic components (**F**) (*figure 6*). The pellets of each centrifugation step were carefully re-suspended in homogenisation buffer containing 250mM sucrose homogenised using a glass pestle. Both peroxisome bearing fractions (**D** and **G**) were used for further purification in density gradients. In western blot a direct comparison of protocol 1 and 2 was performed.

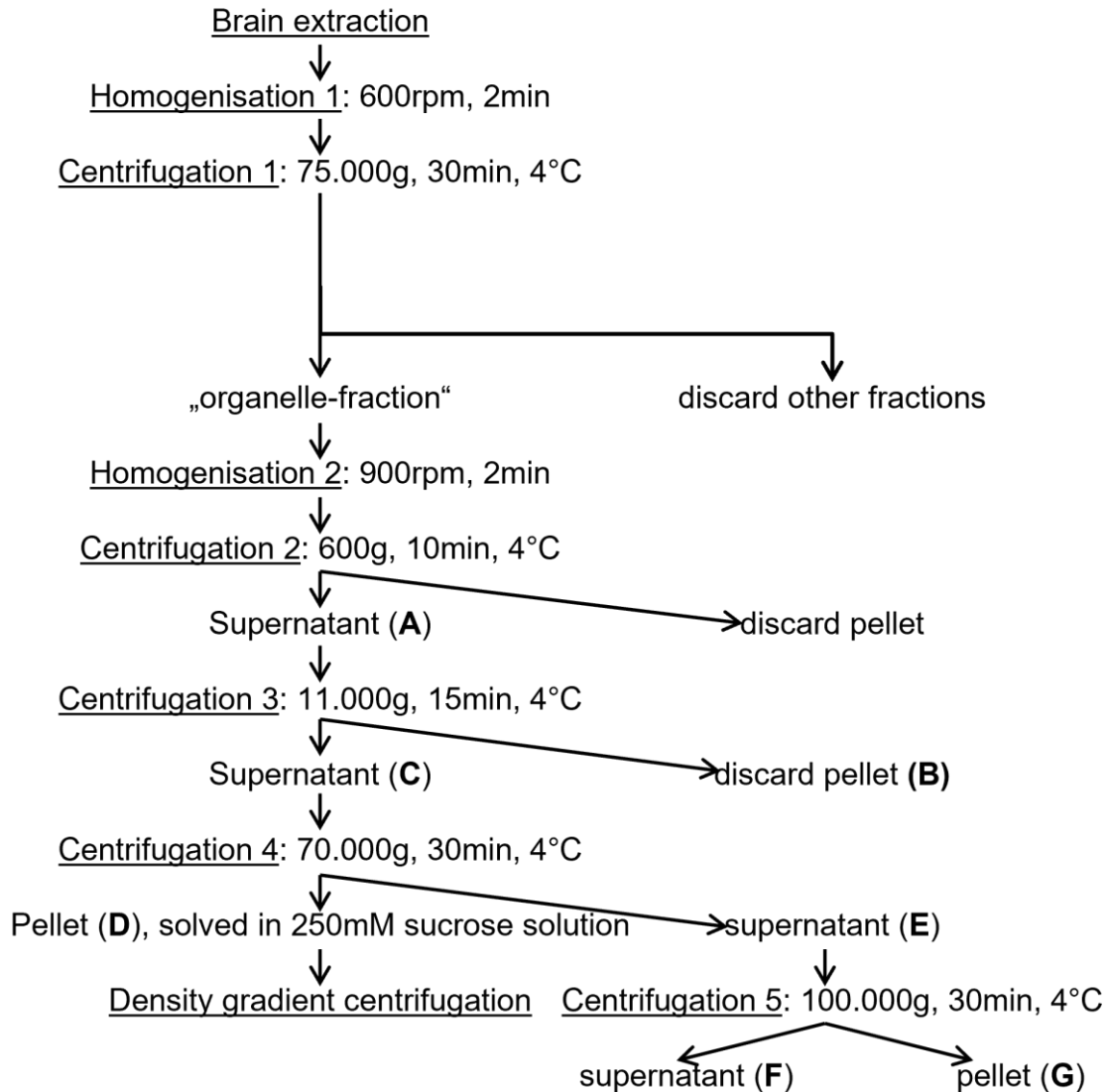


Figure 6: differential centrifugation protocol

After homogenisation, myelin was removed followed by removal of debris and mitochondria leading to a heavy peroxisomal fraction (D) and a light peroxisomal fraction (G).

2.3.10 Further purification via density gradient centrifugation using different gradient media

For optimisation of the purification protocol, additional purification steps with alternative gradient media were performed. Comparisons among gradient media were made using fraction D or fraction G as starting material. Considering the different molecular weight of the gradient media and differences in separation capability, gradients with Nycodenz (iohexol), Optiprep (iodixanol) or sucrose were tested. These three reagents were chosen since they were used in pre-existing peroxisome isolation protocols (Kovacs et al., 2001; Lazo et al., 1991; Posset et al., 2015; Schrader et al., 1994; Singh et al., 1993).

Sucrose (342.2965 Da) was thought to rapidly penetrate cellular organelles due to its comparatively low molecular weight and high osmotic pressure thus increasing the density of organelles. By contrast, Optiprep (1550.191 Da) was due to its comparatively

large particle size considered to accumulate to a lesser degree in organelles. Optiprep has been successfully used in purification of liver peroxisomes from light mitochondria (Islinger et al., 2012a). Nycodenz (821.1 Da) has been successfully used for the purification of brain peroxisomes from young mice (Kovacs et al., 2001) and is postulated to be partially capable of entering peroxisomes through their membrane pores.

For each gradient medium, separation was tested on a continuous density gradient ranging from 1.04 g/ml to 1.15 g/ml for iodixanol, 1.04 g/ml to 1.18 g/ml for sucrose and 1.04 g/ml to 1.14 g/ml for Nycodenz (table 11). Centrifugation time and force were kept constant with 50,000 x g and 150 min respectively. For all these centrifugations a swing-out rotor was used (table 10).

Gradient material	Gradient range
Sucrose	1.04g/ml – 1.18g/ml
Nycodenz	1.04g/ml – 1.14g/ml
Optiprep	1.04g/ml – 1.15g/ml

Table 11: Tested continuous gradients to determine the enrichment of organelles separated by rate zonal sedimentation on continuous gradients of different media.

As step gradients are faster to produce exhibit higher reproducibility and are able to concentrate individual fractions at density boundaries, the continuous sucrose gradient was transferred into a step-gradient: According to separation capability and the observed densities at which organelles accumulated, a sucrose step gradient was created with 2M sucrose preventing attachment of organelles at the ground, a layer of 1,137 g/ml and another of 1,08 g/ml sucrose solutions, adjusted via refractometry, and the sample dissolved in 250mM sucrose on top. Consecutive centrifugations were abbreviated to 40 min.

The consecutive step gradient centrifugations (paragraph 2.3.11) were based on the hereby derived findings. Further experiments on continuous and step gradients were performed after pre-processing with sequential gradient centrifugation.

2.3.11 Protocol 3: Addressing brain peroxisome purification by serial gradient centrifugation

Centrifuges and rotors		
Rotina 420R centrifuge	Hettich Zentrifugen, Tuttlingen, Germany	Centrifugation 1 and 2
Sorvall WX Ultra 100 centrifuge	Thermo Fisher Scientific, Waltham, USA	Centrifugation 3, 4 and gradient centrifugation
Sorvall Surespin 360 swinging bucket ultracentrifuge rotor	Thermo Fisher Scientific, Waltham, USA	Centrifugation 3 and 4
Beckman VTI50 fixed angle rotor	Beckman Coulter, Brea, USA	Gradient centrifugation

Table 12: Centrifuges and rotors used in protocol 3

In the preceding protocols, most organelle separation steps were carried out by differential centrifugation using density gradients only for myelin removal and in the final continuous separation gradient. Examining the results more in detail and taking the amount of protein as measure of organelle count in each step into account, however, most organelles were separated from peroxisomes in the gradient

centrifugation steps. Hence this protocol, focussing on 3 sequential gradient centrifugations, was developed.

To exploit the advantages of both gradient medias, Nycodenz and sucrose, gradients in both media were used in sequence. For the sake of reproducibility and stability of the results, step gradients were used, and continuous gradients were transferred to step gradients whenever possible.

Sucrose solutions were used as primary gradient and homogenisation media because they are easily to produce and feasible for the prevention of osmotic damage in the subsequent analyses. The density of the layers of interest was determined in the experiments concerning gradient media (*paragraph 2.3.10 and 3.2.6*).

2.3.11.1 Protocol layout

The developed protocol consisted of the homogenisation step, two subsequent sucrose step gradients and a final Nycodenz gradient (*figure 7*):

After brain extraction and homogenisation as described in *paragraph 2.3.2 and 2.3.3*, cellular debris was removed from the homogenate. For this purpose, it was centrifuged twice (centrifugation 1 and 2 *figure 7*), first with 1.000 x g, then with 600 x g for 10 minutes each.

The resulting **post-nuclear supernatant (PNS)** was subsequently purified from myelin in the first sucrose step gradient, the **myelin removal gradient**, which was described in *paragraph 2.3.7*. This gradient was centrifuged 90min at 106.000 x g. After the centrifugation, the fluffy myelin layer at the border between the two upper layers of the gradient (0,32M /0,8M) and the supernatant in the upmost layer were removed. The remaining layer (850 mM) below the myelin and the pellet were merged and re-suspended using a glass pistil for further separation on the **organelle separation gradient (OSG)** (*figure 8*). In subsequent experiments the **myelin removal gradient** was complemented by additional sucrose layers extending the gradient to remove further heavy particles (details on the densities added *figure 8*). This in fact resulted in two subsequent **organelle separation gradients (OSGs)**.

The **organelle separation gradient (OSG)** was designed according to the densities at which the organelles peaked in the continuous sucrose gradients (*paragraph 3.2.6.2*). As border effects occur in step gradients which might affect substrate behaviour on the gradient, several different organelle separation gradient constitutions and centrifugation times were tested (*paragraph 2.3.11.2*). Centrifugal force was kept constant with 100,000 x g. After centrifugation, the peroxisome-rich fraction was concentrated by pelleting. This fraction was then resuspended in Nycodenz in gradient buffer and put on a continuous or step gradient made of Nycodenz (*paragraph 2.3.11.3*).

In a final centrifugation, proteins of all derived fractions were pelleted with 100.000 x g for 20min and resolved in homogenisation buffer.

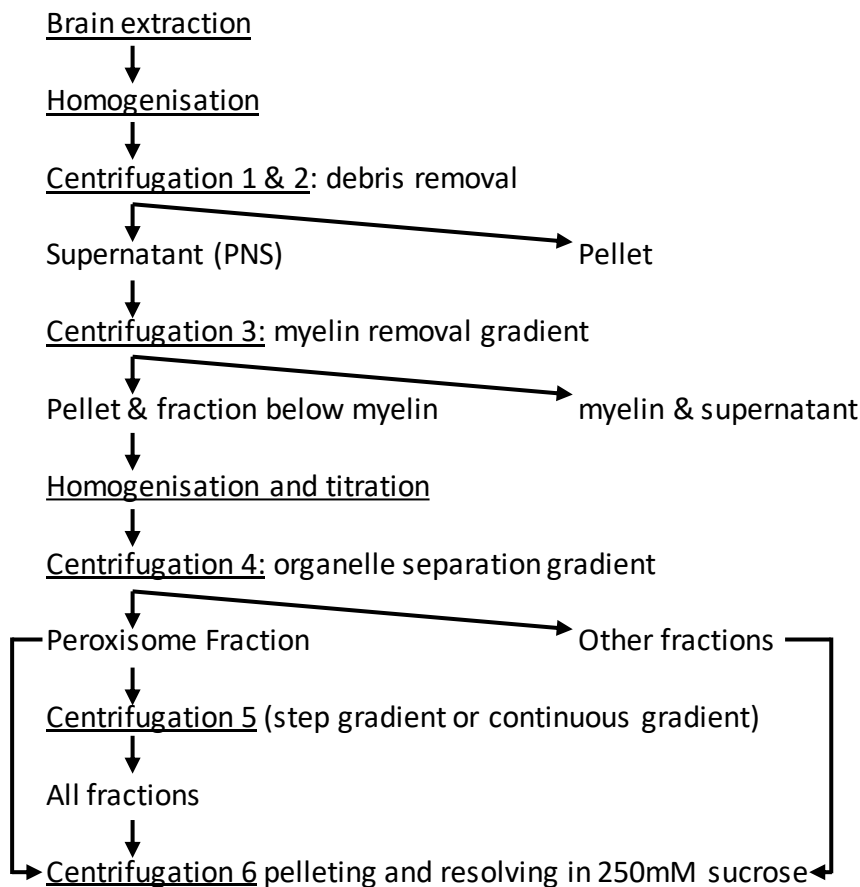


Figure 7: Layout of protocol 3

Using protocol 3 a serial sucrose step gradient centrifugation followed by a Nycodenz gradient centrifugation was tested. The different tested organelle separation gradients (OSG) are highlighted in figure 7.

2.3.11.2 Organelle separation gradient (OSG)

For further separation of organelles after myelin removal, as introduced in protocol 2 (paragraph 2.3.7 and 2.3.9), an organelle separation gradient consisting of several sucrose layers was introduced. Various compositions with different application sites and separation layers as depicted in figure 8 were tested.

Centrifugal force (107,960 x g) and centrifugation time (90 min) were kept constant. Gradients were step by step compared to find a final gradient with best organelle separation and the densities at which the organelles equilibrated. For this purpose, the gradients were harvested band-wise, and all bands were compared by western blot. The collection site, defined by maximum peroxisome concentration was used in the following gradient centrifugation.

Directly on top of the 2M sucrose cushion an organelle-enriched layer was located containing the majority of protein applied on the gradient. As peroxisomes were also present, this layer was further separated on a sucrose step gradient (figure 9) to analyse if this fraction contained peroxisome populations which could be isolated by subsequent density gradient centrifugation.

As the fractions neighbouring the peroxisome-enriched fraction had a high protein content, a repetition of OSG using the peroxisome enriched fraction of the first OSG instead of PNS was tested to reduce contamination of the peroxisome fraction (*paragraph 2.3.11.4*).

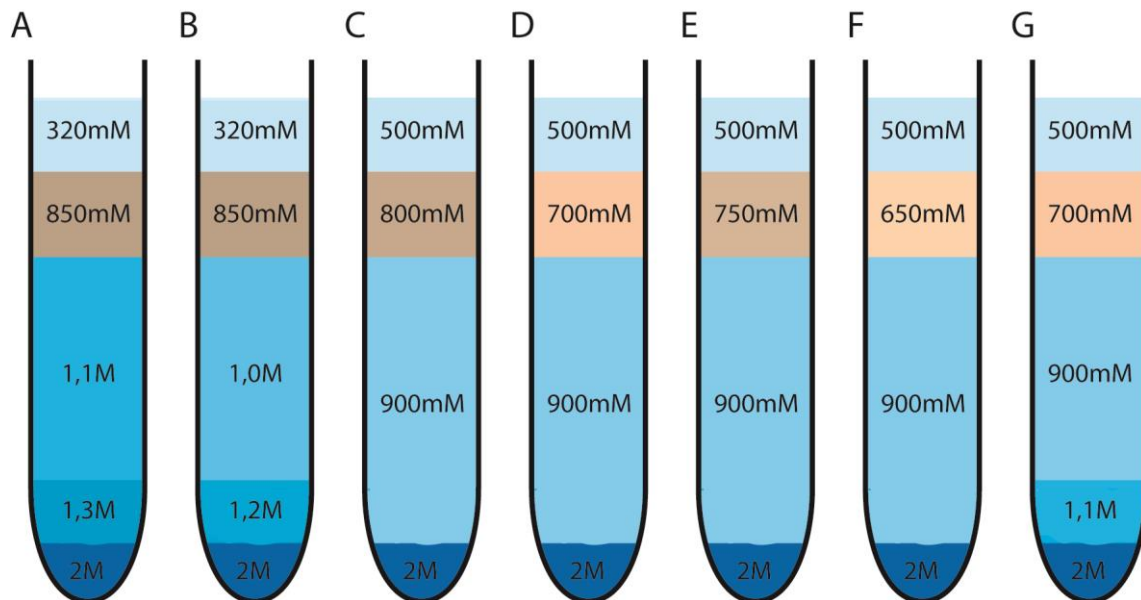


Figure 8: Different tested organelle separation gradients

The sample application site is highlighted in brown, after centrifugation (107,960 x g ; 90min) gradients were harvested band-wise. Organelle distributions are shown in figure 27)

2.3.11.3 Separation of the bottom fraction of gradient for further peroxisomal subpopulations

The bottom fractions of separation shown in figure 28 (*paragraph 3.2.7.2*) contained the vast majority of proteins of the separation. Absolute protein content was about 10 times higher than in the peroxisome-enriched fraction 4 (*figure 28*). Sample constitution differed: Mitochondria were enriched compared to fraction 4, ER signal at similar levels and PEX14 and synaptophysin signal lower than in fraction 4. As the amount of proteins was by far higher than in the other fractions, and as - deviating from PEX14 signal – ACOX1 was enriched in this fraction, a split up of this fraction might reveal further peroxisomal fractions.



Figure 9: Gradient for further separation of the bottom fraction of the organelle separation gradient. Application site was 700 mM sucrose. Sample was thinned to reach this concentration.

The fractions were split up on a gradient consisting of 0.7M, 0.9M, 1.1M, 1.2M, 1.3M, 1.4M and 2M sucrose with application at 0.7M sucrose (*figure 9*). The gradient was harvested band-wise.

2.3.11.4 Combination of 2 organelle separation gradients

To further improve separation on sucrose gradients, the use of a second sucrose gradient was examined. Following the hypothesis that a repetition of the OSG might further deplete the sample of interest from contaminants, OSG from *paragraph* 2.3.11.2 was repeated (*figure 10, A*). In a second step it was complemented by further steps of 0.95M, 1.0M, 1.1M and 1.2M sucrose (*figure 10 B*). Finally, **Gradient G** followed by the same gradient with additional 950mM sucrose layer appeared most promising tested (*figure 10, C*). To shorten the protocol, myelin removal was performed on the OSG when 2 OSG were used.

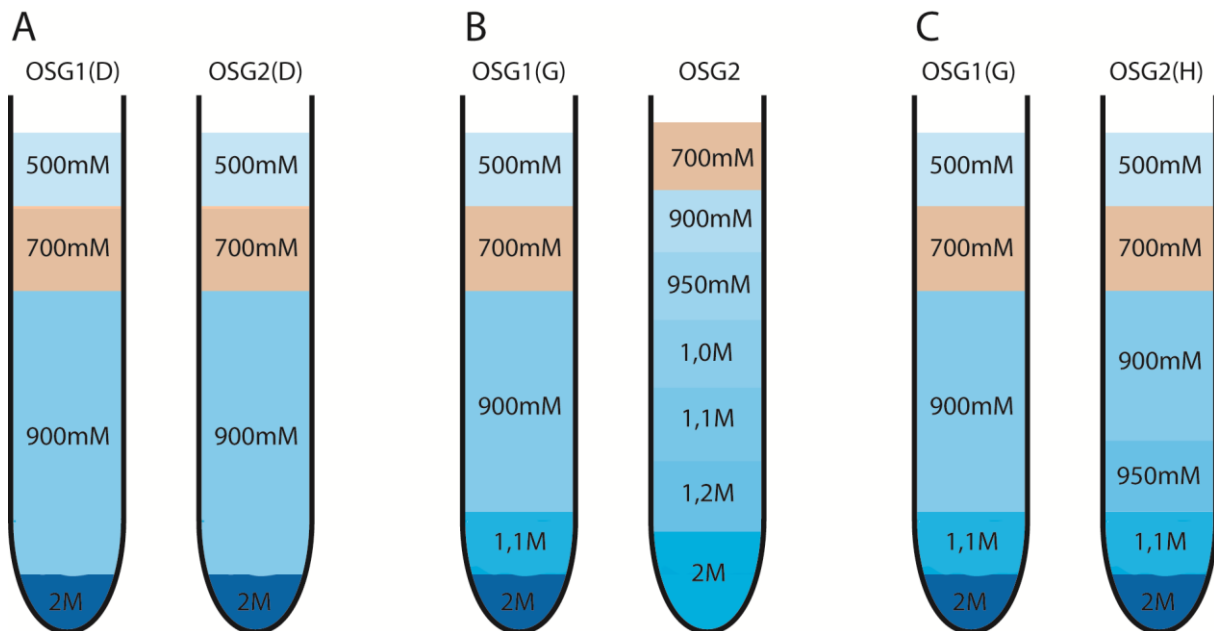


Figure 10: Combinations of 2 subsequent organelle separation gradients

Starting with the repetition of **Gradient D** (A) to achieve further purification of the peroxisome enriched fraction, the separation width was extended towards denser fractions in the second gradient (B) and finally **Gradient G** followed by the same gradient with additional 950mM sucrose layer (C).

2.3.12 Final separation via Nycodenz gradients

With the final Nycodenz gradient, an additional gradient medium was introduced, aiming at better separation from synaptosomes and ER, which had been demonstrated in *paragraph* 3.2.6. All gradients were centrifuged with 142.000 x g in a VTi50 vertical rotor. Acceleration and deceleration speed was set to the lowest value possible.

2.3.12.1 Continuous Nycodenz gradient

Starting from 10-40% (1.052-1.212 g/ml) in protocol 1, gradient range was adapted step by step, according to results of previous experiments to achieve an optimum range with maximum separation length at the band of interest (*figure 25*). Finally gradient range was narrowed to 1.09-1.14 g/ml (*figure 11 A*). To avoid attachment of the sample to the bottom of the gradient at the wall of the tube, a cushion of 40% Nycodenz in gradient buffer was added below lighter gradients. To prevent osmolysis and to shorten migration distance and hence stress level for peroxisomes, sample was applied at the bottom of the gradient. The resulting gradients were harvested ml-wise, density and protein content of the fraction were measured and their organelle content was determined via western blot.

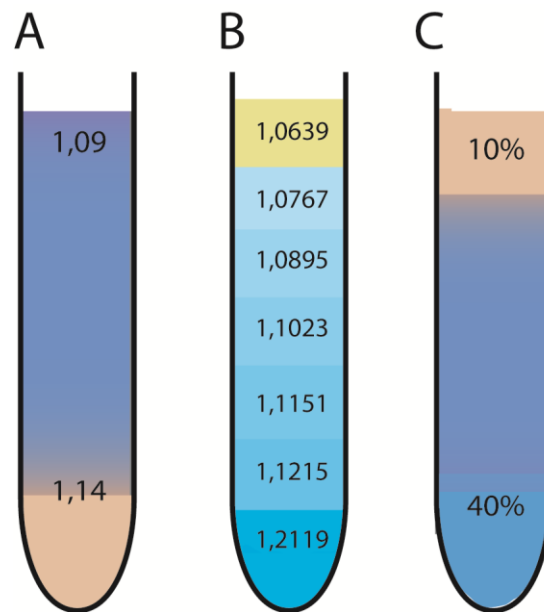


Figure 11: Highlighted nycodenz gradients: Composition of continuous Nycodenz gradient (**A**), Nycodenz step gradient (**B**) and gradient used for testing for peroxisomal “ghosts” (**C**). Application site in (**C**) is hypoosmolar.

2.3.12.2 Nycodenz-step gradient

As demonstrated for sucrose gradients, the introduction of steps positively affects the reproducibility and organelle distribution within the gradient. Steps were chosen according to the densities at which the organelles had enriched in the preceding continuous gradients. As large steps next to the application site prevented organelle penetration into the gradient, small steps of approximately 0.1-0.2g/ml difference were chosen (*figure 11 B*).

Nycodenz step gradient ranged from 1.09g/ml to 1.21g/ml with application from the top of the gradient. As pure Nycodenz would be hypoosmolar, sample was applied in sucrose (250mM) enriched medium. Steps were derived from the densities at which the organelles enriched on continuous gradients (*figure 33*).

2.3.12.3 Testing for peroxisomal “ghosts”

Empty and resealed peroxisomal membranes are referred to as peroxisomal “ghosts”. These “ghosts” might either derive from osmotic damage to the peroxisomes or from spontaneous release of peroxisomal core enzymes (Antonikov et al., 2004a). To differ osmotically damaged peroxisomes from those spontaneously releasing core enzymes and truly ACOX1 and catalase-free peroxisomes, which have been described in immunofluorescence studies (Ahlemeyer et al., 2007), we exposed our pre-purified peroxisomes to osmotic stress:

We applied the sample in a hypoosmolar 10% Nycodenz solution without added sucrose on a continuous Nycodenz gradient and compared the hereby derived fractions to our other purifications (*figure 11 C*).

2.4 Methods for post separation analysis

2.4.1 Bradford protein assay

Protein concentrations are measured via Bradford protein-assay (Bradford, 1976). The test principle is a protein-linkage-induced colour change of Coomassie Brilliant blue from red (absorption maximum 470 nm) to blue (absorption maximum 595 nm).

The samples are diluted with distilled electrolyte-free water until they were within the range of a bovine serum albumin protein linear standard curve ranging from 100 µg/ml to 5 µg/ml. The attenuation is performed in pure water in order to avoid tampered measurements by photometrically active chemicals (Bradford, 1976).

The assay is performed within 96 well plates, on which each sample is applied as triplicate. 5:1 diluted RotiNanoquant serves as detection reagent. Each sample is loaded onto the plate in three replicates. The plate is photometrically measured at 595 nm and 450 nm with 5 flashers per well. Absorption measurement is performed on both wavelengths with a scatter of 9 nm each. After measurement, each triplicate is examined for consistency. The quotient of the absorption at 595 nm and 450 nm is formed, the blank value subtracted and the triplicates averaged. The concentration is calculated using a serially diluted bovine serum albumin (BSA) protein standard from 5 – 100 µg/ml.

2.4.2 Immunoblotting

To examine the organelle distributions in the different fractionation experiments, immunoblots are performed.

2.4.2.1 Preparation of SDS-PAGE gels

Before assembly of the respective gel cassette glass plates were cleaned with ethanol. Subsequently gels with a polyacrylamide concentration of 10% in the separating and 4 % in the stacking gel were cast:

Per 10ml of separation gel 3,1ml of 30% polyacrylamide, are diluted with 4,1ml distilled water and buffered with 2,6ml of 1,5-molar Tris-HCl, pH 8.8. 100 µl of 10% SDS solution are added as denaturing agent. Just before filling the solution inside the gel cassette, 100 µl of a 10% ammonium persulfate solution, a source of free radicals acting as an initiator for gel formation, and 4 µl of TEMED, which stabilizes free radicals and improves polymerization, are added. By stacking a layer of isopropanol on top of the separation gel a flat boundary surface is produced. The isopropanol is removed by washing carefully with distilled water gel polymerization.

The stacking gel is poured on top of the separation gel. It consists of 6.94 ml of 30% polyacrylamide solution, 1.61 ml distilled water, 1.24 ml 0,5molar Tris-hydrochloride buffer, pH 6.8, 100 µl 10% SDS and APS solution each and 10 µl TEMED per 10ml.

2.4.2.2 Sample preparation for Western blot

According to the protein concentrations of each sample determined by the Bradford protein assay, each sample is diluted to an equal protein concentration. As the cellular constituents were separated into different organelle fractions, a loading control for a homogeneously distributed housekeeping protein cannot be applied and comparability depends on protein content. Sample is diluted in TVBE buffer, the denaturation reagent is fivefold concentrated LAEMMLI buffer. The samples are denatured at 95°C for 5 minutes and cooled successively. To track the run of the protein samples, the tracking dye bromophenol blue is used, which runs ahead of most proteins.

As protein standard Thermo Scientific Page Ruler Pre-Stained protein ladder and Page Ruler Pre-Stained protein ladder plus are used. Equal amounts of protein are added to all lanes. Empty wells are filled with LAEMMLI sample buffer.

TVBE buffer	
Substance	Concentration
NaHCO ₃	21mg
EDTA	93,06mg
Ethanol	250µl
2%Triton	1250µl
Distilled water	248,5ml

Table 13: Recipe TVBE buffer

Laemmli-buffer (5x concentrated)	
Substance	Concentration
10%(w/v) SDS	40ml
0.5M Tris	20ml
Mercaptoethanol	10ml
Glycerol	20ml
Bromphenol blue	2.2mg
Distilled water	ad 100ml

Table 14: Recipe Laemmli buffer

2.4.2.3 Electrophoresis

For the SDS-PAGE, a single running buffer is used. Gels are run at constant 110V for approximately 90 minutes until the tracking dye Bromphenol Blue reached the end of the separating gel.

Running buffer	
Substance	Concentration
Tris	25mM
Glycin	192mM
SDS	0.1%(w/v)
Solvent:	Distilled water

Table 15: Recipe Running buffer

2.4.2.4 Western blotting

For further analysis, proteins separated in the SDS-PAGE are transferred to a Polyvinylidene fluoride (PVDF)-membrane (Whatman) by Western blotting via the semidry-blotting procedure according to Towbin (Towbin et al., 1979). After electrophoresis, gels are removed from the separation chamber and placed on the methanol-capacitated Polyvinylidene fluoride (PVDF) membrane. Three blotting-buffer-soaked 0,85 mm Whatman filter papers were added on each side and the stacks were put on the blotting machine with the membrane-side heading to the anode (Towbin et al., 1979)

Per membrane (4.5 x 6cm), a current of 45mA is applied. Voltage is limited to 5V and power to 30W (Towbin et al., 1979).

Blotting buffer	
Substance	Concentration
Tris	3g
Glycin	14.4g
methanol	200ml
Distilled water	ad 1l

Table 16: Recipe blotting buffer

2.4.3 Immunodetection

After blotting, the membranes are blocked by incubation in 5% fat free milk powder in PBST for 60 minutes.

Organelle specific proteins are detected by antibodies to investigate the distribution of peroxisomes, mitochondria, endoplasmic reticulum, synaptosomes and myelin throughout the fractions. Identity, concentration, and origin of the marker antibodies are described below. All antibodies are diluted in PBST containing 1%FCS. For detection, a system of antigen specific primary antibodies and species-specific horseradish-peroxidase coupled secondary antibodies, which bind the species-specific Fc-fragments of primary antibodies, is applied. Primary antibodies are incubated for 90 minutes at room temperature or overnight at 4°C, secondary antibodies for 60 minutes at room temperature. Before addition and after removal of each antibody, the blots are washed 3 times in PBST for 10 min.

Phosphate buffered saline + Tween 20	
di-Sodium hydrogen phosphate dihydrate	1,78g
Potassium dihydrogen phosphate	0,2g
NaCl	8g
KCl	0,2g
Tween 20	1ml
Distilled water	ad 1l

Table17: Recipe PBST

2.4.3.1 Peroxisomal marker

Target	Full name	concentration	animal	source
PEX 14	Peroxisomal biogenesis factor 14 (protein-import to peroxisomes)	1:20.000	rabbit	D. Crane, Griffith University, Australia
PMP 22	22-kDa peroxisomal membrane protein	1:1.000	rabbit	A. Völkl, Heidelberg University, Germany
PMP70	70kDa peroxisomal membrane protein	1:500	rabbit	A. Völkl, Heidelberg University, Germany
Catalase		10µg/ml	rabbit	A. Völkl, Heidelberg University, Germany
ACOX 1	acyl-coenzyme A oxidase 1 (first enzyme of peroxisomal fatty acid beta-oxidation pathway)	1:10.000	rabbit	T. Hashimoto, Shinshu University Japan
ACAD-11 (B12)	acyl-coenzyme A dehydrogenase family member 11	1:1000	mouse	santa cruz biotechnology inc. (sc-514027)
ACBD5	Acyl-CoA Binding Domain containing protein 5	1:1000	rabbit	Sigma Aldrich (HPA012145)

Table 18: Peroxisomal markers

2.4.3.2 Mitochondrial marker

Target	Description	concentration	animal	source
ATP-Synthase	complex 5 of electron transport chain	1:20.000	mouse	BD Transduction Laboratories (#612516)
TOM 20	Mitochondrial Translocase of the Outer Membrane import receptor subunit TOM20	1:5.000	mouse	BD Transduction Laboratories (#612278)
COX 4	Cytochrome-c-oxidase	1:2.000	mouse	Abcam (ab33985)
VDAC1/porin	Voltage-dependent anion selective channel 1 in outer mitochondrial membrane	1µg/ml	rabbit	Abcam (ab15895)

Table 19: Mitochondrial markers

2.4.3.3 ER marker

Target	description	concentration	animal	source
ERp29	Endoplasmic reticulum protein 29	1:5.000	rabbit	Abcam (ab11420-50)
GRP78	Binding immunoglobulin protein also known as 78 kDa glucose-regulated protein	1:10.000	mouse	BD Transduction Laboratories (#610978)
PDI	Protein-disulfide-isomerase	1:500	mouse	Abcam (ab2792)

Table 20: ER markers

2.4.3.4 Synaptosomal marker

Target	description	concentration	animal	source
Synapto-physin	Synaptophysin	1:20.000	mouse	Synaptic Systems (101 011)

Table 21: Synaptosomal markers

2.4.3.5 Myelin marker

Target	description	concentration	animal	source
MBP	Myelin basic protein	1:1.000	rat	Abcam (ab7349)

Table 22: Myelin markers

2.4.3.6 Transfected protein

Target	description	concentration	animal	source
GFP	Green fluorescent protein	1:500	mouse	Sigma Aldrich (MAB3580)
c-Myc	MYC proto-oncogene	1:500	mouse	santa cruz biotechnology inc. (sc-40)

Table 23: Transfected protein markers

2.4.3.7 Secondary antibodies

Target	description	concentration	animal	source
mouse-IgG (Fc-fragment)	Secondary antibody bound to horseradish-peroxidase for imaging	1:5.000	goat	Thermo Fisher
rabbit-IgG (Fc-fragment)	Secondary antibody bound to horseradish-peroxidase for imaging	1:5.000	goat	Thermo Fisher
rat-IgG (Fc-fragment)	Secondary antibody bound to horseradish-peroxidase for imaging	1:5.000	goat	Thermo Fisher

Table 24: Secondary antibodies

2.4.4 Image acquisition

For signal detection, the blot membranes are incubated in two-component detection reagent for 1 minute and placed between two transparent films.

Images of the western blots are acquired with the **Fusion Solo 4M VILBER LOURMAT** acquisition system from **Peqlab (Erlangen, Germany)**, which is operated by the Fusion software from the same provider. Through a pre-exposition, the optimal acquisition time for an area of the image or the whole image is calculated, to grant a maximum image dynamic. Resolution of each image is chosen as high as possible within reasonable time. Maximum acquisition time for each blot is limited by the duration of constant decay of the western blot detection reagent.

All images are taken without gamma correction. The processing of the taken images is surveyed by the “good laboratory practice” tool incorporated in the software, which saves each processing step in the meta-data of the respective image.

Special care is employed to avoid over-saturated signals in images for semi-quantitative analysis. In order to investigate huge concentration differences among samples, oversaturated images are taken if they could not be avoided.

Alternatively, images on radiographic film are taken in the darkroom with estimated fixed exposure times. The film is successively developed and digitalized.

2.4.5 Semi-quantitative analysis of western blot results

In addition to visual analysis of the western blot images taken with **Fusion Solo 4M VILBER LOURMAT (Peqlab, Germany)**, a semi-quantitative analysis is performed with the quantification tool incorporated in the Fusion software. The volume of the single bands per lane is calculated after linear background signal removal. The relative depletion or enrichment of a marker protein is calculated with respect to the homogenate, by calculating the quotient of the respective fraction and the homogenate. The distribution of the relative marker signal in the gradients is then compared to the other marker signals to visualize the organelle distribution throughout the fractions. A real quantification cannot be performed due to lack of respective protein standards.

3 RESULTS

3.1 Peroxisome isolation from cultured cells

Due to the limited capacity of density-gradient, the organelle or organelles of interest had to be pre-purified to a certain degree. After this pre-purification organelles were separated on a continuous density gradient.

3.1.1 Differential centrifugation for pre-purification

After harvesting, the cells were homogenised by frictional force pulling the cell suspension 7x up and down a syringe equipped with a needle.

Remaining large particles and debris and nuclei were removed by centrifugation at 600 g yielding **P1** and the post-nuclear supernatant (**S1**). In the pellet (**P1**) more mitochondria and ER were contained than in the supernatant (**S1**) revealing that cell lysis is still incomplete. Catalase-positive peroxisomes were present at similar levels in both fractions. By this step peroxisomes and the other organelles were hardly affected. The resulting supernatant (**S1**) was re-homogenised by friction to shred the particles even further and set the organelles free (figure 12).

In the subsequent centrifugation, heavy mitochondria, which are the majority of mitochondria, were pelleted (**P1**). Compared to supernatant (**S1**), peroxisomes were enriched in **S2**, while mitochondria and ER were depleted. In the resulting pellet (**P3**), peroxisomes were clearly enriched. ER and mitochondria were enriched compared to **S1**, too. Their enrichment however was relatively lower than that of peroxisomes. According to the significant enrichment of peroxisomes in **P3**, this fraction was chosen for a subsequent purification on a density gradient. In the supernatant (**S3**) and the 100.000xg pellet (**P4**) remained no mitochondria, little peroxisomes and some ER. Note that the mild conditions used for homogenisation led to a low ER content in the microsomal pellet (**P4**), where vesicles derived from a fractionated ER were usually the dominating organelles (figure 12).

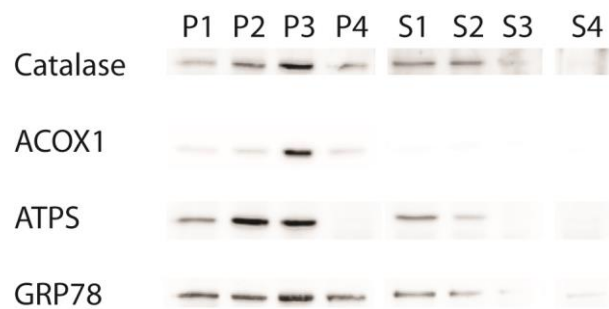


Figure 12: Analysis of differential centrifugation for pre-purification. Pellets (**P**) and Supernatants (**S**) were derived by centrifugation 2-4 and 6 (figure 4). Peroxisomes (ACOX1, Catalase) were enriched in **P3** together with ER (GRP78), part of mitochondria was depleted in centrifugation 3 resulting in **P2**.

3.1.2 Organelle distribution on Nycodenz and Optiprep density gradients

As the protocol is intended compare the buoyant densities of distinct organelles in response to the expression of peroxisome- and ER-bound proteins (VAPB and ACBD5), the final centrifugation has to be a density gradient centrifugation. For this purpose, starting with a broad gradient range, the gradient was successively narrowed to an optimum density range facilitating a maximum separation of individual organelles. As both, Nycodenz and Optiprep have been used in peroxisome purification from cultured cells, the two media were tested. As optimum gradient length for Optiprep 1.10 to 1.16 g/ml could be determined, for Nycodenz the gradient ranged from 1.14 to 1.19g/ml.

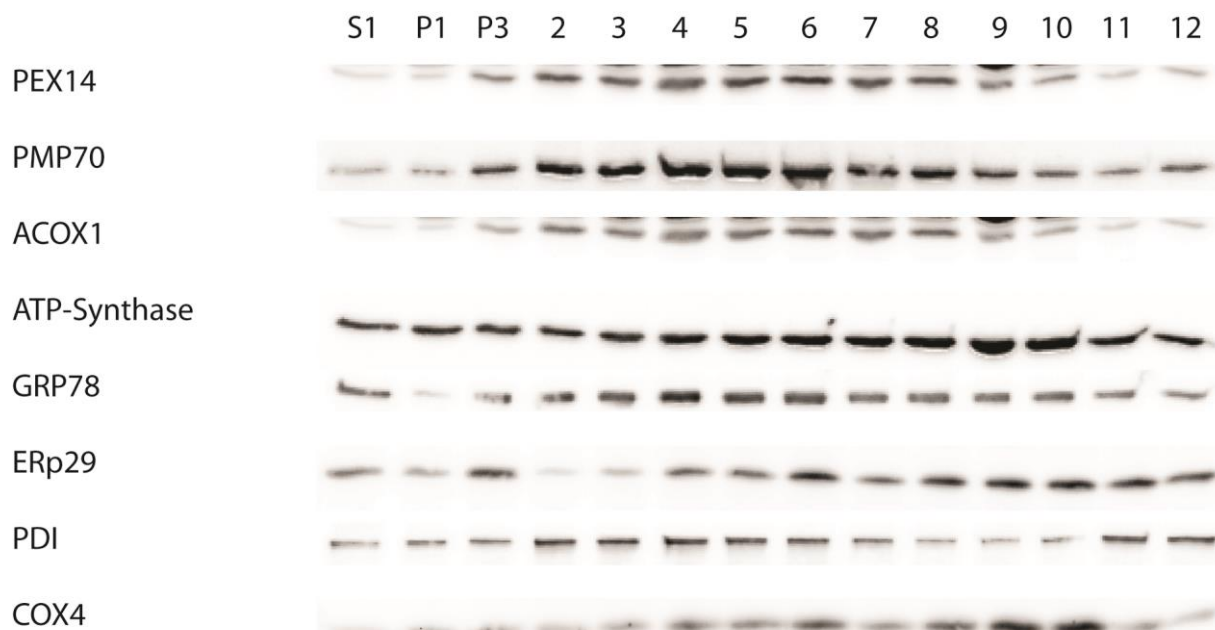


Figure 13: Optiprep gradient 1.10 - 1.16g/ml:

Peroxisomes peaked at 1.14 - 1.15g/ml, while ER signal was present throughout the gradient. While GRP78 and PDI were increased at 1.14 to 1.15g/ml, ERp29 peaked further towards the top of the gradient (1.08 - 1.11g/ml). Hence, even before protein overexpression an overlap of peroxisome (PEX14, PMP70, ACOX1) and ER (GRP78, ERp29, PDI) existed, which limited its application in peroxisome-ER-interactions studies. Concerning mitochondria (ATP-Synthase, COX4) an enrichment at 1.116g/ml could be observed.

In Optiprep gradient (figure 13), Peroxisomes were the densest organelles, they enriched with maximum at 1.126-1.14g/ml. ER signal exhibited differences among markers: GRP78 and PDI signal exhibited a similar distribution pattern. ERp29 (ER). Between the two patterns profound differences existed. While GRP78 and PDI were increased at 1.126 to 1.151g/ml, ERp29 peaked further towards the top of the gradient (1.08 to 1.11g/ml). Most likely, the different bimodal distribution of ER marker proteins in the gradient, points to an enrichment of distinct ER subpopulations at different positions of the gradient. Hereby, GRP78 and PDI-signal overlapped directly with peroxisomal signal at the same density. Mitochondria (ATP-Synthase and COX4) tended to accumulate at the lighter fractions of the gradient.

In un-transfected cells, peroxisomes marked by PEX14, PMP70 and ACOX1 mainly accumulated at the denser part of the Nycodenz gradient at 1.18 to 1.19g/ml (*figure 14*). They were clearly enriched compared to the peroxisome-enriched fraction **P3** and even more compared to the **PNS (S1)**. Mitochondria peaked at lighter densities. Their maximum concentration was at 1.165g/ml. At the main peroxisomal densities they exhibited a similar concentration as in **P3**.

ER markers GRP78 and PDI signal again exhibited a similar distribution pattern. Both were present throughout the gradient but clearly peaked at 1.165g/ml or in lighter fractions.

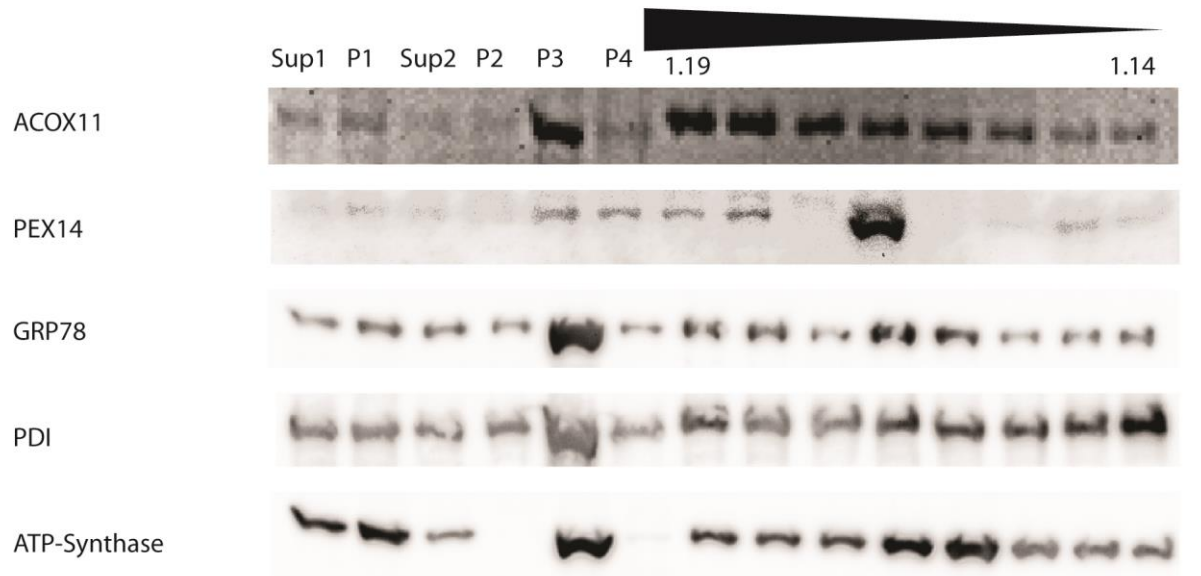


Figure 14: Organelle distribution on Nycodenz density gradient

While Peroxisomes (ACOX11 and PEX14) enriched predominantly at the densest fractions of the gradient (1.18-1.19 g/ml) in untransfected cells, ER (GRP78 and PDI) enriched around 1.65 g/ml but remained present throughout the gradient. Remaining Mitochondria peaked around 1.165g/ml as well.

With respect to the separation of the individual organelles in the distinct gradient media, the comparison of the distribution patterns of marker proteins shown in *figure 13* and *figure 14* showed that in the case of HepG2 cells, organelle separation in Nycodenz is more efficient than in Optiprep: Peroxisome- and ER-enriched fractions did not directly overlap in Nyodenz gradient.

3.1.3 Organelle shift due to ACBD5 and VAPB overexpression

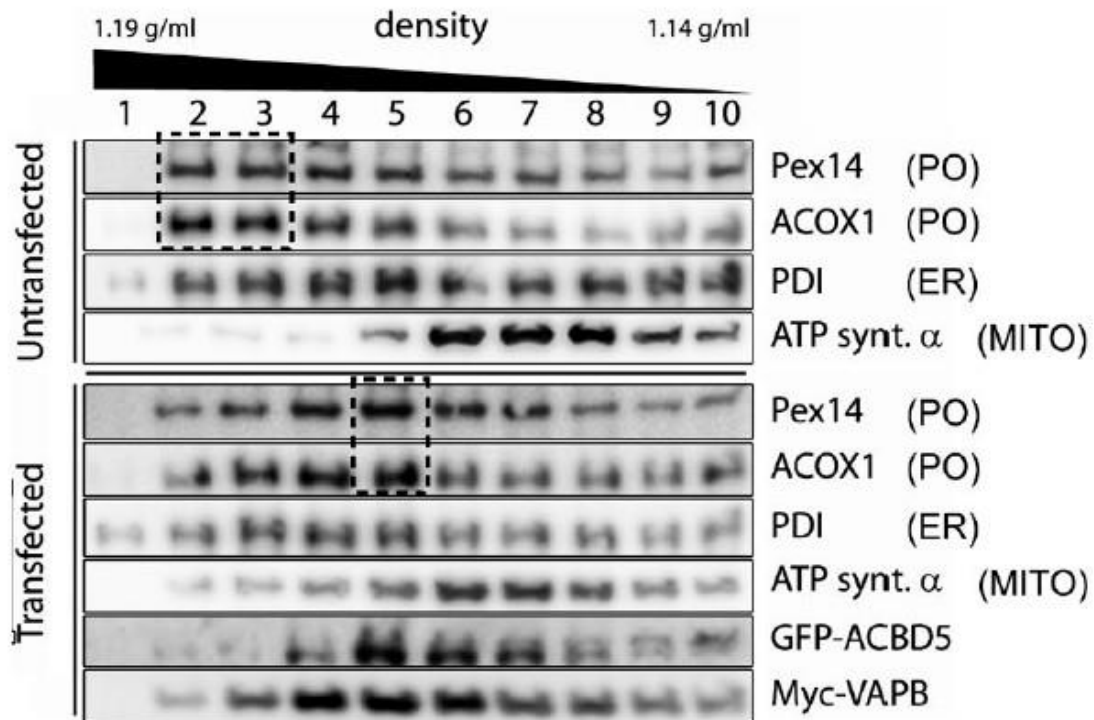


Figure 15: Transfection shift

When peroxisomes were transfected with GFP-ACBD5 and ER with Myc-VABP, peroxisomal signal (PEX14, ACOX1) was shifted towards lighter fractions around 1.65 g/ml from 1.18 g/ml. Hereby an overlap with ER maximum was formed. The transfected proteins Myc-VABP (ER) and GFP-ACBD5 (peroxisomes) peaked at the same densities.

As described above, peroxisomes from untreated HepG2 cells tended to enrich at the bottom of the Nycodenz gradient (*figure 14*). ER was slightly lighter and enriched in the fractions above peroxisomes. Mitochondria were less dense than both organelles and exhibited little overlap with ER and hardly any with peroxisomes. According to the results described above, Nycodenz gradients were applied for the organelle separation of transfected cells. Importantly, after expression of the peroxisomal tail-anchored membrane protein GFP-ACBD5, according to marker proteins peroxisome maximum was shifted to lighter fractions, largely to the same density as ER maximum (*figure 15*). Of note, the expressed proteins GFP-ACBD5 and Myc-VABP were both highly enriched in the respective fractions. The coincidence of the transfected proteins with the respective organelle markers indicates a correct targeting, which was corroborated by immunofluorescence microscopy (Costello et al. 2017). Mitochondria remained at the same densities, which means that they are un-affected by the expression experiments.

3.2 Peroxisome isolation from murine brain

Besides peroxisome isolation from cell culture, we addressed peroxisome isolation from murine brain as it is supposed to grant further insights in brain peroxisome function in living tissue. Due to the interaction of different cell types working on specialized peroxisomal functions peroxisome composition might also be altered compared to cultured cells. As neurons are terminally differentiated cells, cell culture can only be performed with secondary cell lines, e.g. from neuronal tumors or application of growth factors (Gordon et al., 2013).

We started with the examination of the different physical properties of adult and young mice's brain peroxisomes and herewith the applicability of previously developed peroxisome isolation protocols in adolescent mice.

Successively we focused on the development of an isolation protocol examining differential centrifugation and gradient centrifugation for suitability and compared the achieved results.

3.2.1 Protocol 1: Analysis of the physical properties of adult brain peroxisomes using a protocol designed for peroxisome separation from juvenile mouse brain

This protocol combined differential and sucrose step gradient centrifugation followed by Nycodenz density gradient centrifugation, as described by Kovacs and coworkers (Kovacs et al., 2001). A series of differential centrifugation steps was applied to enrich peroxisomes (by decreasing the content of the main contaminating organelles) in a pre-fraction to be further separated by density centrifugation.

3.2.1.1 Peroxisome pre-purification

Peroxisome pre-purification consisted of a series of differential centrifugations, starting with the removal of debris and nuclei (1000 x g) followed by a mitochondria removal step (5,500 x g) and further subfractionation to 2 peroxisomal fractions and a final myelin removal step.

As shown in *figure 16*, the majority of mitochondria were removed by centrifugation at 5.500 x g (**M** (heavy mitochondria fraction)).

Peroxisomes were also slightly enriched in fraction **M** compared to the supernatant (**PMS**). ER was hardly affected. Majority of myelin was also depleted, leading to an enrichment in fraction **M**. Pelletation of these organelles with low density probably derived from association to myelin.

With the subsequent centrifugation (18,000 x g), remaining light mitochondria were pelleted (**L1**) in parallel with parts of ER, peroxisomes and synaptosomes.

After centrifugation of the supernatant of **L1** (**SN**, 106,409 x g), however, all these three organelles were further enriched (**P1**).

In the **L** pellet derived fractions myelin concentration is higher than in the supernatant (**SN**)-derived fractions **P1** and **P2**. Myelin removal step gradient decreased myelin content in both final fractions (*figure 16*: **L1/L1a** vs. **L2** and **P1** vs. **P2**) and lead to a rise in concentration of all other organelles compared to **PNS**. Myelin was found as a fluffy layer at the border of 0.25 and 0.85M sucrose layer.

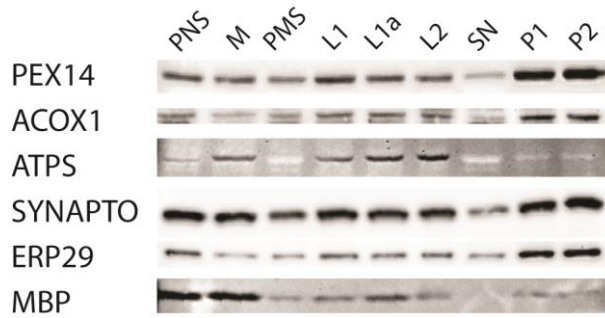


Figure 16: fractions of protocol 1 (adapted after Kovacs et al)

In a first step mitochondria were removed (5,500 x g) from post nuclear supernatant (**PNS**). The supernatant (**PMS**) was further centrifuged to fraction **L1** (18,000 x g) and **P1** (106,409 x g). **L1a** was derived by a repetition of the centrifugation generating fraction **L1**. Both fractions were then applied on myelin removal gradient to generate fractions **L2** and **P2** to be applied on the following Nycodenz gradient.

The peroxisomal markers (**PEX14** and **ACOX1**) were enriched in centrifugation 1 to 8 towards pellet **P1** and **P2**. Mitochondria (**ATPS**, ATP-Synthase) were removed in mitochondria removal step and the subsequent centrifugation. Synaptosomes (**SYNAPTO**, Synaptophysin) were contained in **L-** and **P-**fractions at approximately the same intensity as in **PNS**. ER (**ERP29**) was enriched in **P-**fractions and depleted in **L-**fractions. Hereby it resembled distribution of peroxisomal markers. Myelin was mainly removed in mitochondria removal (**M**), the remaining myelin was successfully removed in the myelin removal gradient (**L1/L1a** vs. **L2** and **P1** vs. **P2**).

3.2.1.2 Nycodenz density gradient

Fraction **L2** was applied to a continuous Nycodenz gradient ranging from 10-40% Nycodenz (figure 17).

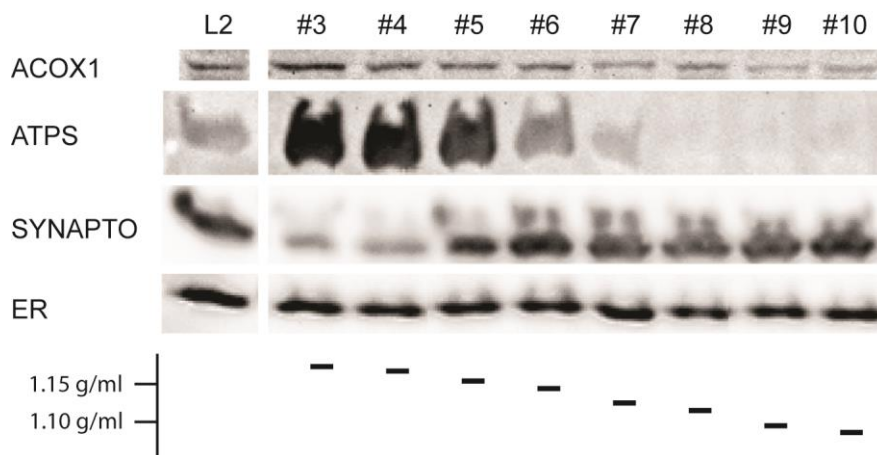


Figure 17: Nycodenz density gradient 10-40%

Using protocol 1 solemnly synaptosomes (Synaptophysin, **SYNAPTO**) could be separated from peroxisomes (**ACOX1**), while peroxisomes and mitochondria (**ATPS**, ATP-Synthase) remained at the same dense fractions towards the bottom of the gradient. ER marker **ERP29** indicated no separation effect of ER from the other organelles.

The peroxisomal marker, **ACOX1** extended almost over the whole gradient length. The maximum concentration was found in the fractions from 1.154 to 1.173g/ml. In contrast to the similarities to the peroxisomal markers in the preliminary centrifugations, synaptophysin was retained in the lighter part of the gradient, forming a plateau around 1.144g/ml. Towards higher densities of the gradient synaptosome content decreased

rapidly. ER-marker ERP29 exhibited an almost even distribution throughout the gradient ATP-Synthase signal was enriched towards the bottom of the gradient and peaked at densities from 1.167 to 1.193g/ml.

In summary, the continuous Nycodenz gradient centrifugation used only efficiently separated synaptosomes from peroxisomes, while it was incapable to split peroxisomes from mitochondria.

3.2.2 Influence of re-homogenisation on myelin content/organelle preservation

After homogenisation, no major particles were visible when the pistil was slowly moved through the homogenate. However, an unneglectable amount of large particles remained, which was pelleted with low force (1000 x g).

Though absolute gain of protein from mice brain was increased by multiple turns of homogenisation and successive centrifugation for debris removal, peroxisome and other organelle content decreased constantly from the supernatant of the first (*figure 18 PNS1*) until the supernatant of the following turns of homogenisation and centrifugation (*PNS2* and *PNS3*). Furthermore, every re-homogenisation process applied shearing forces to the sample (Burden, 2008), which are capable to destroy organelles. The relative peroxisome content appeared to be decreased even stronger than the one of other organelles if signal intensity in western blot was compared. Myelin, indicated by Myelin basic protein, increased with re-homogenisation. The best ratio of PEX14 signal to other marker protein signal in western blot was found in *PNS1*. Hence a re-homogenisation of the pellet of this debris removal centrifugation appeared disadvantageous.

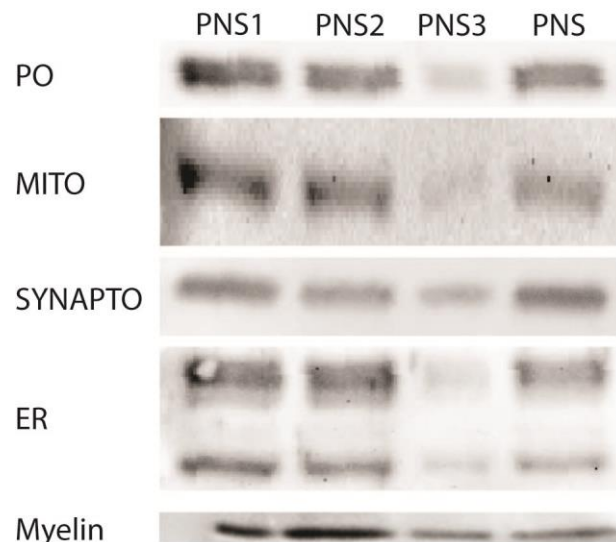


Figure 18: Western blots highlighting the decrease of organelle content with homogenisation and successive centrifugation in the further processed supernatant (PNS1-3) and the resulting mix PNS. Peroxisomes (PO; marker PEX14), mitochondria (MITO, marker ATP-Synthase), synaptosomes (SYNAPTO, marker Synaptophysin) and endoplasmic reticulum (ER, marker ERP29) decreased from *PNS1* to *PNS3*. Peroxisomes appeared to be decreased even stronger than the other organelles. Myelin (marker MBP) approximated the organelle distribution but was enriched in the second cycle.

3.2.3 Myelin removal and by sucrose step-gradients

3.2.3.1 Gradient composition

Several myelin removal gradient compositions were tested (*Methods, protocol 1 and 2*) In brief, an 850mM sucrose layer containing the sample (*figure 19, PNS*) was overlaid with a 250mM sucrose buffer solution (*protocol 1*). After centrifugation, the myelin enriched on top of 850mM sucrose layer as a fluffy white layer (*figure 19, My*) below a clear supernatant (*figure 19, SN*). Below the myelin layer, the 850mM sucrose turned into a yellowish transparent layer (**U**). At the bottom of the tube, a pellet with a brownish core and ochre surrounding was formed, when no 2M sucrose solution was used. The pellet was suspended in fraction **U** (**U+P**). The formed layers were removed separately, special care was taken for the complete removal of all visible white particles of the myelin layer to achieve best myelin removal.

The supernatant (**SN**) contained only little protein. In western blot analysis, the intensity of all organelle markers was low. This observation might derive from the dominance of cytosolic proteins and other light membrane components, which were not analysed by antibodies in this fraction. As expected, myelin was clearly enriched in the myelin layer. However, low concentrations of the organelles were present as well. Peroxisomes, mitochondria, ER and synaptosomes enriched in the region below the myelin layer (**U** and **U+P**). In the yellowish layer below the myelin layer, only little ATP-synthase was found. As the total protein amount in the yellowish layer was low, the fraction was complemented with the underlying pellet (**U+P**). When the pellet was added peroxisome, synaptosome and ER concentrations increased. According to the ATP-signals, mitochondria were almost exclusively contained in the pellet at the bottom of the myelin removal gradient. However, also myelin levels increased to some extent in the pellet fraction (**U+P**). In summary, the myelin removal gradient lead to a substantial but not absolute depletion of myelin in the lower fractions of the gradient. Remaining myelin might either derive from inaccuracies in removal of the myelin layer or attachment to the membranes of organelles, which is further discussed in *paragraph 4.2.3*.

3.2.3.2 Positioning of the myelin removal step

In the majority published isolation protocols for brain peroxisomes, myelin removal was performed after an initial mitochondria removal (Cimini et al., 1993; Kovacs et al., 2001; Posset et al., 2015; Singh et al., 1993) but its use as an initial centrifugation step was also described (Lazo et al., 1991). To assess gradient position we compared post-nuclear supernatant (**PNS**) and mitochondria depleted samples (**PMS**) before and after myelin removal (**PNSZ** and **PMSZ** respectively) concerning myelin and organelle content. Direct mitochondria removal from the **PNS** at 5,500 x g

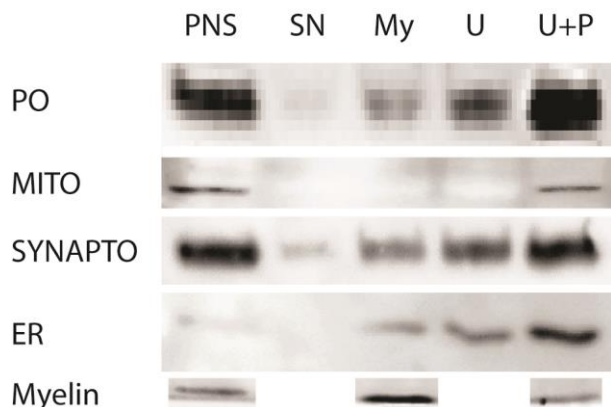


Figure 19: Myelin removal gradient

Fraction PNS was split up on myelin removal gradient. Myelin (MBP) was enriched in myelin fraction, PO (PEX14), MITO (ATP-Synthase), ER (ERP29) and Synaptosomes (Synaptophysin) enriched below. As no peroxisome enrichment step precedes myelin removal, peroxisome signal had to be detected with binning. Myelin signal in SN and U is lacking due to lack of sample material as analysis was derived on a different blot.

significantly removed mitochondria forming the **PMS** (Figure 20). Signal intensity of mitochondrial marker, ATP-Synthase, was clearly depleted. However, in comparison to **PNS** peroxisome concentration and synaptosome concentration and in particular ER were as well slightly increased in the mitochondrial fraction (**M**). Nevertheless, peroxisomes, synaptosomes were more enriched in the **PMS**. Thus, in comparison, an initial myelin removal step as described in paragraph 3.2.4, efficiently enriched peroxisomes, with mitochondria and synaptosomes. When myelin was removed from the **PMS**, peroxisomes were less efficiently enriched in the resulting fraction (**PMSZ**) Of note, ER content signified by ERp29 signals in figure 20 were in parallel increased in the **PMSZ**. In addition, myelin contamination is higher, when mitochondria depletion was performed in the initial separation step. Taking the organelle separating gradient into account (figure 27), dense peroxisomes and mitochondria were depleted in **PMS**-derived gradients (figure 27 gradient **A** and **B**), leading to an overlap of peroxisome and mitochondria maxima. The little existing separation capability of synaptosomes from peroxisomes was lost, as synaptophysin signal stretched in **PMS** derived fractionation over whole gradient length. ER signal of **PMS**-derived fractionation extends over the whole gradient length or forms similar peaks as PEX14 dependent on gradient constitution. Hence position of myelin gradient crucially affects organelle composition and separation capability in the subsequent gradients. In summary, myelin depletion before the differential centrifugation procedure to be advantageous compared to an initial mitochondria-depletion step.

3.2.4 Optimization the differential centrifugation procedure

According to the results show above, myelin depletion was performed with a step gradient containing layers of 2M, 0.88M and 0.32/ 0.25M sucrose. Organelles and myelin enriched according to figure 19.

The “organelle” layer from the myelin removal gradient was further purified by series of centrifugation steps of 900 x g (depletion of erythrocytes, debris, nuclei), 11,000 x g (mitochondria), 70,000 x g (heavy peroxisomal fractions) and 100,000 x g (light peroxisomal fractions) (figures 6 and 21).

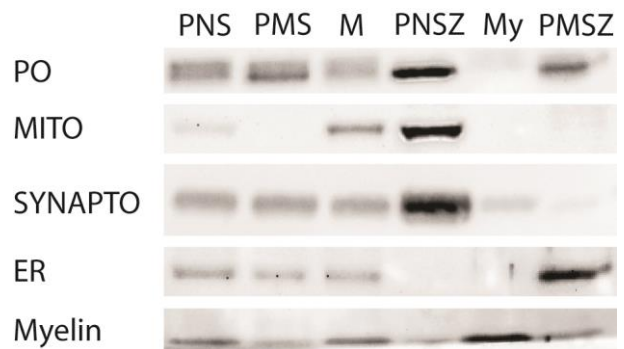


Figure 20: Test concerning the position of myelin gradient.

Western blot describing organelle and myelin distribution depending on the position of myelin removal gradient: Peroxisomes (PO, PEX14), mitochondria (MITO, ATP-Synthase), synaptosomes (SYNAPTO, Synaptophysin), endoplasmic reticulum (ER, ERP29) and myelin (MBP).

Post-nuclear supernatant fraction (**PNS**), which is derived by debris removal (1,000 x g) from the homogenate is either directly applied on myelin removal gradient or further processed by after mitochondria removal as described in literature (Cimini et al., 1993; Kovacs et al., 2001; Posset et al., 2015; Singh et al., 1993). By this centrifugation (5,500 x g) mitochondria are pelleted (**M**) and the supernatant (**PMS**) is applied on myelin removal gradient. **PNSZ** and **PMSZ** are the organelle fractions harvested after myelin removal gradient, **My** denotes for the fluffy myelin layer.

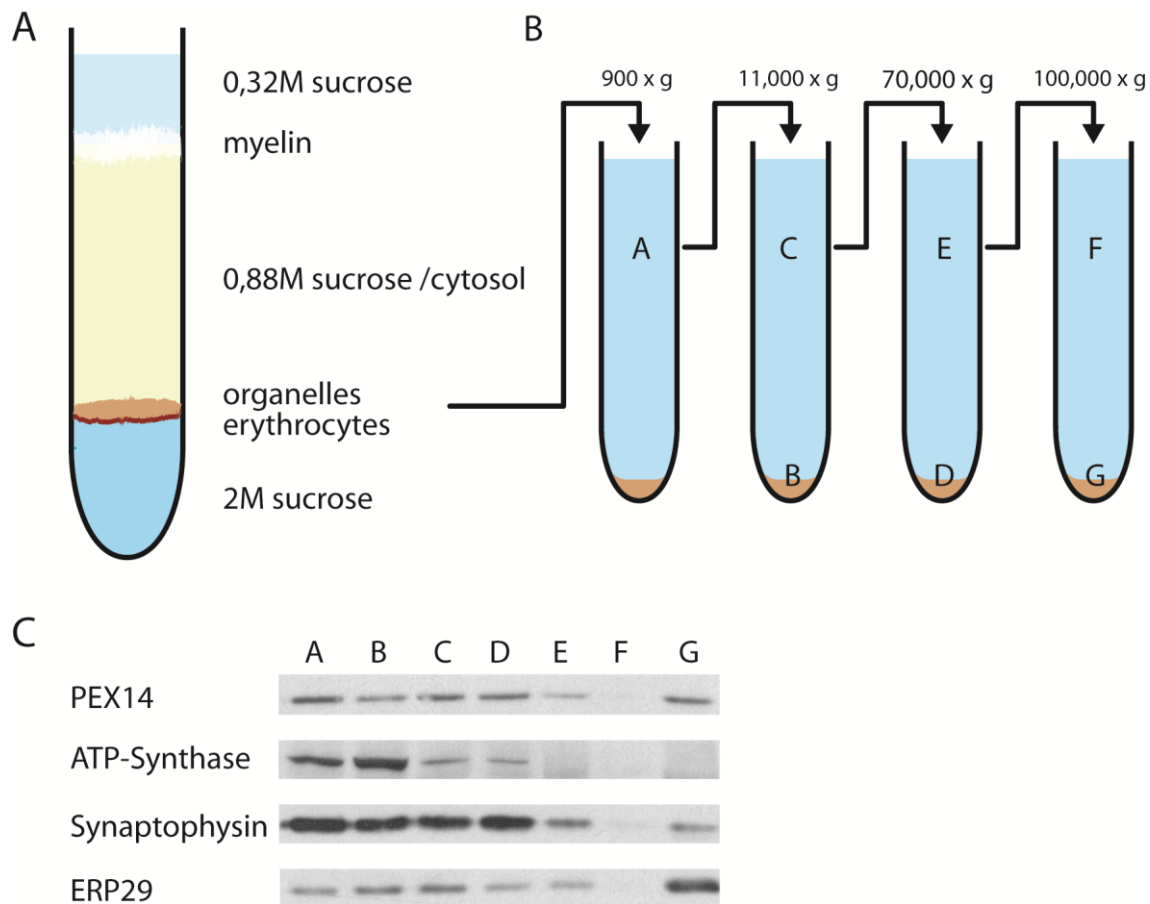


Figure 21: Myelin removal gradient (A) and following differential centrifugation steps (B) and fractions derived by differential centrifugation (C)

Myelin was enriched as a fluffy layer at the border between the 0.32 and the 0.88M sucrose step (figure 19). A yellowish cytosol layer was found below the myelin layer. At the border to 2M sucrose a reddish erythrocyte layer below the brownish “organelle” layer could be found. This was further purified by debris removal to **A** and mitochondria depletion to the fractions **D** and **G**. Peroxisomes (PEX14) were enriched in fractions **D** and **G**. While **D** contained a higher mitochondria (ATP-Synthase) and synaptosome (Synaptophysin) concentration, ER (ERp29) concentration was higher in **G**.

While mitochondria were efficiently separated in the 11.000 x g pellet (figure 21 **B**), peroxisomes could be found enriched in substantial amounts in two subsequent pellets from the 70,000 x g (**D**) and the 100,000 x g (**G**) centrifugation. However, both fractions contained differing contaminations. According to the synaptophysin signal, synaptosomes could be found substantial concentration in fraction **D**, microsomes enriched together with peroxisome in the 100.000 x g pellet.

In summary, organelles were separated into three major fractions: Fraction (**B**) contained most mitochondria. Fraction **D**, containing organelles sedimenting at forces among 11.000 x and 70.000 x g, had the highest peroxisome concentration. In the lightest fraction (**G**), pelleting between 70.000 x g and 100.000 x g, ER was enriched. Synaptosomes and peroxisomes were also abundant but in lower concentrations than in **D**. Mitochondria were depleted. Consequently, fraction **D** was chosen for further purification of peroxisomes via density gradient centrifugation.

3.2.5 Protocol 2: adaptations aiming to improve peroxisome isolation capacity by differential and gradient centrifugation

After an initial gradient for myelin removal, the sample was fractionated by differential centrifugation. The peroxisome-enriched sample from the differential centrifugation procedure was further separated by a density gradient, for which different gradient media were tested and compared.

Since the method for PO isolation published by Kovacs (Kovacs et al., 2001) failed to purify PO from adult mouse brain, we attempted to adjust centrifugation parameters for a more successful purification protocol. The order and parameters of the differential centrifugation procedure were varied. A crucial step of the isolation procedure is the elimination of myelin. To avoid that the hydrophobic myelin interacts with organelle membranes in the pellets produced by differential centrifugation, the myelin removal step was transferred to the beginning of the isolation procedure.

3.2.6 Analysis of different gradient media in the final purification steps

Due to the incomplete separation from other organelles the fractionations described above (*paragraph 3.2.1. and 3.2.4*), had to be further purified to remove remaining contaminating organelles. The adaptation of centrifugation parameters in the differential centrifugation with changes in the centrifugation forces did not sufficiently improve the composition of the pelleted fractions towards a better enrichment of peroxisomes. Peroxisomes, mitochondria, ER and synaptosomes appear to exist in broad spectrum of sizes, densities and weights extending beyond the borders of the fractions achieved by differential centrifugation. By gradient centrifugation different separation parameters are introduced with density and sedimentation speed. To use possible effects of the density generating medium, the media Optiprep, sucrose and Nycodenz were tested and compared.

3.2.6.1 Optiprep

Gradient centrifugation with Optiprep has been successfully used in peroxisome isolation from liver (Islinger et al., 2012a) and cultured cells (*paragraph 3.1*). Hence, its applicability for the purification of brain peroxisome was assessed. Sample distribution in Optiprep gradients, spread across the whole gradient length from 1.04g/ml to 1.13g/ml (*figure 22 and 23A*). A prominent double band and two single bands were formed after centrifugation. The double band was located at the top of the gradient and is attributed to two fractions (**#4, #5**). This double layer was followed by a clear intermediate and a broad whitish, partly transparent layer. This layer was split up into two fractions for investigation. Bordered from this layer by another clear interphase, a weak, but clearly distinguishable layer was found close to the ground of the gradient. To identify organelle position, gradient was eluted at constant volumes of 1 ml (*figure 23*). and band-wise orientating on visible turbidity.

In line with the band pattern, majority of proteins accumulated at approximately 1.07 - 1.09 g/ml (**#4/5**) – the position of the double band.

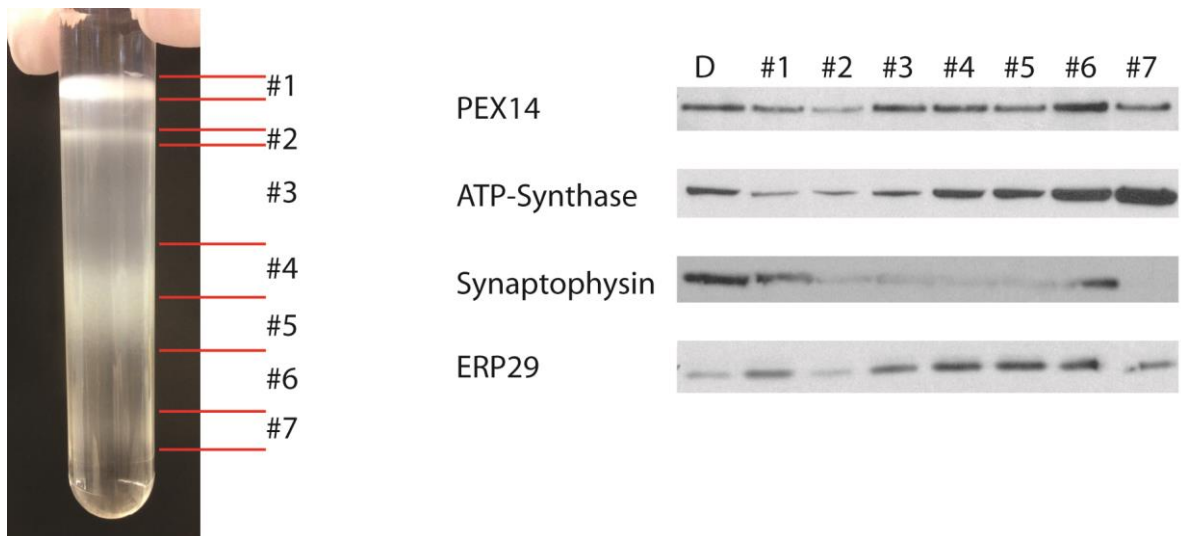


Figure 22: Fraction D separated on Optiprep gradient

The sample was split into different fractions which accumulated in 3 bands (**#2, #4/#5, #7**) on the gradient. Peroxisomes (PEX14) tended to accumulate in fraction **3-6** with Maximum in fraction **6**, while mitochondria (ATP-Synthase) increased in content towards the denser fractions. Synaptosomes (Synaptophysin) was enriched towards the top of the gradient but extended over the whole gradient length. ER (ERP29) was not separated from peroxisomes.

Band intensities for the peroxisome marker PEX14 peaked just below the major protein band at approximately 1.103 / 1.106g/ml e. A second, lower peroxisomal signal peak appeared on top of the main protein band. It appeared at densities around 1.07g/ml. In experiments with band-wise harvesting (*figure 23*), this second peak could not be detected, which derives most probably from averaging with surrounding less enriched gradient. Both PEX14 peaks exhibited enrichment compared to fraction **D**, which was also present in surrounding fractions. In the fractions lighter than 1.05g/ml only little PEX14 was found.

According to the ATP-Synthase signal, most mitochondria gradually accumulated in the high-density fractions (maximum between 1.113/1.116 g/ml).

Synaptophysin signal differences among the fractions were low. Synaptophysin predominantly enriched in the lighter fractions of the gradient and peaked at 1.058g/ml. However, it remained present for the whole range of the gradient. In band-wise harvesting hardly any differences in intensity were found.

In band-wise harvesting, ERP29 signal appeared to be highest in the lower part of the broad band and the top-part of the double layer.

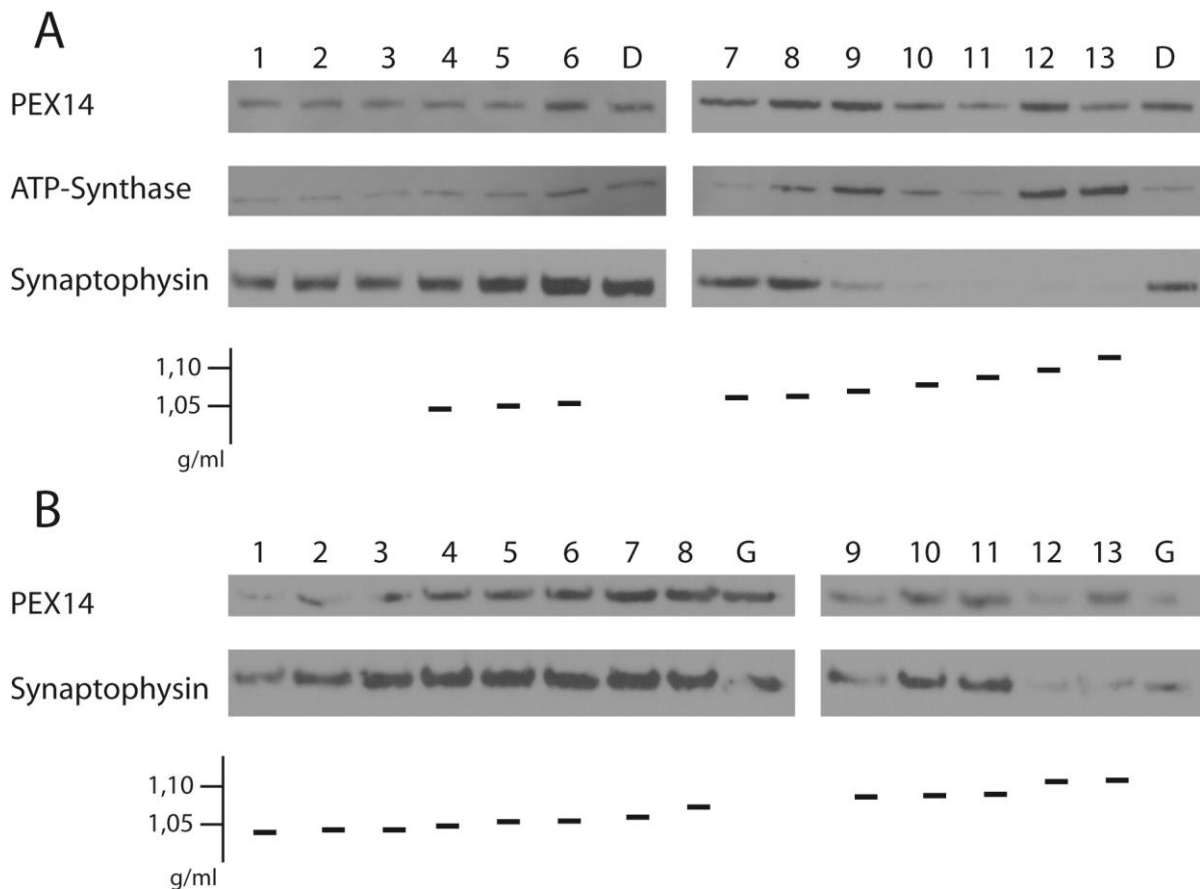


Figure 23: organelle distribution on continuous Optiprep gradients

Fraction **D** (part **A**) and fraction **G** (part **B**) were applied on continuous Optiprep gradients (1,03-1,14g/ml). Gradients were harvested ml-wise. Organelle distribution was demonstrated by ATP-Synthase (mitochondria), PEX14 (peroxisome) and Synaptophysin (synaptosome). In **G**-gradient (**B**), ATP-Synthase fluorescence did not exceed background activity. To grant comparability, starting fractions were applied on both blots. In both gradients (part **A** and **B**), peroxisomes exhibited a peak around 1.07g/ml (#8/#9), while an additional peak at 1.10g/ml (#12) was only found in ml-wise harvested **D**-gradient.

Those clear differences between results from ml-wise and band-wise harvested gradients hinted, that the visible bands did not necessarily go all along with single enriched organelles. The band appearing at highest density seemed to derive mainly from mitochondria. The large, semi-transparent band might be due to ER over the whole band and, mainly at the upmost part of this layer, peroxisomes and synaptosomes, which accumulated there in higher concentrations but were present throughout it. Highest concentrations of peroxisomes were found below this large layer together with a high concentration of mitochondria. The upmost layers were constituted of ER, peroxisomes and synaptosomes but of none in extraordinary amounts. None of these bands was attributed to only a single organelle. Hence layer-wise harvesting seemed not to be advantageous. Peroxisomes appeared to be separated to 2 fractions. Separation capability concerning mitochondria from heavier peroxisomes appeared to be low, the same was the case for light mitochondria from ER and synaptosomes.

3.2.6.2 Sucrose

As sucrose served already as medium in the preceding differential centrifugation, sucrose was investigated concerning its suitability in differential centrifugation. According to the idea that sucrose is capable of penetrating organelles, an extended gradient range from 1.04g/ml, corresponding to 300-320mM sucrose solution, to 1.18g/ml was chosen. To avoid attachment on the ground a 2M sucrose cushion was added below the gradient.

After centrifugation, an untransparent, clearly distinguishable white band appeared in the lowest third of the gradient. Directly below it, a second band formed, which contained several white clusters. Further towards the bottom the gradient appeared clear. Above, the white band was less distinguishable. Towards the top of the gradient the gradient was semi-transparent turbid. Turbidity decreased towards the top of the gradient, leaving the upper third of the gradient clear.

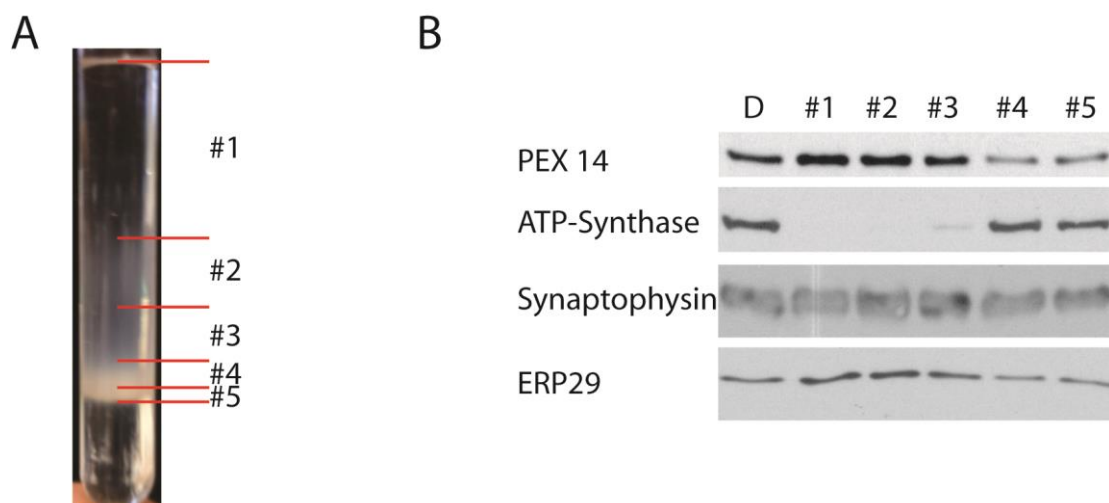


Figure 24: Saccharose gradient

Fraction **D** derived from pre-purification (paragraph 2.3.9) applied on continuous sucrose gradient. The sample formed various bands (**A**). Harvested band-wise (**B**), peroxisomes (PEX14) accumulated at densities around 1.1 g/ml, while mitochondria (ATP-Synthase) accumulated at the densest fractions. Concerning ER (ERP29) and synaptosomes (synaptophysin) only little differences among the fractions could be observed.

In Bradford assay, relevant protein concentrations were only detected in layers with higher density than 1.09g/ml, where no turbidity was visible. These fractions were hence only examined in summary (*figure 24 #1*) via western blot due to insufficient protein content. The gradient part with highest density, deriving from the 2M sucrose cushion, also appeared clear and contained no measurable protein content.

PEX14-signal had its maximum at a density of 1.105 g/ml (*figure 24 #2*). It was clearly enriched compared to fraction **D** in this fraction and the neighbouring fraction. Towards heavier fractions, signal decreased. ERP29 exhibited a similar signal distribution as PEX14 with a peak in the same fractions and a decrease in concentration at heavier fractions. ATP-synthase peaked at 1.151g/ml and 1.165 g/ml with concentrations similar or slightly elevated compared to **D**. In the two fractions with maximum PEX-signal, no ATP-Synthase signal was detectable. Synaptophysin, however, showed an almost even distribution throughout the fractions.

Majority of organelles appeared to accumulate in heavier fractions, indication diffusion inside organelles. Whereas peroxisomes could be clearly separated from mitochondria, the gradient exhibited a similar distribution pattern of peroxisomes and ER and showed hardly any focussing effect on synaptosomes.

3.2.6.3 Nycodenz

The Nycodenz gradient ranging from 1,04g/ml to 1,14g/ml exhibited turbidity along the whole gradient apart from a small area on top (*figure 25*). The density range of the gradient was reduced according to results achieved in protocol 1 (*paragraph 3.2.1.2*). The two untransparent bands corresponded to comparatively high protein concentrations. They were located at densities of approximately 1.07 and 1.11g/ml.

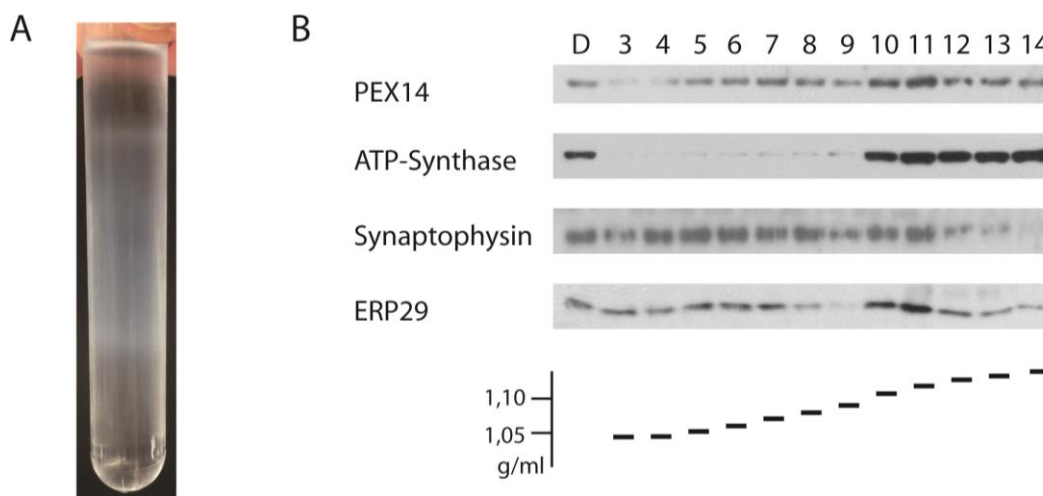


Figure 25: Nycodenz gradient 1.04-1.14 g/ml

Band-distribution on Nycodenz gradient after centrifugation (A). With less pronounced bands than in sucrose and Optiprep, gradients were harvested ml-wise. Results of ml-wise harvested Nycodenz-gradient (B). While peroxisomes (PEX14) accumulated mainly around 1.10 g/ml (#11) and 1.13 g/ml (#14), Mitochondria (ATP-Synthase) increased towards the densest fraction, Synaptosomes (Synaptophysin) could be separated from peroxisomes as they enriched at the top of the gradient. ER (ERP29) remained present throughout the gradient.

The upmost fractions with protein concentrations below 0.03mg/ml were not investigated in Western blot.

PEX 14 signal had 2 clearly distinguishable maxima, hinting at 2 different fractions: The first at a density of 1.10-1.11g/ml and the second at 1.13-1.14g/ml. The first maximum at 1.10-1.11g/ml clearly exceeded **D** in signal intensity - thus hinting at clear enrichment. In the lightest fractions, hardly any PEX14-signal was detectable. ER-marker, ERP29 exhibited a split distribution. Whilst in the lightest fractions above 1.08g/ml, ERP29 was present at levels slightly below that of fraction **D**, it was enriched at fractions above 1.11g/ml. Peak ERP29 level was only a single fraction heavier than that of PEX14. ATP-Synthase signal rose with density of the fraction. Above 1.09g/ml hardly any signal could be detected, at 1.11g/ml it reached concentration of **D** and rose till the dense end of the gradient(#14). The synaptophysin signal stretched across a broad range of the gradient but tended to enrich towards the lighter fractions of the gradient (1.04-1.08g/ml and coinciding PEX14 maximum). All synaptophysin signal maxima appeared in similar intensity.

Whilst peroxisomes were separated into three fractions, of which the two lightest were close to ER and synaptosomal signals. The third and heaviest fraction contained mitochondria and ER as major contaminants. Majority of synaptosomes appeared to accumulate towards the top of the gradient, mitochondria to the bottom. ER also tended to accumulate towards the lighter fractions of the gradient but remained present throughout it.

3.2.6.4 Comparison among the gradient media

Overall organelle distribution and the distribution of the single organelles differed clearly among the gradient media. In sucrose, cellular organelles enriched at higher densities than in Optiprep and Nycodenz. Whereas hardly any protein content was present above 1.09g/ml in sucrose gradients, major protein amounts were found in concentrations until 1.04g/ml in both Nycodenz and Optiprep gradients, which in turn reached only until 1.13g/ml compared to sucrose, where proteins could be measured up to densities of 1.17g/ml.

PEX 14 exhibited a single peak signal at 1.105g/ml in sucrose gradient. In Optiprep gradient - apart from this maximum - a second maximum at 1.07g/ml appeared. And in Nycodenz a third peak at 1.13-1.14g/ml appeared (*figures 22-25*). Surprisingly, main PEX14 signal remained at the same position.

In all gradient media, ATP-Synthase signal rose towards heavier fractions. Whereas it rose to the level of fraction **D** in the neighboring fraction to PEX14 maximum in Nycodenz and Optiprep, it reached the signal intensity of fraction **D** at 1.151g/ml in Sucrose. This was a difference of approximately 0.05g/ml, and by far more than the 0.01g/ml distance in the other two media (*figures 22-25*). Thus, sucrose gradient permits the best separation of peroxisomes from mitochondria.

ERP29 signal distribution in sucrose was similar to that of PEX14. Peaks were in the same fractions. In Optiprep, ERP29 signal was mainly orientated in lighter layers than PEX14 signal. IN ERP29 however ERP29 exhibited a split with presence in light and heavy fractions but little presence in the middle (*figures 22-25*). Concerning disposal of ER, Optiprep and Nycodenz appear to be advantageous.

In both, sucrose and Optiprep gradient, synaptophysin signal differences among the fractions were lower than in Nycodenz gradient. In Optiprep and Nycodenz, synaptophysin appeared to enrich predominantly in the lighter fractions of the gradient, in sucrose the distribution appeared even. Nycodenz seemed to be slightly advantageous compared to Optiprep in separation from synaptosomes as differences among fractions were clearer (*figures 22-25*).

In summary, Nycodenz appears to be the most advantageous gradient medium for the separation of peroxisomes from synaptosomes. As sucrose permitted best the separation from mitochondria, a combination of both gradients appears advantageous.

3.2.6.5 Transfer of the continuous sucrose gradient to a step-gradient

To gain a better reproducible and faster separation, i.e. for further use in combination with a Nycodenz gradient, continuous sucrose gradient was transferred into a step gradient. The protein distribution in the step gradient was assessed in respect to the continuous gradient (*figure 22 and 23*). The step gradient consisted of fraction **D** in 250mM sucrose solution on top of layers of 1.08g/ml (625mM), 1.137g/ml (1,07M) and 2M sucrose solution, whose densities derived from results in *paragraph 3.2.6.2 (figure 26 A)*. The gradient was balanced with 250mM sucrose solution. After centrifugation, the gradient exhibited three distinguishable bands (*figure 26 B*). An untransparent white band appeared at the border of 1.137g/ml and 2M sucrose solution, a double band consisting of a more optically dense and a less optically dense band at the border of 1.08g/ml to 1.137g/ml dense sucrose solution. This double band extended over a wider range than the others. A third band appeared at the border of 250mM to 1.08g/ml dense sucrose solution. The top of the gradient with 250mM sucrose solution and the 2M sucrose solution remained clear, in the rest of the gradient – also among the bands – turbidity was visible. Due to the clearly visible bands, this gradient was harvested band-wise, as highlighted in *figure 26*. Protein content increased with density. PEX14 signal peaked in **S3**, which conforms to the expected position from continuous gradient. It was clearly enriched compared to fraction **D**. Elevated signal levels

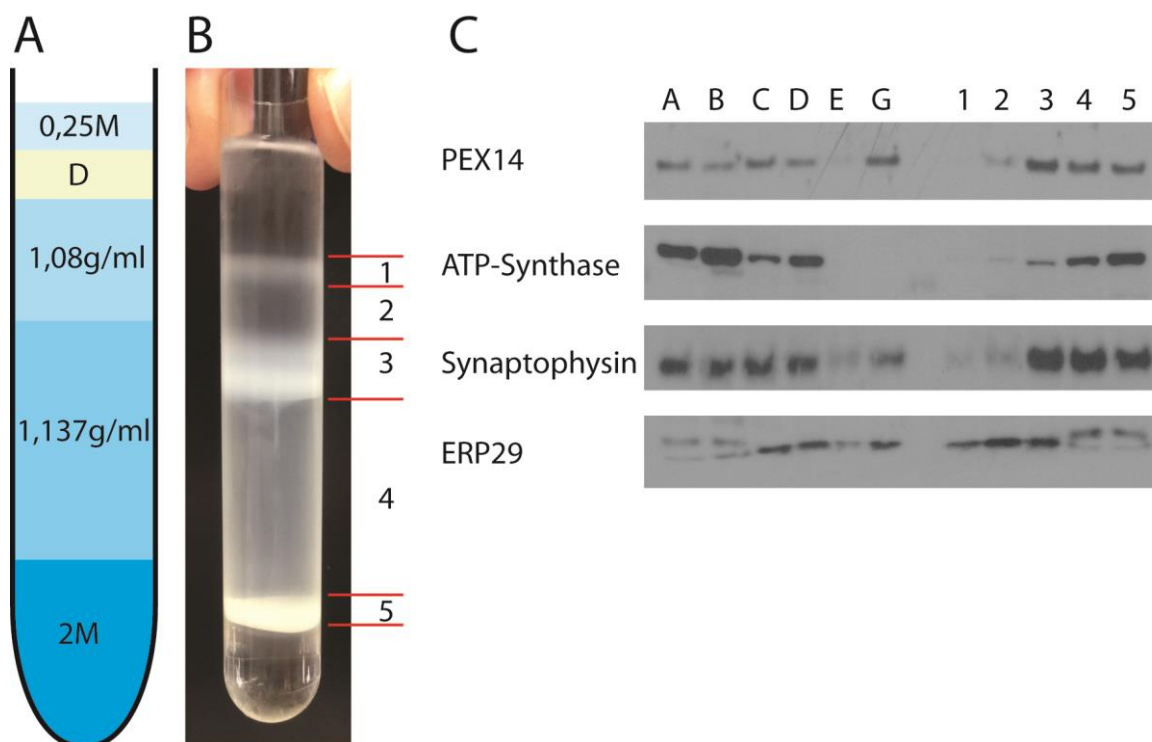


Figure 26: sucrose step gradient

Constitution of the sucrose gradient and application site of fraction **D** (**A**). Gradient after centrifugation and definition of the further fractions **1-5**, henceforth named **S1-S5** (**B**). 250mM sucrose supernatant and the clear 2M sucrose cushion were discarded. First band formed fraction **S1**, the double band fraction **S3**, which was also investigated in two separate sub-bands (**S3a** and **S3b**) and the third band formed fraction **S5**. The intermediate parts of the gradient formed fraction **S2** and fraction **S4**. Western blot of the differential centrifugation (**A-G**) and sucrose gradient (**1-5**) with peroxisomal (PEX14), mitochondrial (ATP-Synthase), synaptosomal (synaptophysin) and ER markers (ERP29) (**C**). Peroxisomes enriched at **S3**, mitochondria towards **S5**, synaptosomes in **S3-S5** and ER in **S2-S3**.

compared to **D** were also present in **S4** and **S5**. ATP-Synthase signal increased towards denser fractions. Its peak was in fraction **S5** with slight elevation compared to fraction **D**. Signal decreased strongly towards lighter fractions. From **S3** on only light signal was visible. This distribution went also along with that in continuous gradient. In difference to the continuous gradient, synaptophysin signal followed PEX14 signal, but with less clear enrichment compared to fraction **D**. Peak synaptophysin appeared in fraction **S4** just below PEX14 peak. The ERP29 signal enriched in fraction **S2** and **S3**. The tendency to the lighter fractions appeared to be more emphasized than in the continuous gradient.

In summary, fraction **S3** had the highest peroxisome concentration with clear mitochondrial depletion and less clear ER depletion. Synaptosomes were less clearly separated from peroxisomes. The split of fraction **S3** into two drastically reduced yield in the two fractions. Peroxisome to synaptosome-ratio appeared unaffected by the split. Hence fraction **S3** was best suited for further processing. Apart from the procedure's inherent advantages, sucrose step gradients appeared to be superior to continuous gradients in organelle separation, which was further emphasized in *paragraph 3.2.7*.

3.2.7 Protocol 3: improvement of the isolation protocol by serial step gradient centrifugation

Based on the findings (*paragraph 3.2.6.5*), that sucrose step gradients are capable to separate the respective cellular organelles from peroxisomes, their use as replacement for the previously described differential centrifugation and combinations of gradient centrifugations with different gradient media was tested. These gradients were combined with an improved homogenisation according to *paragraph 3.2.2* and an extended debris removal procedure. The necessity of myelin removal step was tested, as well as the myelin removal procedure was altered as described in *paragraph 3.2.3*. These preliminary centrifugations were combined with a Nycodenz gradient, as Nycodenz gradients proved best to be capable to separate peroxisomes from synaptosomes.

3.2.7.1 Organelle separation gradient (sucrose)

Various compositions of and sample applications on this sucrose step gradient were tested. Distribution pattern differed widely and was highly affected by the steps (*figure 27*).

Most peroxisomes were capable to migrate until into 950mM sucrose solutions independent of the density of the applied sample. Here the maximum peroxisome concentration was found. Less peroxisomes were capable to penetrate denser layers, i.e. 1M or 1.1M sucrose. Confronted with denser layers, they accumulated at the borders to these denser solutions. The peroxisome maximum concentration equilibrated in 900mM / 950mM sucrose layer, which corresponds to densities of approximately 1.12g/ml. This density was similar to that in continuous sucrose gradient (*paragraph 3.2.6.2; figure 24*), where peroxisomes peaked at 1.11 g/ml. Sample application affected mainly peroxisome content in lighter and denser fractions than the peak fraction. The denser the applied sample was, the higher relative content in dense fractions and the lower that in lighter fractions. The position of the peak was hardly affected. The best distribution was achieved by sample application at 700mM and collection at 900mM sucrose (*Figure 27, gradient D and G*).

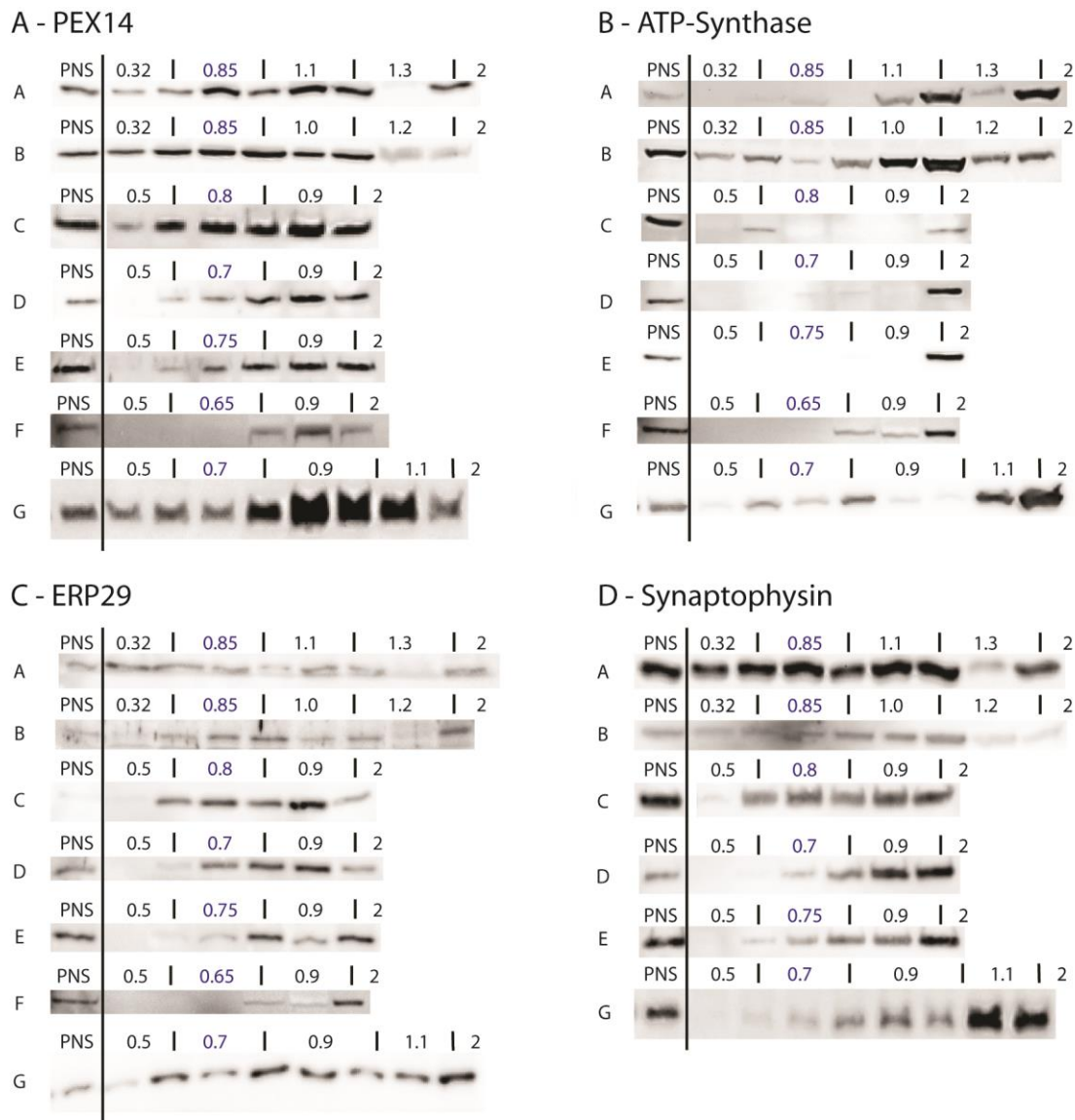


Figure 27: Organelle distribution in different OSGs

Peroxisome (A-PEX14), mitochondria (B-ATP-Synthase), ER (C-ERP29) and synaptosome (D-synaptophysin) distribution on different OSGs. The localization of the different fractions on the gradient in respect to the different layers (in sucrose molarity) is noted above the respective blot. Application site is highlighted with blue.

Mitochondria, marked by ATP-synthase, were usually found at the bottom of the gradient. Their maximum concentration was usually found at the border to the 2M sucrose cushion. While in 900mM and 950mM sucrose solution hardly any mitochondria were found or signal was not detectable, mitochondria concentration rose in the band below 950mM sucrose solution and further to the bottom. Mitochondria exhibited a second, but by far smaller peak at about 1.09 - 1.10g/ml, corresponding to 700mM – 800mM sucrose, i.e. the band on top of the 900mM sucrose layer. The major peak corresponded to that expected from continuous gradients, while the lighter one exhibited no equivalent in continuous gradient. This lighter peak might derive as remains from the application.

ER signal was present over the whole length of the gradient. The distribution pattern appeared to be highly dependent on the application density and the gradient constitution. In separations with application in 850mM sucrose ER concentration peaked at the bottom of the gradient independent of constitution A second, but less

elevated peak was located at a density of about 1.08g/ml at the border among 850mM and 320mM sucrose. An alteration to 500mM on top of the application permitted penetration of this layer. The third and smallest signal elevation was found at the border from 850mM to 1M or higher concentrated sucrose. The insertion of a 900mM or 950mM sucrose layer led to an enrichment or even a peak in this layer and at the bottom of it leading to a more even distribution in the gradient and enlarged the concentration at the bottom of the gradient. With decreasing density of application site, concentration above 900mM sucrose layer increased. If an application in 700mM sucrose was chosen, ER was concentrated in the upper part of the gradient on top of 900mM sucrose layer. A minor peak was found underneath the 900mM layer. Concentration was slightly decreased compared to the starting fraction in 900mM sucrose layer, which was confirmed by both ERP29 and GRP78 signal. If the sample was applied in lighter fractions, i.e. 650mM sucrose, the denser peak was shifted towards 900mM sucrose layer. This dependency on the application site hints that ER-vesicles are apparently highly permeable to sucrose and hence gain weight dependent on the application density.

Synaptophysin appeared to fairly uniformly distributed over the whole length of the gradient in similar concentration as **PNS**. In most gradient compositions, a slight increase towards denser gradient fractions was found. In gradients with application on 700mM sucrose, a layer of 900mM and 1,1M sucrose underneath, synaptophysin concentration peaked with strong increase in the bottom fraction. In 900mM sucrose, slight depletion compared to PNS was found.

3.2.7.2 Optimised organelle separation gradient

According to the results from the different OSGs shown in the preceding paragraph, a discontinuous gradient with the following sucrose concentration was chosen for organelle prefractionation. This gradient consisted of 5 layers with sucrose concentrations of 500mM, 700mM, 900mM, 1.1M and 2M (*figure 28 A*). The sample was applied into the second layer of 700 mM sucrose. The 1.1M sucrose layer gave the fraction 4 more reproducibility as it separated the peroxisome-enriched fraction from the bottom fraction with high protein content. The gradient was harvested band wise with each band differing visibly (*figure 28 B*). Protein content increased exponentially towards the bottom of the gradient.

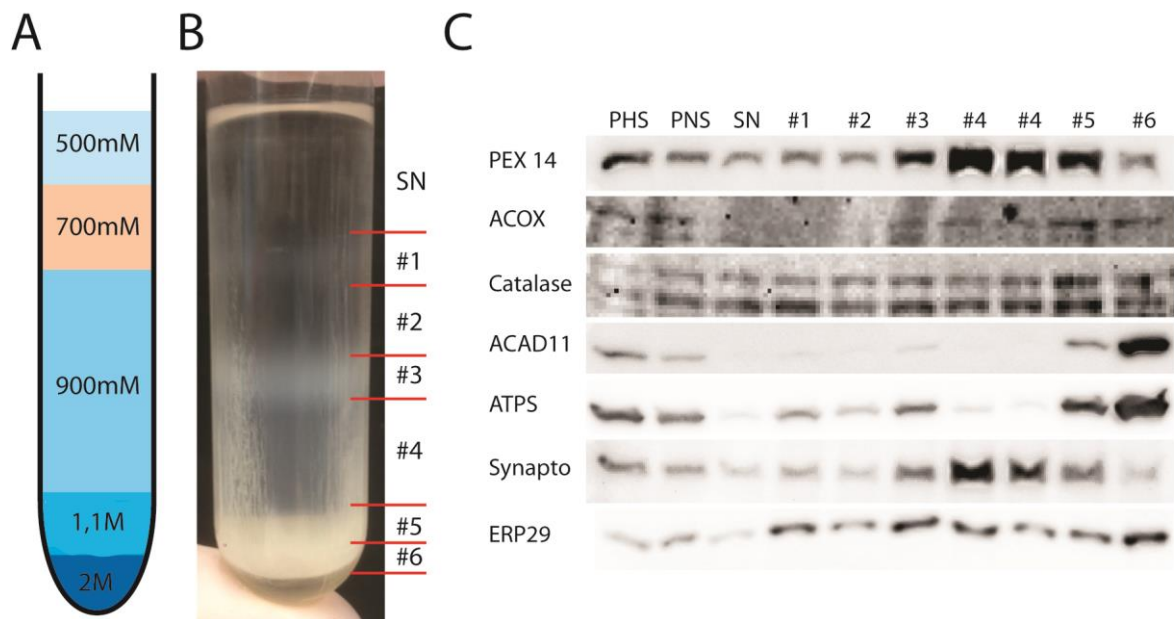


Figure 28: final OSG blot and quantification of the main markers

Gradient steps (A). By centrifugation 2 white bands (#1 and #3) and an ochre and brownish double layer appeared (#5 and #6). At the top was a clear supernatant, between the two white bands a further fairly colored layer, and between the lower white and the ochre band the yellowish 900mM sucrose layer, which was further processed. The double-band consisted of an upper ochre part and a brownish lower part (B). Marker proteins in the harvested bands (C): While peroxisomes (PEX14, ACOX and Catalase) enriched at fraction 4, Mitochondria (ATP-Synthase) accumulated towards fraction 6. ACAD11, which is reported to be expressed in mitochondria and peroxisomes, appeared to be present mainly on mitochondria. As observed in experiments with sucrose gradients, synaptosomes (Synapto; Synaptophysin) could not be separated from peroxisomes. ER distributed mainly towards the bottom of the gradient. Fraction 4 was applied twice on the gradient.

PEX14 peaked in 900mM sucrose at 1.12g/ml (figure 28 C fraction 4) and decayed towards lighter and heavier fractions. Signal intensity enriched in average 3-4 times in fraction 4. In heavier fractions, a plateau formed at 2-fold starting concentration. Being both present in mitochondria and peroxisomes in brain, ACAD11 signal differed from PEX14 signal with enrichment in the densest layer (figure 28) – thus indication a mainly mitochondrial localization in our sample.

In 900mM sucrose layer, hardly any ATP-synthase was detectable, forming a minimum. Below, ATP-Synthase increased in fraction 5 to starting concentration reaching a maximum with multiple signal enrichment in the bottom fraction. Compared to other separations, peroxisome-fraction 4 contained little mitochondria through the separation of 900mM and 2M sucrose layer. In the band above peroxisomes, at the border among 700mM and 900mM sucrose, a second, less pronounced ATP-Synthase peak was located.

Synaptophysin signal followed PEX14-Signal peaking at 1.12g/ml. Though peak was less pronounced than in PEX14, separation of peroxisomes and synaptosomes seems insufficient.

ER concentration was enriched at the top and the bottom of the gradient. The highest concentrations were in the bottom fraction (#6) and fractions 1 and 3. In the peroxisome fraction 4, ER was slightly enriched.

3.2.7.3 Separation of the bottom fraction of gradient for further peroxisomal subpopulations

The bottom fractions of separation shown in *figure 28* (*paragraph 3.2.7.2*) contained the vast majority of proteins of the separation. Absolute protein content was about 10 times higher than in the peroxisome-enriched fraction **4** (*figure 28*). Peroxisome and synaptosome concentration were lower than in fraction **4** but both elevated compared to PNS. The bottom fraction contained the majority of mitochondria. Enrichment of mitochondrial marker compared to PNS signal was 3,5 to 16 times, compared to fraction **4** even more. ER concentration was slightly reduced compared to **PNS** to similar levels as fraction **4**. As the amount of proteins was by far higher than in the other fractions, and as - deviating from PEX14 signal – ACOX1 was enriched in this fraction, a split up of this fraction might reveal further peroxisomal fractions. The peroxisomes contained might deviate from those observed in fraction **4** concerning enzyme composition.

The fractions were split up on a gradient consisting of 0.7M, 0.9M, 1.1M, 1.2M, 1.3M, 1.4M and 2M sucrose with application at 0.7M sucrose. By centrifugation six bands formed (*figure 29*). The upmost band was located at the border among application site and 0.9M sucrose (1.113g/ml, 0.887M), the second at border among 0.9M and 1.1M sucrose (1.125g/ml, 0.976M), the third in the 1.1M sucrose solution (1.139g/ml, 1.086M), the fourth at the border 1.2 to 1.3 M sucrose solution (1.157g/ml, 1.23M), the fifth in the 1.3M sucrose solution (1.157g/ml, 1.284M) and the last at the border 1.3/1.4M sucrose solution (1.169g/ml, 1.322M). The gradient was harvested band-wise.

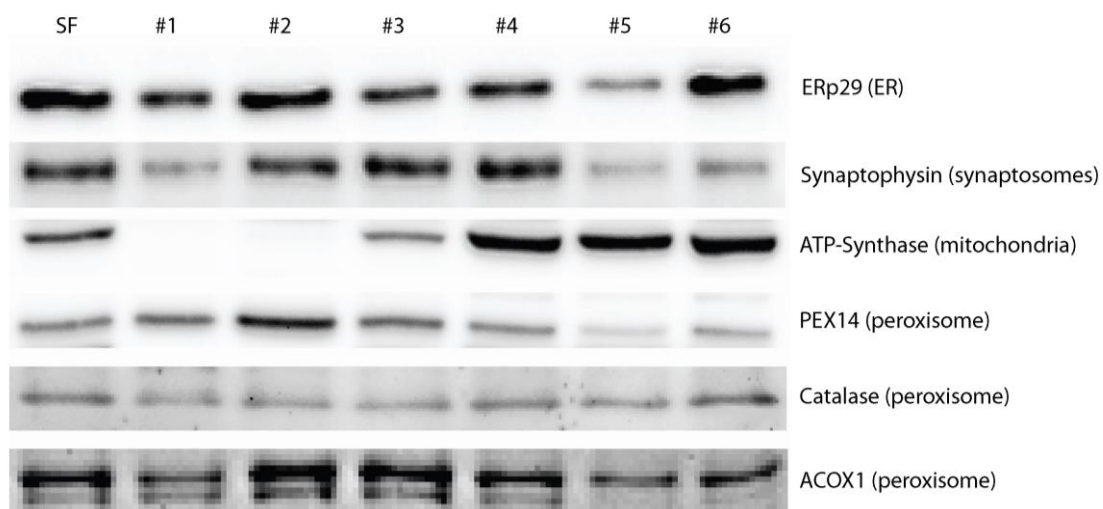


Figure 29: split-up of OSG bottom fraction

In order to distinguish the peroxisomes present in the bottom fraction of the OSG, fraction 5 and 6 (SF) - containing highest Catalase and ACOX-Signal in figure 27 - were further separated on a sucrose step gradient. The resulting band wise harvested fractions revealed two peroxisomal signal peaks at fraction 2 (1.125g/ml, PEX14 and ACOX1) and at fraction 6 (1.169g/ml, catalase and ACOX1, only little PEX14). The different abundancy of peroxisomal proteins hints at different peroxisomal subpopulations.

ATP-Synthase was not present at the two top bands, increased at band **3** to the level of PNS and peaked at band **4**. Below signal formed a plateau over the other 2 bands with an increase to almost double the starting concentration (*figure 29*).

ERP29 was mainly present at fraction **2** and **6** with maximum at fraction **2** (1.125g/ml). The heavy ER vesicles appeared to enrich at 1.169. Signal however was lower than that of the starting fraction (**SF**) (*figure 29*).

Synaptophysin signal reached its maximum in 1.14g/ml and 1.16g/ml band. Below it decreased to the same concentrations as in **PNS** (*figure 29*).

PEX14 and ACOX 1 peaked at band **2** and **3** but remained present throughout the fractions with similar intensity as the applied fraction. Peroxisomes of various densities were present throughout the bands, which hints at different subpopulations.

Catalase differed from PEX14 and ACOX signal. Catalase peaked at band **6** (1.169g/ml) of the gradient (*figure 29*). The presence of an ACOX signal in the same fraction can be seen as proof of their peroxisomal allocation, as catalase might also appear in cytosol and ACOX might appear in mitochondria. Peroxisomes are the only location where both are present. Taking the differences from PEX14 pattern into account, this observation could be attributed to a peroxisomal subpopulation of heavy peroxisomes with catalase and ACOX. The presence of peroxisomal subpopulation fits to observations in publications and immuno-fluorescence microscopy.

3.2.7.4 Combination of two serial sucrose organelle separation gradients (OSG)

Further purification of peroxisomes in sucrose was tested by two serial sucrose gradients. Fraction with maximum peroxisome concentration derived in the OSG was hence applied on a second gradient. To shorten the protocol, myelin removal was performed on the OSG.

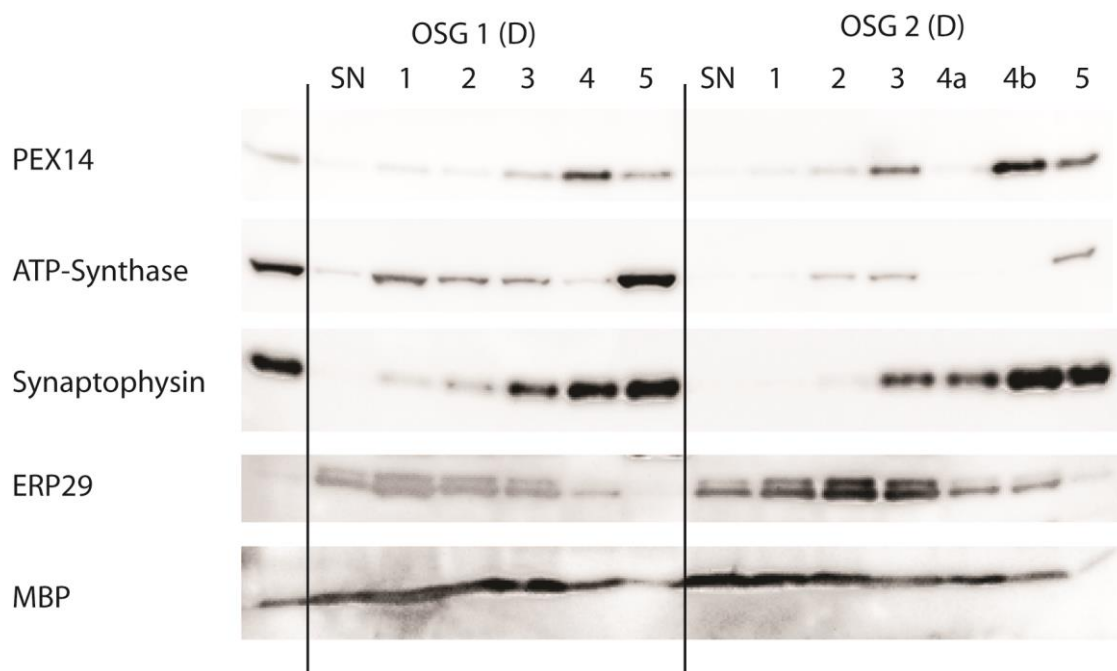


Figure 39: Combination of 2 OSGs by repetition of OSG D (figure 10)

Peroxisome enriched fraction derived by Gradient **D** (composition *figure 27*) was applied on an identical gradient. This led to an elevation of peroxisomal signal (PEX14, **#4b**) and synaptosomal signal (Synaptophysin) and depletion of ER (ERP29), Myelin (MBP) and mitochondrial (ATP-Synthase) signal in the gradient. In contrast to the other organelles and Myelin, peroxisomal signal became more focused, while other organelles signal tended to spread more over the gradient indicating a purification effect of the second OSG.

The 2nd gradient's organelle distribution resembled the first gradient (*figure 30-32*): Alike in the 1st gradient, peroxisomes enriched in 900mM sucrose layer at 1.117g/ml and in the layers additionally added below in the 2nd gradient (950mM). Signal in the

less dense parts of the gradient and at the bottom was comparatively lower in the 2nd gradient. The higher signal intensity of the peak peroxisomal fraction indicated further peroxisome enrichment by the second gradient.

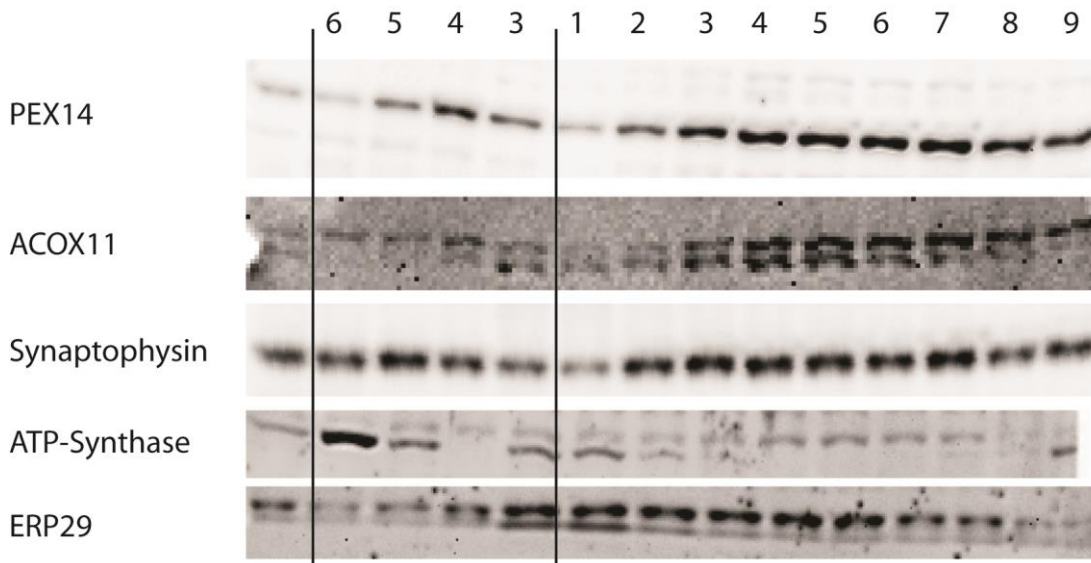


Figure 31: Combination of 2 OSGs with G-Gradient as OSG1 and a second OSG focussing on spreading signal towards the denser fractions until 1.2M sucrose layer (layers: figure 10). Fraction 4 of the first OSG was applied on OSG 2. ER enriched towards the top of the gradient, synaptophysin peaked slightly below. At denser fractions (0,95-1.1M sucrose) peroxisomes denoted by PEX14 and ACOX11 were enriched. Mitochondria were deriched by OSG 1 and were found mainly in the densest fractions of the subsequent gradient.

All organelles were comparatively low concentrated at the less dense fractions of the 2nd gradient.

ER signal peaked at lighter layers (1.083g/ml) than in the 1st gradient, where signal peaked at 1.12g/ml. Below 1.09g/ml signal decreased strongly and reached PNS level at 1.117g/ml.

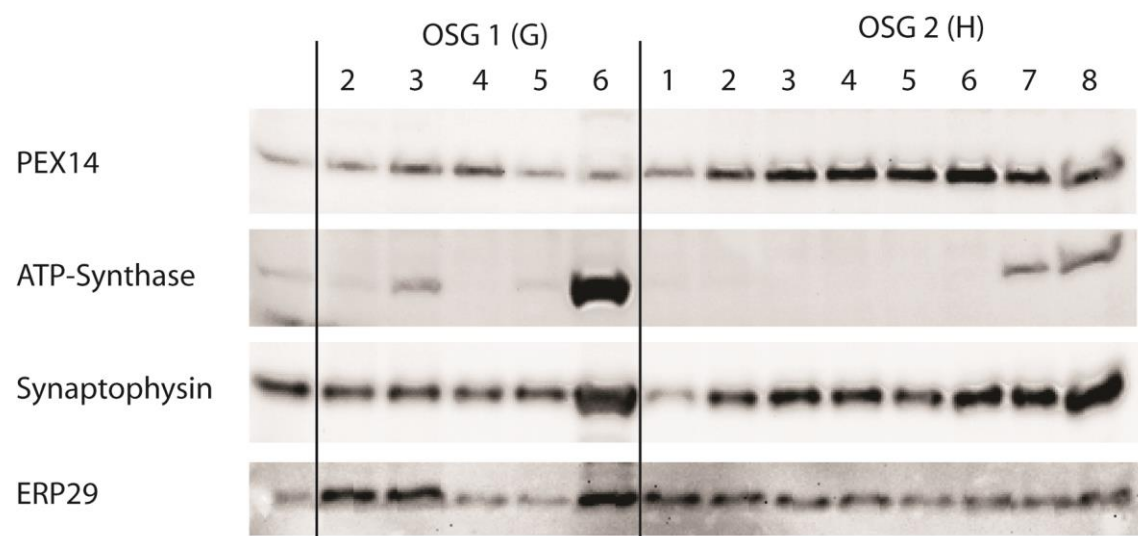


Figure 32: 2 OSGs with 0,95M and 1,1,M sucrose layers (gradient H, figure 10) Fraction 4 from gradient 1 was applied on gradient 2. Adding the additional layers of 0.95M and 1.1M sucrose to the gradient an even further purification of fraction 4 could be achieved (#6). However, compared to the combination of 2 OSGs with less bands, peroxisomes were less focussed.

Synaptophysin signal was spread up at the bottom of the gradient. It reached a plateau below the peroxisome peak.

ATP-Synthase maximum was found at the bottom, whose position corresponds enrichment in the 1st gradient. Signal level exhibited no enrichment compared to PNS in the maximum and clear derichment over the rest of the gradient.

All organelle patters were shifted towards the density of the starting fraction (900mM). Addition of layers approximating the density of the starting fraction improved separation of the organelles. In summary, the 2nd gradient increased peroxisome concentration and purification from ER and mitochondria. However, with sucrose alone, organelles could not be sufficiently purified. As experiments described in *paragraph 3.2.6* showed improvement of separation capability with the use of different gradient media, we pursued this approach.

3.2.8 Further purification on Nycodenz gradients

Compared to sucrose, Nycodenz separated mitochondria less efficiently from peroxisomes. By contrast synaptosome and ER separation were more efficient in Nycodenz (*paragraph 3.2.6*). Thus, we evaluated if a Nycodenz-gradient could be efficiently used for the further separation of the peroxisome-enriched fraction (*figure 28 #4* - 1.115g/ml) of the sucrose-based OSG.

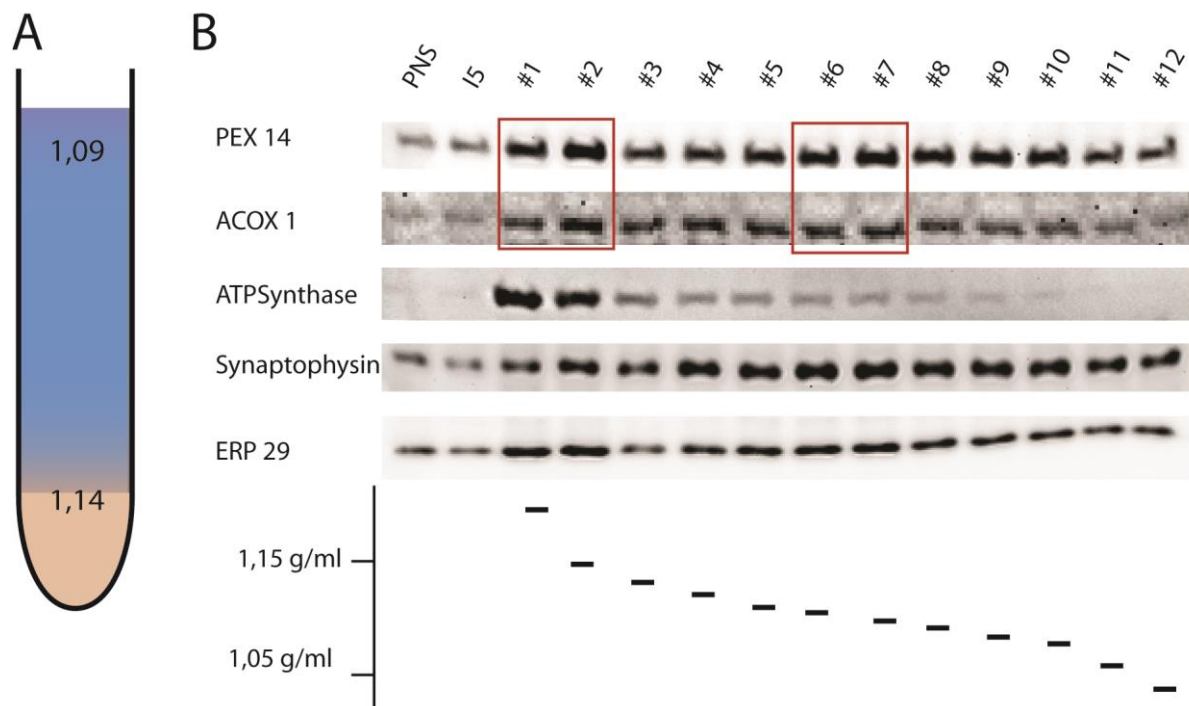


Figure 33 Final separation on continuous Nycodenz gradient 1.09 – 1.14 g/ml
 Continuous Nycodenz gradient 1.09-1.14g/ml with application from the bottom of the gradient in 1,2g/ml Nycodenz. Weight was adjusted with gradient buffer (A). Peroxisomes (PEX14, ACOX1) enriched at the bottom of the gradient (1.14g/ml; #1 and #2) together with mitochondria (ATP-Synthase). A second peak was at 1.10-1.12mg/ml (#6 and #7), which coincided with synaptosome and ER maxima (B). ER (ERP29) and synaptosomes (synaptophysin) extend over the whole gradient. Peroxisome maxima are highlighted with a

Independent from application site or continuity of gradient, peroxisomes accumulated at 2 major densities: The lighter peak was exhibited at about 1.10 – 1.11g/ml, the heavier at 1.14 – 1.17g/ml (*figures 25 and 33, 34*). Peroxisomal membrane protein PEX14, a quite ubiquitous peroxisomal marker, identified the peroxisomal peaks at 1.10 – 1.11 and 1.15 – 1.17g/ml. As both, ACOX and PEX14 were detectable in the

two signal peaks, these could be attributed to intact peroxisomes. The fraction applied on the Nycodenz - gradient did not contain catalase peak signal in the preceding OSG (paragraph 3.2.7.2), which hints at a further peroxisomal subpopulation, that was not split up in the Nycodenz – gradient (paragraph 3.2.7.3). Though localization of peaks remained consistent, the different gradients however differed in how pronounced the peaks were.

Mitochondria, determined by ATP-Synthase, tended to accumulate at the bottom of gradients. In some gradients, this dense ATP-Synthase peak overlapped with the denser PEX14 peak.

ER and synaptosomes tended to accumulate around 1.08-1.09g/ml - further towards the top of the gradient than peroxisomes and mitochondria. With by far lower intensities signal remained present until the bottom of the gradient. In single experiments peak differed and were also present in the denser parts of the gradient but signal was less than 2-times enriched compared to the starting fraction.

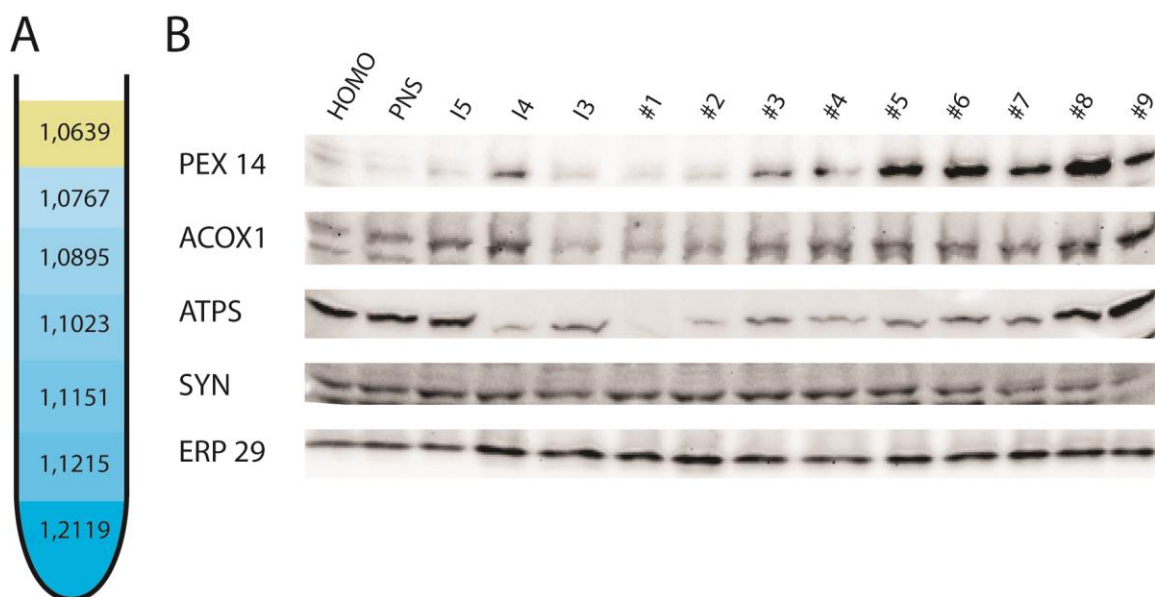


Figure 34: Nycodenz step gradient

(A) Nycodenz step gradient 1.09-1.21g/ml with application of fraction **I4** from the top of the gradient. Application in sucrose (250mM) enriched fraction. Steps were derived from the densities at which the organelles enriched on continuous gradients. (B) Peroxisomes (PEX14, ACOX1) enriched in the second densest fraction of the gradient (1.12g/ml) slightly above mitochondria (ATP-Synthase 1.18g/ml). In comparison to the continuous gradient, only a slight signal increase at 1.10mg/ml was detected. Synaptosomes and ER both enriched in the fractions further to the top of the gradient. Whilst peroxisomes were enriched compared to the fraction derived by OSG, mitochondria concentration remained at a similar level, thus giving further proof of the incapability of Nycodenz gradient to separate mitochondria from peroxisomes. On the step gradient, a better separation from synaptosomes and ER could be achieved than on continuous gradient (figure 33).

The loss of weight in synaptosomes, ER and myelin lighter in sucrose-free Nycodenz-gradient seemed to derive from sucrose leaving the organelles and Nycodenz being incapable to enter them. As mitochondria and some peroxisomes gained weight, an uptake of Nycodenz appeared plausible.

3.2.8.1 Testing for peroxisomal “ghosts”

Peroxisomal marker pattern differed among the membrane protein PEX14 and the matrix proteins catalase and ACOX1 (figures 28, 29 and 33), which might be explained either by dissociation from peroxisomal membrane and matrix – i.e. the formation of

peroxisomal “ghosts” or derive from truly ACOX1 and catalase-free peroxisomes, which have been described in immunofluorescence studies (Ahlemeyer et al., 2007). A third explanation might be the spontaneous release of peroxisomal core enzymes (Antonenkov et al., 2004a).

To differ peroxisomal “ghosts” formed by osmolysis of peroxisomes or osmolarity-dependent spontaneous release of matrix enzymes (Antonenkov et al., 2004a) from ACOX1 or catalase-free peroxisomes, peroxisomes were applied in hypoosmolar solution (*figure 34*). Peroxisomes were reported to exhibit no further release of core enzymes when exposed to pure 16-40% Nycodenz solution (Antonenkov et al., 2004a). When applied in hypoosmolar solution, peroxisomal membrane protein PEX14 enriched at a second peak at 1.05-1.07g/ml apart from the peak at 1.10-1.11g/ml. To a comparatively lower degree synaptosomes and mitochondria were also present. Exhibiting no enrichment of peroxisomal core enzyme ACOX and being only present in gradients, where sample was applied hypoosmolar solutions, these PEX14 signals were likely to derive from peroxisomal “ghosts” (*figure 34*).

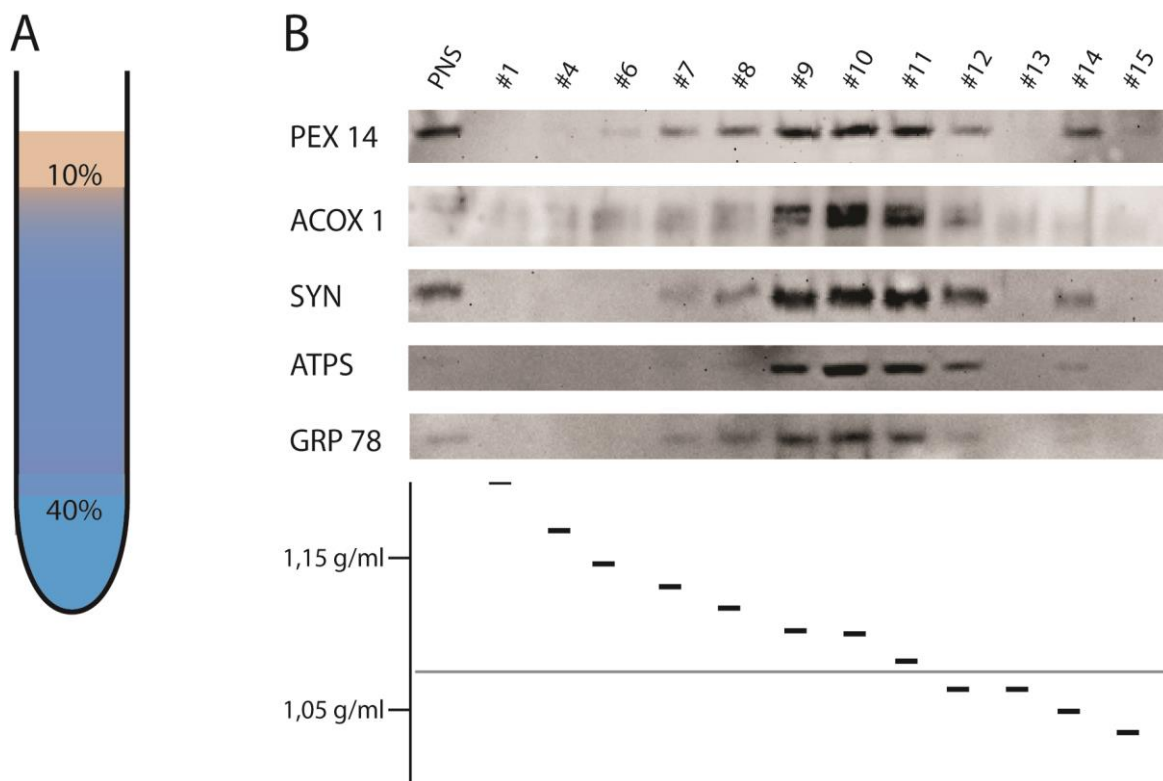


Figure 35: effect of osmolarity on peroxisomes

To further investigate the effect of peroxisomal “ghosts” formed by osmolysis of peroxisomes and differ it from peroxisomes spontaneously releasing their core enzymes (Antonenkov et al., 2004a), peroxisomes were applied in hypoosmolar solution. Peroxisomes were reported to exhibit no further release of core enzymes when exposed to pure 16-40% Nycodenz solution (Antonenkov et al., 2004a). (A) Sample derived by OSG was applied in hypoosmolar, sucrose-free 10% Nycodenz solution on a gradient ranging from 10 to 40% Nycodenz in gradient buffer. (B) Apart from the peak at 1.10-1.11g/ml peroxisomal membrane protein PEX14 enriched at a second peak at 1.05-1.07g/ml. To a comparatively lower degree synaptosomes (Syn, synaptophysin) and mitochondria (ATPS, ATP-Synthase) and ER (GRP78) were also detectable at these low densities. Exhibiting no enrichment of peroxisomal core enzyme ACOX and being only present in gradients, where sample was applied hypoosmolar solutions, these PEX14 signals were likely to derive from peroxisomal “ghosts”.

4 DISCUSSION

Proteomic studies in isolated organelles and interaction assays play an important role in the understanding of organelle function. The isolation protocols described in the previous sections of this thesis should contribute to the deciphering peroxisomal functions. For each protocol separately, integrity of peroxisomes is discussed, and results are compared to published data and integrated into existing knowledge.

4.1 Peroxisome isolation from cultured cells

The developed purification procedure of peroxisomes from cultured cells differs from published procedures (Hosoi et al., 2017) by the use of a continuous gradient as final centrifugation step. The isolation protocol was optimized for the analysis of the interaction between two individual organelles peroxisomes and the ER using a transfection based density-shift-assay.

4.1.1 Resulting marker and organelle pattern in Nycodenz and Optiprep gradients

The identical pattern of the applied peroxisomal markers, PEX14 (surface), PMP70 (surface), Catalase (matrix) and ACOX1 (matrix) in the density gradient and the preceding centrifugations indicates intact peroxisomes. Hence the homogenisation procedure with its frictional force produces intact organelles. During differential centrifugations the majority of mitochondria was removed, whereas ER and peroxisomes accumulated mainly in the fraction applied on density gradient (*figure 16*). ER markers in Optiprep gradient enriched at the less dense fractions of the gradient. They overlapped with the peroxisomal markers. In Nycodenz gradient, peroxisomes enriched at approximately the same density as in Optiprep gradient. ER was enriched mainly at the lighter fractions with more distance to peroxisomes but also partly at denser fractions. The wide range of densities over which ER signal was present in both media might derive from the fractionation of ER tubules and resealing of ER into vesicles of different sizes during homogenisation (Burden, 2008; de Araujo et al., 2015).

While in Optiprep gradient of untransfected cells, signal of mitochondrial, ER and peroxisomal markers widely overlap, the enrichments of these markers are better separated in Nycodenz gradient and exhibit less overlapping signal. In the peroxisomal peak fractions, even no mitochondrial signal could be detected. Hence, Nycodenz is better suited as gradient medium for the final continuous gradient. Optimum gradient range could be determined to 1.14 to 1.19g/ml, which is denser than the gradients used in brain tissue.

4.1.2 Peroxisome-ER interaction – application of the new developed protocol

Among ER and peroxisomes a close interaction is known. Several metabolic pathways, e.g. ether phospholipid and polyunsaturated fatty acid biosynthesis, include reactions located in peroxisomes and ER. Furthermore, peroxisomes can form by growth and division (fission) from pre-existing organelles and by de novo synthesis through vesicle formation from the ER (Costello and Schrader, 2018; Dimitrov et al., 2013; Islinger et al., 2012b). As peroxisomal membrane lipids derive in majority from ER and several peroxisomal membrane proteins appear to be translated on ER-bound ribosomes, direct contact might be required for peroxisome biogenesis as well.

Ultrastructural studies confirmed that peroxisomes are often located close to ER tubules and suggest of a physical interaction (Fahimi et al., 1993; Gulyas and Yuan, 1977; Novikoff et al., 1972; Zaar et al., 1987).

Proteins mediating this interaction and association and the exact interaction sites were not completely known yet. A genome-wide interaction study (Huttlin et al., 2015) identified a potential binding of the exclusively peroxisomal protein ACBD5 and the protein VAPB located on ER:

VAPB is a member of the VAP-family of ER membrane proteins. They are known to be involved in membrane contact of ER to mitochondria (De Vos et al., 2012), Golgi apparatus (Kawano et al., 2006; Mesmin et al., 2013), vesicles directed to plasma membrane (Jansen et al., 2011) and endosomes (Rocha et al., 2009). All members of this protein family consist of a C-terminal trans-membrane domain, indicating its nature as a tail-anchored transmembrane protein, and an N-terminal major sperm protein (MSP) domain (Lev et al., 2008). A highly conserved sequence contained in the MSP-domain (Lev et al., 2008) indicates its crucial role in VAP function. The MSP-domain in VAP-proteins interacts with SNAREs, viral proteins and FFAT (double phenylalanine in an acidic tract)-motif-containing proteins (Kawano et al., 2006; Lev et al., 2008; Loewen et al., 2003; Murphy and Levine, 2016). Colocalization of VAPB with peroxisomal proteins in fluorescence microscopy studies indicate an interaction with peroxisomes (Hua et al., 2017).

The exclusive peroxisomal protein ACBD5 contains such a FFAT-motif. Hence it is a possible binding partner for VAPB mediating peroxisome-ER-interaction. Loss of binding when FFAT-motif is mutated (Costello et al., 2017a) and persistence in mutations of Acyl-CoA-binding site indicate an interaction via the FFAT-motif (Kragelund et al., 1999; Nazarko et al., 2014). Interaction was also shown by an increase in peroxisome mobility in ACBD5 or VAP depleted cells (Costello et al., 2017a; Hua et al., 2017).

Furthermore, a direct interaction between ACBD5 and VAPB was shown in *in vitro* binding assays (Costello et al., 2017a).

Both these independent experiments confirmed the results we achieved in our experiments: After co-expression of GFP-ACBD5 and Myc-VAPB in HepG2 cells we were able to demonstrate a shift in density of ER and peroxisomes towards a common fraction on the final Nycodenz gradient of our isolation protocol. Experiments with single expression of one of these proteins did not result in the density shift described. Hence the shift could only be attributed to an interaction and not to a gain in density through e.g. a higher protein load of the organelles or a change in organelle morphology.

Interestingly, peroxisomes purified from livers of ACBD5-deficient mice, show a converse behavior. In this situation, considerably higher amounts of peroxisomes were found in the high-density region of Optiprep gradients if compared to wild-type controls (Darwisch et al., 2020). The results suggest an intricate interaction between peroxisomes and the ER facilitated by the tethering proteins ACBD5 and VAPB, which influence the density of peroxisomes by attached fragments of the ER, which can even be found in isolated peroxisomes analyzed by electron microscopy (Zaar et al., 1987)

4.1.3 Function of interaction

Proof of interaction among ER and peroxisomes via VAPB and ACBD5 gives an explanation to the observed close ultrastructural association among peroxisomes and ER (Costello et al., 2017a). Increased peroxisomal mobility and lower peroxisomal membrane growth in absence of VAPB and/or ACBD5 suggest, that the interaction could play an important role in organelle positioning and delivery of membrane lipids required for peroxisome growth (Costello et al., 2017a; Hua et al., 2017; Wang et al., 2018). Concerning shared metabolic pathways among ER and peroxisomes a direct interaction would be increase the efficacy of these metabolic pathways. So, plasmalogen synthesis is impaired when the VAPB-ACBD5 tether is disrupted (Hua et al., 2017). ACBD5 appears also to be involved in VLCFA metabolism, as it is reported that ACBD5 can bind VLCFAs in vitro (Yagita et al., 2017). In case reports, cytosolic VLCFA-accumulation was reported in ACBD5 deficiency (Abu-Safieh et al., 2013; Ferdinandusse et al., 2017; Yagita et al., 2017). With ACBD5 involved in ER-PO-binding (Costello et al., 2017a), interaction in lipid metabolism appears possible.

Between VAPB and ACBD4 a similar protein interaction was demonstrated (Costello et al., 2017b). As ACBD5-knockdown affected peroxisomal mobility and lowered peroxisomal membrane growth even in the presence of ACBD4 (Hua et al., 2017), the tether appears not to be capable to replace VAPB-ACBD5 interaction.

4.2 Peroxisome isolation from murine brain

Organelle isolation from tissue gives additional insights to organelle function. In contrast to cell culture, where cells are grown in a defined environment, organelles separated from a tissue are influenced by the interactions among the different cell types in the tissue and the whole animal's metabolism. While cultured cells are best suited for experiments involving a single or few cell types, organelles isolated from tissue can be used to examine the organelles' role in the interaction with various cell types forming the tissue.

Brain tissue consists of various cell types and subtypes with specific distinct functions: Metabolic pathways of glial cells and neuronal cells are intertwined with each other, e.g. in the regulation of released neuronal transmitters, or are only exerted in a specific cell type like myelin formation, D-serine degradation (Wolosker et al., 2008), ROS-metabolism, VLCFA formation and metabolism.

Peroxisome derived diseases, e.g. peroxisomal biogenesis disorders (PBD) or single enzyme deficiencies often go along with a pronounced neuronal phenotype (Braverman et al., 2016; Darwisch et al., 2020; Schrader et al., 2015; Steinberg et al., 2006; Trompier et al., 2014; Wanders, 2014; Wanders et al., 2015; Waterham et al., 2016). CNS manifestation includes abnormal myelination (Baes and Aubourg, 2009), demyelination (Steinberg et al., 2006), axonal degeneration and neuronal migration defects (Faust et al., 2005; Power and Moser, 1998; Waterham et al., 2016). These alterations associated with peroxisome malfunction hint at the crucial role of peroxisomes in brain, making brain peroxisomes an important field in peroxisome research.

To be of use in disease models and in brain research, mice were chosen for the development of brain peroxisome isolation protocol.

Organelle isolation from tissue bears different difficulties than isolation from cultured cells. In a first step the tissue must be disrupted and in addition to the separation from cellular contents organelles must be purified from the extracellular matrix contained in the sample. Furthermore, tissue specific properties must be incorporated in the organelle separation protocol.

Pre-existing protocols were developed for use in nascent or new-born mouse or rat brain, before the onset of the major steps in myelination of the axons (Cimini et al., 1993; Gaunt and de Duve, 1976; Kovacs et al., 2001; Lazo et al., 1991; Posset et al., 2015; Singh et al., 1989; Singh et al., 1993). Our protocol was intended to extend the field of investigation on the use in a fully developed brain.

4.2.1 Comparison of peroxisome isolation from adult mice with those published for young mice

As a starting point, we tested the peroxisome purification protocol developed for young mice from 0 to 25 days of age by Kovacs et al (Kovacs et al. 2001) for effectivity in adult mice. The comparison of the results derived by us (*paragraph 3.2.1*) to those published by Kovacs et al (Kovacs et al., 2001) indicated differences among adult and infant mice.

The homogenisation used by Kovacs et al maximized yield but at the cost of relative peroxisome concentration, which was higher after the first centrifugation than in the mixed fraction (*paragraph 3.2.2*).

In the differential centrifugation steps, our results resembled those described by Kovacs et al: Like published by Kovacs for young mice, the majority of mitochondria was concentrated in the “mitochondrial fraction” **M** (Kovacs et al., 2001). Maximum myelin concentration determined by myelin basic protein (MBP) antibody in our experiments and by proteolipid protein antibody and 2',3'-Cyclic-nucleotide 3'-phosphodiesterase (CNPase) activity by Kovacs et al. (Kovacs et al., 2001) was obtained in the “mitochondrial fraction” **M**.

Both fractions **L** and **P** were described to obtain some myelin proteolipid protein (Kovacs et al., 2001). Even after removal of myelin by the myelin removal gradient, fractions were reported to contain still little myelin (Kovacs et al., 2001). Majority of myelin was detected in the 0.25M/0.85M sucrose interphase, (Kovacs et al., 2001) but even in the final supernatant (**FS**) some myelin was still detected (Kovacs et al., 2001). This distribution pattern coincided with the results presented in this work for adult mice. In contrast to the experiments published by Kovacs et al (Kovacs et al., 2001), highest peroxisome concentration in our experiments could not be determined in the fractions **L** and its derivate **L2** but in **P** and its derivate **P2**. While fraction **L2** contained peroxisomes sedimenting among 5.500 x g and 18.000 x g, fraction **P2** contained peroxisomes sedimenting among 18.000 x g and 106.401 x g.

Sedimenting at higher centrifugal force, most peroxisomes of adult mice appear to have a lower sedimentation rate than those of mice aged less than 14 days. With the sedimentation rate correlating with particle size and weight, this demonstrates that adult mice's peroxisomes appear to be smaller and lighter.

This observation of lighter peroxisomes in differential centrifugation in sucrose coincides with the results of the Nycodenz gradient: On the Nycodenz gradient, peroxisomes obtained by preparation from adult mice were found at maximum densities between 1.154 to 1.173g/ml and were, hence, much lighter than those described for infant mice, (1.167-1.2 g/ml) (Kovacs et al., 2001). A 40-fold enrichment of peroxisomes (Kovacs et al., 2001) could not be reproduced as enzyme activity of

marker enzyme catalase was not strong enough detectable in adult mice brain samples.

In our experiments also peroxisomal markers (PEX14, ACOX1) extended over the whole gradient length and exhibited less distinct enrichment than reported in young mice (Kovacs et al., 2001). Together these peroxisomal markers indicate that the preexisting procedure appears not to be capable to focus peroxisomes. This might derive from a higher variability of peroxisomes.

The observed ACOX signal, which enriched more clearly at the denser fractions of the gradient, suggests heterogeneity of peroxisomal protein content, i.e. the presence of peroxisomal subpopulations, containing less of beta-oxidation enzymes. A different explanation might be a partial disruption of peroxisome membranes during the isolation procedure resulting in a dissociation of matrix proteins. As peroxisomal membrane protein (PEX14) and non-membrane bound peroxisomal enzymes (i.a. ACOX) were not enriched in cytosolic fractions disruption appears implausible. Furthermore, it would remain unclear why only peroxisomes from adult mice should be affected, when identical frictional forces in homogenisation, centrifugation forces and solutions are used (*paragraph 3.2.1 and 3.2.2*). Additionally, the intentionally produced peroxisomal “ghosts” appear to enrich in less dense fractions (*paragraph 3.2.8.1*). Hence peroxisomal subpopulations appear to be more plausible. This hypothesis is supported by the results published (Ahlemeyer et al., 2007; Kovacs et al., 2001), which describe an alteration in protein expression and hence peroxisomal function during brain development.

As peroxisomes in our experiments were less dense than described, the relative position to mitochondria was changed in the gradient: While in the results published by Kovacs et al peroxisomes were denser than mitochondria (Kovacs et al., 2001), in our experiments mitochondria reached equilibrium at slightly higher densities than peroxisomes in adult mice. With maxima so close, signals of mitochondria and peroxisomes partially overlapped.

Whereas ER signal in our experiments extended over the whole length of the gradient, only the lighter half of the gradient was described to contain the majority of the immunoreactivity for Grp94 (ER) with decreasing intensity towards the denser fractions (Kovacs et al., 2001).

Synaptosomes, which were not investigated by Kovacs et al (Kovacs et al., 2001), enriched clearly towards the top of the gradient and separated well from peroxisomes. They might have been a part of the CNPase determined membranes, amongst others myelin, which were described to be only abundant in the light parts of the gradient (Kovacs et al., 2001).

While ER and mitochondria were most efficiently separated from peroxisomes in the differential centrifugation series, the Nycodenz gradient was better suited to deplete peroxisomes from Synaptosomes.

In summary, the procedure published by Kovacs et al. did not achieve an appropriate separation of peroxisomes from other organelles in adult mice. The fractions with highest peroxisomal content were still contaminated by mitochondria and ER. Only synaptosomes could be sufficiently separated from peroxisomes.

4.2.2 Differences in physical properties of peroxisomes

Though peroxisomes could not be sufficiently purified, differences in physical properties of peroxisomes were observed.

Sedimenting at higher centrifugal force, most peroxisomes of adult mice have a lower sedimentation rate than those of mice aged less than 14 days. With the sedimentation rate correlating with particle size and weight, this demonstrates that adult mice's peroxisomes are smaller and lighter. This is also supported by the peroxisome marker maximum on Nycodenz gradient, which is also shifted to less dense fractions than described by Kovacs et al (Kovacs et al., 2001).

The observed lower sedimentation rate in differential centrifugation, which hints at a higher peroxisome content of lower size and weight in adult brain might represent changes in enzyme content: Catalase positive-peroxisomes are larger than catalase-negative ones (Holtzman, 1982). A further size difference exists among catalase-positive neuronal and glial peroxisomes (Holtzman, 1982). As catalase content decreases with the end of myelination during adolescence (Ahlemeyer et al., 2007; Arnold and Holtzman, 1978; Lazo et al., 1991), relative content in these large peroxisomes decreases. With Kovacs et al focus on isolation of peroxisomes at the peak of myelination (Kovacs et al., 2001), the leading peroxisomal subpopulation might represent peroxisomes in oligodendrocytes containing proteins involved in myelin formation.

The observed differences in physical properties hint, that peroxisomes, organelles and brain composition differ between juvenile and adult mice. Peroxisomal function seems to alter during adolescence and with them peroxisomal protein composition. In addition, the abundance of peroxisomes decreases by half during postnatal development, also exhibiting prominent differences between distinct brain regions and cell types (Ahlemeyer et al., 2007). Whereas peroxisome content decreases in neurons, it remains constant in ependyma, epithelial cells of the choroid plexus and glial cells (Ahlemeyer et al., 2007). In hippocampal neurons a decrease in neuronal peroxisome content could also be observed with aging (Fanelli et al., 2013). With lower peroxisome content in the brain of adult mice will therefore lead to higher contamination rates in the peroxisome enriched fractions.

Kovacs et al determined catalase enzyme activities to identify peroxisomal fractions (Kovacs et al., 2001). Of note, catalase abundance exhibits a clear age-dependent decline, which explain why catalase activities could not be successfully performed in adult brain samples in this work. Whereas Kovacs et al. detected significant catalase concentrations (Kovacs et al., 2001), catalase could only be detected in samples with high protein concentration in our experiments. Signal intensity per protein content is extraordinarily low, which hints at a decrease in content of catalase-positive peroxisomes or catalase expression. This decrease of catalase-positive peroxisomes has been reported for neurons in cerebrum and cerebellum (Arnold and Holtzman, 1978), oligodendrocytes (Lazo et al., 1991) and white matter in general (Ahlemeyer et al., 2007). Two distinct hypotheses address the change in catalase content: Houdou et al. suggest a close relationship among myelinogenesis in the developing human brain and catalase-positive glia (Houdou et al., 1991), which is supported by the decrease of catalase-positive particles in oligodendrocytes with aging (Lazo et al., 1991).

The decrease of high levels of catalase at birth and during postnatal brain development, are hypothesized to protect the neurons from oxidative injury during birth (Ahlemeyer et al., 2007). Ahlemeyer et al were able to relate the high abundance of

peroxisomes and the observed peak of catalase around birth to the course of nerve growth factor expression (Ahlemeyer et al., 2007; Nikolaou et al., 2006), which has been shown to stabilize the catalase mRNA level in the brain (Sampath and Perez-Polo, 1997) and to induce peroxisomal proliferation in Hep-G2 cells (Schrader et al., 1998).

Other peroxisomal enzymes also alter with aging. Number of ACOX1-positive peroxisomes decreases almost ubiquitously in postnatal murine brain (Ahlemeyer et al., 2007). The number of peroxisomes stained with immunofluorescence by peroxisomal thiolase decays too apart from ependyma (Ahlemeyer et al., 2007). The extent varies among tissue and area in the central nervous system (Ahlemeyer et al., 2007).

These observations in PEX14, catalase, ACOX1 and peroxisomal thiolase immunofluorescence indicate a decrease of peroxisome content and shift in peroxisomal enzyme constitution, which denotes for a functional change. Hence it appears plausible, that physical properties, such as mass, size, and density, which affect behaviour in centrifugation, alter as well. This explains the shift of the density maximum to lighter fractions as well as the differing peroxisomal pattern. The broader extent of peroxisomal signal in the gradient, however, might also be explained by the change in detected peroxisomal proteins (*paragraph 4.2.4*).

4.2.3 Other alteration in aging

Apart from changes in peroxisomes, the general molecular composition of murine brain alters as well. Myelin content, marked by MBP and CNPase of oligodendrocytes, increases during postnatal development (Ahlemeyer et al., 2007; Cuzner and Davison, 1986). Myelin is the major contaminant, which can inhibit organelle separation on Nycodenz gradient (Kovacs et al., 2001). Its removal is the major difficulty in brain peroxisome purification (Lazo et al., 1991). The phase of myelin and membrane production during growth is also reflected by the increased ER content (Silvestre et al., 2009). The expression of ER markers increases in situations of high proliferation and membrane expansion (Silvestre et al., 2009). Raised chaperone expression in proliferative situations is thought to reflect protein synthesis for membrane proteins and proteins for secretion (Silvestre et al., 2009).

As response to a lack of need for active membrane biogenesis by the cell, ER shrinks by autophagy (Silvestre et al., 2009). In accordance with the decrease, relatively more ER membrane marker proteins are present in embryonic brain cells than in adult cells (Silvestre et al., 2009). This change, however, only affects abundance, nor size, mass or density. As the tubular ER network is also fractionated by homogenisation, particle size depends mainly on homogenisation. Though antibody testing results vary, the broader distribution pattern in our experiments coincide partly with the enzyme assay results by Kovacs et al. (Kovacs et al., 2001).

Mitochondria are reported to undergo activity-dependent alterations (Williams et al., 1998). With stimulation via NMDA receptors, close mitochondria alter their shape and size (Peng et al., 1998). Other alterations concerning mitochondrial shape and abundance have been reported in response to stimulation with glucocorticoids and estrogen (Ahmad et al., 2013; Hara et al., 2014; Picard and McEwen, 2014). Age and redox state dependent mitochondrial alterations include a shift from tubular to blob or donut-shaped form (Ahmad et al., 2013; Hara et al., 2014; Liu and Hajnoczky, 2011; Picard and McEwen, 2014). Increase of donut-shaped mitochondria has been reported to be associated with decline of working memory (Hara et al., 2014). In summary, adult brain mitochondria show a higher variability in morphology than those of infant mice.

Hence, the differences in most organelles can be attributed to changes during aging. The broader distribution pattern of peroxisomes over almost the whole gradient length might more probably derive from the abundance of peroxisomes of different density than from the use of a different antibody.

4.2.4 The issue of different antibodies

Kovacs and coworkers identified peroxisomes by the peroxisomal enzymes catalase, acyl-CoA oxidase, sterol carrier protein 2 and HMG-CoA-reductase (Kovacs et al., 2001). In our experiments, we preferentially used the peroxin PEX14, which is an inherent part of peroxisome formation machinery (Grant et al., 2013). Whereas enzyme content varies, peroxines are present on all peroxisomes. I.e., catalase and DAAO expression are lower in adult than in nascent mice (Ahlemeyer et al., 2007; Holtzman, 1982). Hence, the intensity of the PEX14 immunofluorescence staining in neurons and astrocytes is higher than that of peroxisomal enzymes (Ahlemeyer et al., 2007). With PEX14 and additional to peroxisomal enzymes, most peroxisomes are labelled. This enables the detection of further peroxisomal subpopulations, for example from Purkinje cells, which are neither detectable with catalase nor ACOX or peroxisomal thiolase (Ahlemeyer et al., 2007). High signal intensity and ubiquitous abundance make Pex14 a suitable marker protein for identification of all peroxisomes in the central nervous system, especially those in neurons (Ahlemeyer et al., 2007). However, distinguishing among peroxisomal subpopulations is not possible with PEX14 labelling. As all subpopulations are labelled, the detected signal is a summarized signal and is broader than that of an enzyme expressed in a subpopulation. Signal differences observed among PEX14 and the peroxisomal enzymes in our experiments affirm this hypothesis. However, the alteration in density maximum cannot be fully explained by this effect. A more plausible explanation might be an alteration in the peroxisomal subpopulation pattern with age as described in fluorescence microscopy studies (Ahlemeyer et al., 2007).

The antibodies used for detection of the other organelles vary as well but exhibit less significant differences. In both experiments established markers and antibodies were used. Mitochondrial markers glutamate dehydrogenase is located on mitochondria and nuclei (Lai et al., 1986), whereas ATP-Synthase is solely located in mitochondria (Lee et al., 1990). As nuclei are removed early in the centrifugation, this double expression is of minor importance. ER markers Grp94 (Glucose-regulated protein 94) (Marzec et al., 2012) and ERP29 (Sargsyan et al., 2002) are both chaperones located in the lumen of ER and do not contain trans-membrane domains. With ER being fractionated during homogenisation, differences are more likely to derive from this procedure. Hence, the main differences in signal pattern of mitochondria and ER appear not to derive from the antibodies. As Kovacs et al did not screen for synaptosomes (Kovacs et al., 2001), these results could not be compared.

4.2.5 Peroxisome separation from adult mice's brain tissue

To overcome the insufficient purification of peroxisomes from adult mice with the protocol developed for pups, new protocols were developed investigating each single step of the isolation protocol.

4.2.5.1 Homogenisation

Brain tissue is homogenised mechanically as brain tissue is not sufficiently disrupted chemically (Burden, 2008). Containing a complex extracellular matrix, tissue is not primarily sensitive to chemicals (Burden, 2008). Introducing unwanted molecules in the lysate and/or denaturing proteins (Burden, 2008), they render them undesirable in organelle or protein purification schemes.

Multiple rounds of mechanical homogenisation allow a better disruption of tissues (Burden, 2008; Graham, 2002a), however, the applied shearing forces will as well destroy intracellular membrane bounded particles (Graham, 2002a). Furthermore, shear forces may cause nuclear rupture and DNA release causing aggregation and loss of material into the nuclear pellet (de Araujo et al., 2015).

Thus, it is required to establish a homogenisation strategy balancing efficient tissue dissociation and organelle preservation. In this study, it was demonstrated that in adult brain repeated rounds of homogenisation to increase organelle yield is at a high cost in peroxisome preservation (*figure 16*). Hence this procedure was reduced to a single homogenisation and a centrifugation with 1000 x g, sufficient to remove nuclei (Sporn et al., 1962) and debris.

4.2.5.2 Myelin removal

With the increase in myelin content (Cuzner and Davison, 1986; Kovacs et al., 2001) myelin removal gains utmost importance. As the presence of myelin impairs peroxisome (Kovacs et al., 2001) and other organelle isolation (Islinger et al., 2011), this step is crucial. The myelin removal gradient described by Cimini et al (Cimini et al., 1993) and used in further publications (Kovacs et al., 2001) was adapted, to decrease the remaining myelin concentration in the subcellular fractions. The alteration in lipid composition of myelin with aging starting at day 15-20 in rat brain and the appearance of a new dense subfraction of myelin might cause this effect (Cuzner and Davison, 1986). Starting with day 15-20, the dense myelin fraction increase compared to the light one (Fujimoto et al., 1976).

As described in literature (Cimini et al., 1993; Kovacs et al., 2001), in our experiments myelin enrichment in a fluffy layer floating above at least 700mM sucrose could be examined. Organelle markers enriched mainly at denser layers. Fractions above the 700 mM sucrose layer contained a substantial amount of myelin, but low concentrations were still present in denser layers. Variation in density of the lighter layer, to which the boarder was formed did not affect the formation of the visible myelin layer. This corroborates with the observations in myelin subfractionation, where myelin was found in bands at 0.4, 0.5-0.6 and 0.7M sucrose, of which the visible fluffy main layer was the one in 0.5-0.6M sucrose (Cuzner and Davison, 1986). Similar subpopulations were also described by Cruz et al. (Cruz and Moscarello, 1985). As morphological correlate of the different myelin fractions, electron microscopy showed that the lighter myelin fractions contained multilamellar, compact myelin, whereas the denser fractions contained smaller myelin fragments with fewer lamellae (Cruz and

Moscarello, 1985; Fujimoto et al., 1976). To avoid myelin contamination the further processed fraction was the 0.9M or denser fraction.

However, some remaining myelin could be still found in the 0.9 M sucrose fraction. In summary, the myelin depletion gradient leads to a relative but not absolute reduction of myelin in the organelle layers (and pellet) of the gradient. Remaining myelin might be associated to the lipid bilayer of other organelles. A further explanation is that during homogenisation in sucrose myelin forms distinct subpopulations with different composition which enrich at different densities (Cruz and Moscarello, 1985). To further decrease myelin content, we repeated the myelin removal step by addition of a 500mM sucrose layer on top of the subsequent organelle separation gradient (OSG). Hereby, a distribution of myelin to similar densities like in the myelin depletion gradient could be detected, which supports the hypothesis that remaining myelin derives from a saturation effect in myelin removal gradient.

4.2.5.3 Addressing the issue of peroxisome isolation by differential centrifugation

Tests with differential centrifugation were performed according to the following approach: initial myelin removal (Cimini et al., 1993) and several differential centrifugation steps were combined with a final density gradient centrifugation. Major differences in procedure compared to protocol 1 (Kovacs et al. 2001) were - in addition to the change in order of debris and myelin removal - the forces applied in differential centrifugation steps. After mitochondria removal, sample was split into a heavy and a light peroxisomal fraction, which were purified by further centrifugation.

To reduce the mitochondria concentration by differential centrifugation, centrifugation velocity was elevated if compared to protocol 1 (Kovacs et al. 2001). While mitochondria could be indeed successfully reduced by these changes, the separation of peroxisomes from other organelles was not increased. The low effect on synaptosome and ER concentration might derive from the fact, that the observed ER-particles and synaptosomes are generated by fractionation and resealing of ER- and cell-membranes during homogenisation. More promising results for the separation of ER and synaptosomes could be observed on continuous gradients after the differential centrifugation (*paragraph 3.2.6 and 3.2.8*), thus, gradient centrifugation seems to be advantageous. As a similar purification from mitochondria could also be achieved by the organelle separation gradient and as each centrifugation step bears the risk of organelles sticking together, a differential centrifugation for mitochondria removal was omitted in subsequent protocols.

4.2.6 Density gradient centrifugation in adult mice's brain peroxisome isolation - differences among the gradient media

As the exact density and sedimentation properties of brain peroxisomes have not been determined so far, peroxisome purification was amended by density gradient centrifugation. It was carried out after preliminary centrifugation steps to optimize peroxisome yield in relation to applicable organelle amounts.

The separation medium-dependent differences in the densities at which organelles enrich highlight the important role of the separation medium for organelle purification. Percoll, which is also used in organelle separation was not tested because

peroxisomes and endoplasmic reticulum band at the same densities and cannot be resolved (Graham, 2002b).

The tested gradient media, sucrose, Nycodenz and Optiprep are the gradient media commonly used in density gradient centrifugation (Graham, 2015). The three gradient media differ in molecular mass. With a molecular mass of 342.30 g/mol sucrose is by far lighter and smaller than Nycodenz (821 g/mol) (Rickwood et al., 1982) and Optiprep (1550 g/mol) (Graham, 2015).

As peroxisomes are osmotically sensitive particles (Antonenkov et al., 2004a), osmolarity of medium plays an important role. According to van't Hoff equation osmotic pressure depends on the molar concentration (n/V) of the solution and the absolute temperature (T) (Rasouli, 2016). R denotes for the general gas constant

$$P = \frac{n}{V} * R T$$

Density of a solution does not affect its molarity, so that solutions of a certain density made from molecules of different molecular mass exert a different osmotic pressure (Graham, 2015; Manner and Islinger, 2017; Rasouli, 2016):

Nycodenz has about the 2.4-fold molecular mass of sucrose, Optiprep about the 4.5-fold. Hence a sucrose solution contains the 2.4-fold number of molecules per litre than a Nycodenz solution of the same density. In the case of an Optiprep solution it is even the 4.5-fold. Using van't Hoff equation, this would result in a 2.4-fold or 4.5-fold osmotic pressure, which would be exerted on the organelles. This would result in a higher water-flow out of the organelles and a shrinking of those. The shrinking of the organelles results in a higher concentration of the solid parts of the organelles and hence a gain of weight per volume – a gain of density. According to the medium properties organelles are supposed to enrich at higher densities in sucrose solutions than in the other solutions.

The problem going along with the osmotic pressure is osmolysis, to which peroxisomes are quite sensitive (Antonenkov et al., 2004a) In order to overcome problems concerning osmolysis, as Nycodenz and Optiprep solutions with little density would lead to hypoosmolar solutions, 250mM sucrose was added to these solutions (Graham, 2015). When buffered with sucrose isoosmolar solutions, optiprep solutions remain isoosmolar (Graham, 2015).

4.2.6.1 Sucrose

Brain peroxisomes, like other organelles, are freely permeable to sucrose (Gaunt and de Duve, 1976). Hence, organelles increasingly take up gradient medium during centrifugation and consequently enrich at higher densities than in other media (Ford et al., 1982). Compared to the other gradient media, the highest concentrations of sucrose are needed to reach a certain density (Graham, 2015). Hence, sucrose solutions have the highest osmolarity and exert highest osmotic pressure (Graham, 2015). Hypoosmotic solutions causing cells to disrupt were not applied.

In continuous sucrose gradients, the peroxisomal marker PEX 14 enriched at a maximum of 1.105g/ml with signal decrease towards the denser fractions of the gradient. Mitochondria enriched at 1.151g/ml and 1.165g/ml. Endoplasmic reticulum signal peaked at 1.105g/ml but was present from the lightest fractions of the gradient and decreased towards the denser fractions. Synaptosomal marker synaptophysin exhibited an even distribution. In summary, sucrose gradients were capable to clearly separate mitochondria from peroxisomes but failed in separation from ER and synaptosomes.

Peroxisomes in our experiments hence were by far lighter than the DAAO-positive or catalase-positive peroxisomes of newborn mice purified on sucrose gradients, which enriched at 1.18g/ml and 1.16g/ml (Gaunt and de Duve, 1976). This coincides with the findings of a lower sedimentation rate in differential centrifugation which points to a lower peroxisome size and density than that of newborn mice. With the density on continuous sucrose gradient corresponding the 0,9M sucrose layer at which peroxisomes enrich in OSG and myelin depletion gradient and the presence of peroxisomal matrix proteins in these fractions (*paragraph 3.2.7.1*) the detected signal is probable to derive from intact peroxisomes and not from peroxisomal ghosts. As peroxisomes are reported to remain intact at that osmolarity (Cimini et al., 1993; Kovacs et al., 2001) hyperosmolar damage appears improbable.

The mitochondrial peak observed in this study (1.151g/ml -1.165g/ml.) coincides with former values published for brain tissue of about 1.165g/ml (Whittaker, 1967). This is lighter than the equilibrium density in other tissues, for example 1.19-1.21g/ml in jejunum (Ford et al., 1982).

The broad distribution of synaptophysin corresponds well to the results by Whittaker et al, where synaptosomes enriched between 1.11-1.19g/ml (Whittaker, 1967).

As well, ER is reported to equilibrate at the broad range of 1.09-1.15g/ml in sucrose gradients (Ford et al., 1982). Even though these published densities do not derive from brain tissue, the broad distribution of ER, which might derive by the fractionation of the ER during homogenisation, could also be observed in our samples as well as the relative orientation of mitochondria towards the denser parts of the gradient.

4.2.6.2 Optiprep

In Optiprep gradient, peroxisomes enriched at 1.103-1.107g/ml. Mitochondria enriched at the same densities and below, which approximates the reported densities of brain mitochondria (1.12g/ml) (Bergemalm et al., 2010). In comparison to organelles isolated from rat liver tissue (Graham, 2002b; Islinger et al., 2010; Islinger et al., 2006), peroxisomes and mitochondria were both less dense. Synaptosomes predominated in the lighter fractions of the gradient but were present throughout it, ER signal only slightly differed from peroxisomal signal. While peroxisomes and mitochondria could not be separated, it worked well for the separation of synaptosomes from peroxisomes. With peroxisomes not osmotically disrupted in Optiprep solutions without major osmoles (Antonenkov et al., 2004a) and Optiprep remaining isoosmolar when buffered with sucrose isoosmolar solutions (Graham, 2015), osmolar cell damage in our experiments is implausible.

4.2.6.3 Nycodenz

In Nycodenz, the peroxisomal marker PEX14 can be found across a wide density range: 1.06-1.14g/ml.

All these peroxisomal fractions are by far lighter than those achieved by protocol 1, which peak between 1.154 to 1.173g/ml or those described by Kovacs et al for nascent mice (Kovacs et al., 2001). This difference might derive from the difference in sedimentation rate in the preparation of the fractions applied on the gradients. While in the tests of gradient media performed after pre-processing with differential centrifugation peroxisomes sedimenting between 11.000 x g and 70.000 x g were tested, the peroxisomes according to the protocol described by Kovacs et al (Kovacs et al., 2001) (protocol 1), peroxisomes sedimenting between 5.500 x g and 18.000 x g

were applied. As a higher sedimentation rate equals a higher density and particle size, it is plausible, that the peroxisomes, which were pre-processed according to protocol 1, enrich at higher densities than those derived by protocol 2.

A similar difference could be observed in mitochondria, which are enriched towards the bottom of the gradient. In preparations derived from protocol 2, mitochondria are accumulated in fractions denser than 1.11g/ml, in those derived from protocol 1 mitochondrial marker peaks at densities from 1.167 to 1.193g/ml. The latter fits well to the equilibrium density for jejunal mitochondria (Ford et al., 1982).

Endoplasmic reticulum tends to accumulate in the lighter fractions of the gradients which was also reported by Kovacs et al (Kovacs et al., 2001).

These findings confirm those from oligodendrocyte culture, where peroxisomes could be well separated from ER and mitochondria (Singh et al., 2000).

Synaptosomes also tended to the less dense fractions at the gradient.

4.2.6.4 Differences among the gradient media due to medium uptake

Tests exhibited differences in the densities at which the organelles enriched dependent on gradient medium: Overall organelle distribution and the distribution of the single organelles differ clearly among the gradient media. In sucrose, cellular organelles enrich at higher densities than in Optiprep and Nycodenz, and corroborate previous publications (Ford et al., 1982). As the used gradient media do not affect protein weight (Ford et al., 1982; Rickwood et al., 1982), and as isolated proteins, e.g. catalase, exhibit far higher equilibrium densities (Ford et al., 1982), the separated organelle markers have to be organelle-bound.

As separation length, centrifugation force and time are kept constant, these parameters could not be made responsible for the differential outcome. Frictional forces should also play only a minor role in a liquid compound.

Assuming that the fractions, loaded upon the gradient, are of the same composition, the densities of the organelles must be changed in at least one gradient medium. This could either happen through medium uptake into the organelles or through interaction of the organelle and the medium, e.g. by osmotic pressure.

Organelles are compartments separated by at least one lipid bilayer from the surrounding liquid. Lipid bilayers act as semi-permeable membranes and permit a flow of water and the passing of selected small molecules through the lipid membrane. Hereby membrane permeability, i.a. membrane pores determine organelle density by medium uptake. Sucrose is known to permeate into mitochondria, synaptosomes and ER (Sambasivarao and Sitaramam, 1983; Sitaramam and Sarma, 1981). A sucrose uptake is also described in peroxisomes (Gaunt and de Duve, 1976).

Sensitivity to osmosis and osmolarity-dependent density changes are described for peroxisomes (Antonikov et al., 2004a): Peroxisomal membranes permit free diffusion for particles up to 300 to 400 Dalton (Rokka et al., 2009), which coincides with the size of sucrose molecules. This might explain the observed shift in the gradient as all observed organelles seem to be permeable for sucrose. Assuming, that the organelle permeability for larger molecules like Nycodenz and Optiprep is more limited, it seems plausible, that organelles enrich at lighter positions in these media.

The second factor influencing organelle density is osmotic pressure and its effect on water content and hereby the relative size of the isolated organelles. As shrinking of the organelles results in a higher concentration of the solid parts of the organelles and hence a gain of weight per volume – a gain of density – differences among the gradient media might be explained.

The observed differences in density might be result of an interplay of these factors.

4.2.7 Peroxisome pre-purification using a series of sucrose density-gradients

Apart from gradient medium, gradient composition, centrifugation and application site on the gradient, results of gradient centrifugation are highly affected by the sample pre-processing. As separation capability of the continuous sucrose gradient could be successfully transferred to a step gradient and separation differed most among sucrose and Nycodenz medium, a sequence of gradient centrifugations was assessed using sucrose step gradients as pre-purification procedure. For the choice of the steps pre-existing separations were considered.

Alike described, myelin was first removed to avoid contamination of the sample (Kovacs et al., 2001), using an interphase among 700-900mM sucrose and 250-500mM sucrose. This procedure was stepwise developed from one described by Cimini et al (Cimini et al., 1993). On the same gradient, peroxisomes were separated from mitochondria and other organelles.

As described in literature, the majority of synaptosomes enriched along the border of 0.9 and 1.2M sucrose (Whittaker, 1967) or 0.8M and 1.2M sucrose (Bai and Witzmann, 2007). Mitochondria enriched at 1.5M sucrose (Whittaker, 1967). Booth and Clarke also observed a synaptosome enrichment at less dense fractions than mitochondria in sucrose gradients (Booth and Clark, 1978). Peroxisomes were present both in 0.9M sucrose layer and the phase below, a 1.1M interphase above a 2M sucrose cushion. Here also most mitochondria enriched. Synaptosomes were also present in both layers but with a clear enrichment in the denser layer.

4.3 Peroxisomal subpopulations derived

With a series of sucrose gradients followed by a Nycodenz gradient different peroxisomal fractions – characterized by PEX 14 enrichment - were separated. On sucrose step gradient, peroxisomes enriched in 0.9M and 1.1M sucrose solution, of which the latter was characterized by catalase maximum. Colocalization of ACOX, catalase and PEX14 signal indicates intact peroxisomes. With its density equilibrating in 1.1M sucrose solution (1.139g/ml, 1.086M) and at the border 1.2 to 1.3 M sucrose solution (1.157g/ml, 1.23M) in subsequent fractionation on step gradient, this fraction corresponds to the densest peroxisomes purified in this protocol. These densest peroxisomes enriched at similar densities as DAAO-positive or catalase-positive peroxisomes of new-born mice purified on sucrose gradients, which enriched at 1.18g/ml and 1.16g/ml (Gaunt and de Duve, 1976).

Majority of peroxisomes enriched in 900mM sucrose and were hence by far lighter than the DAAO-positive or catalase-positive peroxisomes of new-born mice (Gaunt and de Duve, 1976). These peroxisomes were further purified on Nycodenz gradients, where they enriched at 1.09g/ml and 1.13g/ml and were hence at similar densities as those described by Singh et al (Singh et al., 1989). Presence of low levels of ACOX1 though not of catalase indicates intact peroxisomes as well as the reproducibility independent of step or continuous gradient.

4.3.1 Assessing for peroxisomal “ghosts”

As described by Antonenkov et al peroxisomes released their core enzymes and formed empty “ghosts” even at isoosmolar solution (Antonenkov et al., 2004a). Especially when exposed to hypoosmolar solutions these ghosts were formed

(Antonenkov et al., 2004a). To distinguish the fractions, we purified from peroxisomal “ghosts” we applied our pre-purified peroxisomes intentionally on hypoosmolar levels of Nycodenz. This led to the appearance of an increased peroxisomal membrane protein signal without detection of peroxisomal core enzymes in fractions at 1.05-1.07g/ml. This supports the hypothesis that the beforementioned peroxisomal fractions consisted indeed of intact peroxisomes.

4.3.2 peroxisomal subpopulations

Apparently the peroxisomal fractions isolated on sucrose density gradient and Nycodenz gradient (*paragraph 3.2.7 and 3.2.8*) differ in protein constitution, which hints at different peroxisomal subpopulations. Only in the densest peroxisomes catalase could be detected via western blotting. Thus this fraction could be the correlating fraction to that isolated in nascent mice (Kovacs et al., 2001). Considering the large difference in peroxisomal size described (0,1-0,52 μ m) (Lazo et al., 1991) and the fact that catalase positive peroxisomes are described to be comparatively large (Holtzman, 1982), this densest fraction might derive from those catalase-positive peroxisomes. Considering that this densest fraction could not be purified to a similar extent as in nascent mice using protocol 1 (*paragraph 4.2.1*), this subpopulation might represent the peroxisomes in myelination, hence the oligodendrocytes' peroxisomes. Further support is given by the fact that catalase content decreases over time in brain after myelin formation (Ahlemeyer et al., 2007; Kovacs et al., 2001).

Being clearly denser than peroxisomal “ghosts” (*paragraph 4.3.1*) the other 2 subpopulations separated on Nycodenz gradient might derive from further peroxisomal subpopulations. Apart from a decrease in peroxisome content with age (Ahlemeyer et al., 2007; Antonenkov et al., 2004a; Arnold and Holtzman, 1978; Holtzman, 1982; Nagase et al., 2004) a decrease of catalase positive peroxisomes has also been reported (Ahlemeyer et al., 2007; Houdou et al., 1991; Kovacs et al., 2001), which might highlight less abundant peroxisome subpopulations - apart from the myelin components (i.e. squalene) producing peroxisomes - after myelin formation. Diversification of brain peroxisomes was also reported in immunofluorescence studies (Ahlemeyer et al., 2007; Antonenkov et al., 2004a; Arnold and Holtzman, 1978; Holtzman, 1982; Houdou et al., 1991; Nagase et al., 2004). Diversification apparently results in differences in peroxisome density, which might explain the spread of peroxisomes over different densities, which is supported by the described catalase-correlated differences of peroxisome size in neurons and glia (Ahlemeyer et al., 2007; Arnold and Holtzman, 1978). The change in protein/enzyme content might also explain the change in density of peroxisomes.

The peroxisomal diversification during aging can be seen in the elevated peroxisome concentration in fractions with less detectable catalase content, which also could be correlated to alterations in overall catalase content during aging

The hypothesis of the presence of various peroxisomal subpopulations is supported by the presence of peroxisomal subpopulations in other tissues (Angermüller and Fahimi, 1988; Islinger et al., 2012a; Islinger et al., 2010; Schrader et al., 1994).

In summary, with our isolation procedure in brain peroxisome isolation we are capable to isolate different peroxisomal subpopulations. Furthermore, we further assessed the physical properties of brain peroxisomes and gave further evidence of the osmosensitivity of peroxisomes (Antonenkov et al., 2004a).

5 SUMMARY

This study aimed to provide tools for the investigation of peroxisomes in adult brain tissue and in cell culture.

In cultured cells, we developed a procedure capable to deal with transfected peroxisomes and able to perform density-shift-assays. Using this procedure, we were able to demonstrate ER-peroxisome interaction mediated through VAPB and ACBD5 using co-precipitation.

With our studies on brain peroxisome purification and the developed procedures we were capable to differ peroxisomal subpopulations and to assess the density of brain peroxisomal “ghosts”. Furthermore, we further assessed the physical properties of brain peroxisomes considering the enrichment in different gradient media and gave further evidence of the osmosensitivity of peroxisomes.

6 LITERATURE

- Abu-Safieh, L., M. Alrashed, S. Anazi, H. Alkuraya, A.O. Khan, M. Al-Owain, J. Al-Zahrani, L. Al-Abdi, M. Hashem, S. Al-Tarimi, M.A. Sebai, A. Shamia, M.D. Ray-Zack, M. Nassan, Z.N. Al-Hassnan, Z. Rahbeeni, S. Waheeb, A. Alkharashi, E. Abboud, S.A. Al-Hazaa, and F.S. Alkuraya. 2013. Autozygome-guided exome sequencing in retinal dystrophy patients reveals pathogenetic mutations and novel candidate disease genes. *Genome Res.* 23:236-247.
- Ahlemeyer, B., I. Neubert, W.J. Kovacs, and E. Baumgart-Vogt. 2007. Differential expression of peroxisomal matrix and membrane proteins during postnatal development of mouse brain. *J Comp Neurol.* 505:1-17.
- Ahlemeyer, B., J.F. Vogt, V. Michel, P. Hahn-Kohlberger, and E. Baumgart-Vogt. 2014. Microporation is an efficient method for siRNA-induced knockdown of PEX5 in HepG2 cells: evaluation of the transfection efficiency, the PEX5 mRNA and protein levels and induction of peroxisomal deficiency. *Histochem Cell Biol.* 142:577-591.
- Ahmad, T., K. Aggarwal, B. Pattnaik, S. Mukherjee, T. Sethi, B.K. Tiwari, M. Kumar, A. Micheal, U. Mabalirajan, B. Ghosh, S. Sinha Roy, and A. Agrawal. 2013. Computational classification of mitochondrial shapes reflects stress and redox state. *Cell Death Dis.* 4:e461.
- Angermüller, S., and H.D. Fahimi. 1988. Heterogenous staining of D-amino acid oxidase in peroxisomes of rat liver and kidney. *Histochemistry.* 88:277-285.
- Angermüller, S., M. Islinger, and A. Volkl. 2009. Peroxisomes and reactive oxygen species, a lasting challenge. *Histochem Cell Biol.* 131:459-463.
- Antonenkov, V.D., and J.K. Hiltunen. 2012. Transfer of metabolites across the peroxisomal membrane. *Biochim Biophys Acta.* 1822:1374-1386.
- Antonenkov, V.D., R.T. Sormunen, and J.K. Hiltunen. 2004a. The behavior of peroxisomes in vitro: mammalian peroxisomes are osmotically sensitive particles. *Am J Physiol Cell Physiol.* 287:C1623-1635.
- Antonenkov, V.D., R.T. Sormunen, and J.K. Hiltunen. 2004b. The rat liver peroxisomal membrane forms a permeability barrier for cofactors but not for small metabolites in vitro. *J Cell Sci.* 117:5633-5642.
- Arnold, G., and E. Holtzman. 1978. Microperoxisomes in the central nervous system of the postnatal rat. *Brain Res.* 155:1-17.
- Assayag, K., E. Yakunin, V. Loeb, D.J. Selkoe, and R. Sharon. 2007. Polyunsaturated fatty acids induce alpha-synuclein-related pathogenic changes in neuronal cells. *Am J Pathol.* 171:2000-2011.
- Baboota, R.K., A.B. Shinde, K. Lemaire, M. Fransen, S. Vinckier, P.P. Van Veldhoven, F. Schuit, and M. Baes. 2019. Functional peroxisomes are required for beta-cell integrity in mice. *Mol Metab.* 22:71-83.
- Baes, M., and P. Aubourg. 2009. Peroxisomes, myelination, and axonal integrity in the CNS. *Neuroscientist.* 15:367-379.
- Bai, F., and F.A. Witzmann. 2007. Synaptosome proteomics. *Subcell Biochem.* 43:77-98.
- Baumgart, E., A. Volkl, T. Hashimoto, and H.D. Fahimi. 1989. Biogenesis of peroxisomes: immunocytochemical investigation of peroxisomal membrane proteins in proliferating rat liver peroxisomes and in catalase-negative membrane loops. *J Cell Biol.* 108:2221-2231.

- Bergemalm, D., K. Forsberg, V. Srivastava, K.S. Graffmo, P.M. Andersen, T. Brannstrom, G. Wingsle, and S.L. Marklund. 2010. Superoxide dismutase-1 and other proteins in inclusions from transgenic amyotrophic lateral sclerosis model mice. *J Neurochem.* 114:408-418.
- Berger, J., F. Dorninger, S. Forss-Petter, and M. Kunze. 2016. Peroxisomes in brain development and function. *Biochim Biophys Acta.* 1863:934-955.
- Biringer, R.G. 2020. The enzymology of human eicosanoid pathways: the lipoxygenase branches. *Mol Biol Rep.* 47:7189-7207.
- Booth, R.F., and J.B. Clark. 1978. A rapid method for the preparation of relatively pure metabolically competent synaptosomes from rat brain. *Biochem J.* 176:365-370.
- Bottelbergs, A., S. Verheijden, L. Hulshagen, D.H. Gutmann, S. Goebels, K.A. Nave, C. Kassmann, and M. Baes. 2010. Axonal integrity in the absence of functional peroxisomes from projection neurons and astrocytes. *Glia.* 58:1532-1543.
- Bradford, M.M. 1976. A rapid and sensitive method for the quantitation of microgram quantities of protein utilizing the principle of protein-dye binding. *Anal Biochem.* 72:248-254.
- Braverman, N.E., G.V. Raymond, W.B. Rizzo, A.B. Moser, M.E. Wilkinson, E.M. Stone, S.J. Steinberg, M.F. Wangler, E.T. Rush, J.G. Hacia, and M. Bose. 2016. Peroxisome biogenesis disorders in the Zellweger spectrum: An overview of current diagnosis, clinical manifestations, and treatment guidelines. *Mol Genet Metab.* 117:313-321.
- Burden, D.W. 2008. Guide to the Homogenization of Biological Samples. *Random Primers.*
- Calder, P.C. 2020. Eicosanoids. *Essays Biochem.* 64:423-441.
- Camoës, F., N.A. Bonekamp, H.K. Delille, and M. Schrader. 2009. Organelle dynamics and dysfunction: A closer link between peroxisomes and mitochondria. *J Inherit Metab Dis.* 32:163-180.
- Chan, A., A. Schummer, S. Fischer, T. Schroter, L.D. Cruz-Zaragoza, J. Bender, F. Drepper, S. Oeljeklaus, W.H. Kunau, W. Girzalsky, B. Warscheid, and R. Erdmann. 2016. Pex17p-dependent assembly of Pex14p/Dyn2p-subcomplexes of the peroxisomal protein import machinery. *Eur J Cell Biol.* 95:585-597.
- Chu, B.B., Y.C. Liao, W. Qi, C. Xie, X. Du, J. Wang, H. Yang, H.H. Miao, B.L. Li, and B.L. Song. 2015. Cholesterol transport through lysosome-peroxisome membrane contacts. *Cell.* 161:291-306.
- Cimini, A.M., S. Moreno, M. Giorgi, B. Serafini, and M.P. Ceru. 1993. Purification of peroxisomal fraction from rat brain. *Neurochem Int.* 23:249-260.
- Costello, J.L., I.G. Castro, C. Hacker, T.A. Schrader, J. Metz, D. Zeuschner, A.S. Azadi, L.F. Godinho, V. Costina, P. Findeisen, A. Manner, M. Islinger, and M. Schrader. 2017a. ACBD5 and VAPB mediate membrane associations between peroxisomes and the ER. *J Cell Biol.* 216:331-342.
- Costello, J.L., I.G. Castro, T.A. Schrader, M. Islinger, and M. Schrader. 2017b. Peroxisomal ACBD4 interacts with VAPB and promotes ER-peroxisome associations. *Cell Cycle.* 16:1039-1045.
- Costello, J.L., and M. Schrader. 2018. Unloosing the Gordian knot of peroxisome formation. *Curr Opin Cell Biol.* 50:50-56.
- Cruz, T.F., and M.A. Moscarello. 1985. Characterization of myelin fractions from human brain white matter. *J Neurochem.* 44:1411-1418.
- Cui, S., Y. Hayashi, M. Otomo, S. Mano, K. Oikawa, M. Hayashi, and M. Nishimura. 2016. Sucrose Production Mediated by Lipid Metabolism Suppresses the Physical Interaction of Peroxisomes and Oil Bodies during Germination of *Arabidopsis thaliana*. *J Biol Chem.* 291:19734-19745.

- Cuzner, M.L., and A.N. Davison. 1986. The Lipid Composition of Rat Brain Myelin and Subcellular Fractions during Development. *Biochem J*.
- Darwisch, W., M. von Spangenberg, J. Lehmann, O. Singin, G. Deubert, S. Kuhl, J. Roos, H. Horstmann, C. Korber, S. Hoppe, H. Zheng, T. Kuner, M.L. Pras-Raves, A.H.C. van Kampen, H.R. Waterham, K.V. Schwarz, J.G. Okun, C. Schultz, F.M. Vaz, and M. Islinger. 2020. Cerebellar and hepatic alterations in ACBD5-deficient mice are associated with unexpected, distinct alterations in cellular lipid homeostasis. *Commun Biol*. 3:713.
- Dastig, S., A. Nenicu, D.M. Otte, A. Zimmer, J. Seitz, E. Baumgart-Vogt, and G.H. Luers. 2011. Germ cells of male mice express genes for peroxisomal metabolic pathways implicated in the regulation of spermatogenesis and the protection against oxidative stress. *Histochem Cell Biol*. 136:413-425.
- de Araujo, M.E., G. Lamberti, and L.A. Huber. 2015. Homogenization of Mammalian Cells. *Cold Spring Harb Protoc*. 2015:1009-1012.
- De Duve, C. 1960. Intracellular Localization of Enzymes. *Nature*. 187:836-836.
- De Duve, C., and P. Baudhuin. 1966. Peroxisomes (microbodies and related particles). *Physiol Rev*. 46:323-357.
- De Munter, S., D. Bamps, A.R. Malheiro, R. Kumar Baboota, P. Brites, and M. Baes. 2018. Autonomous Purkinje cell axonal dystrophy causes ataxia in peroxisomal multifunctional protein-2 deficiency. *Brain Pathol*. 28:631-643.
- De Vos, K.J., G.M. Morotz, R. Stoica, E.L. Tudor, K.F. Lau, S. Ackerley, A. Warley, C.E. Shaw, and C.C. Miller. 2012. VAPB interacts with the mitochondrial protein PTPIP51 to regulate calcium homeostasis. *Hum Mol Genet*. 21:1299-1311.
- Deak, F., R.E. Anderson, J.L. Fessler, and D.M. Sherry. 2019. Novel Cellular Functions of Very Long Chain-Fatty Acids: Insight From ELOVL4 Mutations. *Front Cell Neurosci*. 13:428.
- Dean, J.M., and I.J. Lodhi. 2018. Structural and functional roles of ether lipids. *Protein Cell*. 9:196-206.
- Delille, H., N. Bonekamp, and M. Schrader. 2006. Peroxisome and Disease - An Overview. *International Journal of Biomedical Science*.
- Delmaghani, S., J. Defourny, A. Aghaie, M. Beurg, D. Dulon, N. Thelen, I. Perfettini, T. Zelles, M. Aller, A. Meyer, A. Emptoz, F. Giraudet, M. Leibovici, S. Dartevelle, G. Soubigou, M. Thiry, E.S. Vizi, S. Safieddine, J.P. Hardelin, P. Avan, and C. Petit. 2015. Hypervulnerability to Sound Exposure through Impaired Adaptive Proliferation of Peroxisomes. *Cell*. 163:894-906.
- Demarquoy, J., and F. Le Borgne. 2015. Crosstalk between mitochondria and peroxisomes. *World J Biol Chem*. 6:301-309.
- Devchand, P.R., H. Keller, J.M. Peters, M. Vazquez, F.J. Gonzalez, and W. Wahli. 1996. The PPARalpha-leukotriene B4 pathway to inflammation control. *Nature*. 384:39-43.
- Diano, S., Z.W. Liu, J.K. Jeong, M.O. Dietrich, H.B. Ruan, E. Kim, S. Suyama, K. Kelly, E. Gyengesi, J.L. Arbiser, D.D. Belsham, D.A. Sarruf, M.W. Schwartz, A.M. Bennett, M. Shanabrough, C.V. Mobbs, X. Yang, X.B. Gao, and T.L. Horvath. 2011. Peroxisome proliferation-associated control of reactive oxygen species sets melanocortin tone and feeding in diet-induced obesity. *Nat Med*. 17:1121-1127.
- Dimitrov, L., S.K. Lam, and R. Schekman. 2013. The role of the endoplasmic reticulum in peroxisome biogenesis. *Cold Spring Harb Perspect Biol*. 5:a013243.

- Dixit, E., S. Boulant, Y. Zhang, A.S. Lee, C. Odendall, B. Shum, N. Hacohen, Z.J. Chen, S.P. Whelan, M. Fransen, M.L. Nibert, G. Superti-Furga, and J.C. Kagan. 2010. Peroxisomes are signaling platforms for antiviral innate immunity. *Cell*. 141:668-681.
- Elliott, K.A., and M.K. Birmingham. 1949. The effect of pH on the respiration of brain tissue; the pH of tissue slices. *J Biol Chem*. 177:51-58.
- Errico, F., S. Rossi, F. Napolitano, V. Catuogno, E. Topo, G. Fisone, A. D'Aniello, D. Centonze, and A. Usiello. 2008. D-aspartate prevents corticostriatal long-term depression and attenuates schizophrenia-like symptoms induced by amphetamine and MK-801. *J Neurosci*. 28:10404-10414.
- Fahimi, H.D., E. Baumgart, and A. Volkl. 1993. Ultrastructural aspects of the biogenesis of peroxisomes in rat liver. *Biochimie*. 75:201-208.
- Fanelli, F., S. Sepe, M. D'Amelio, C. Bernardi, L. Cristiano, A.M. Cimini, F. Cecconi, M.P. Ceru, and S. Moreno. 2013. Age-dependent roles of peroxisomes in the hippocampus of a transgenic mouse model of Alzheimer's disease. *Molecular Neurodegeneration*.
- Faust, P.L., D. Banka, R. Siriratsivawong, V.G. Ng, and T.M. Wikander. 2005. Peroxisome biogenesis disorders: the role of peroxisomes and metabolic dysfunction in developing brain. *J Inherit Metab Dis*. 28:369-383.
- Ferdinandusse, S., S. Denis, P.L. Faust, and R.J. Wanders. 2009. Bile acids: the role of peroxisomes. *J Lipid Res*. 50:2139-2147.
- Ferdinandusse, S., K.D. Falkenberg, J. Koster, P.A. Mooyer, R. Jones, C.W.T. van Roermund, A. Pizzino, M. Schrader, R.J.A. Wanders, A. Vanderver, and H.R. Waterham. 2017. ACBD5 deficiency causes a defect in peroxisomal very long-chain fatty acid metabolism. *J Med Genet*. 54:330-337.
- Ford, T., D. Rickwood, and J.M. Graham. 1982. Buoyant Densities of Macromolecules, Macromolecular Complexes and Cell Organelles in Nycodenz Gradients. *Anal Biochem*.
- Fransen, M., C. Lismont, and P. Walton. 2017. The Peroxisome-Mitochondria Connection: How and Why? *Int J Mol Sci*. 18.
- Fujimoto, K., B.I. Roots, R.M. Burton, and H.C. Agrawal. 1976. Morphological and biochemical characterization of light and heavy myelin isolated from developing rat brain. *Biochim Biophys Acta*. 426:659-668.
- Gabalton, T. 2010. Peroxisome diversity and evolution. *Philos Trans R Soc Lond B Biol Sci*. 365:765-773.
- Gaunt, G.L., and C. de Duve. 1976. Subcellular distribution of D-amino acid oxidase and catalase in rat brain. *J Neurochem*. 26:749-759.
- Geuze, H.J., J.L. Murk, A.K. Stroobants, J.M. Griffith, M.J. Kleijmeer, A.J. Koster, A.J. Verkleij, B. Distel, and H.F. Tabak. 2003. Involvement of the endoplasmic reticulum in peroxisome formation. *Mol Biol Cell*. 14:2900-2907.
- Giannopoulou, E.A., L. Emmanouilidis, M. Sattler, G. Dodt, and M. Wilmanns. 2016. Towards the molecular mechanism of the integration of peroxisomal membrane proteins. *Biochim Biophys Acta*. 1863:863-869.
- Gonzalez, F.J., J.M. Peters, and R.C. Cattley. 1998. Mechanism of action of the nongenotoxic peroxisome proliferators: role of the peroxisome proliferator-activator receptor alpha. *J Natl Cancer Inst*. 90:1702-1709.
- Gordon, J., S. Amini, and M.K. White. 2013. General overview of neuronal cell culture. *Methods Mol Biol*. 1078:1-8.
- Graham, J.M. 2002a. Homogenization of Mammalian tissues. *ScientificWorldJournal*. 2:1626-1629.

- Graham, J.M. 2002b. Purification of peroxisomes in a preformed iodixanol gradient in a fixed-angle rotor. *ScientificWorldJournal*. 2:1536-1539.
- Graham, J.M. 2015. Fractionation of Subcellular Organelles. *Curr Protoc Cell Biol*. 69:311-3122.
- Grant, P., B. Ahlemeyer, S. Karnati, T. Berg, I. Stelzig, A. Nenicu, K. Kuchelmeister, D.I. Crane, and E. Baumgart-Vogt. 2013. The biogenesis protein PEX14 is an optimal marker for the identification and localization of peroxisomes in different cell types, tissues, and species in morphological studies. *Histochem Cell Biol*. 140:423-442.
- Guimaraes, S.C., M. Schuster, E. Bielska, G. Dagdas, S. Kilaru, B.R. Meadows, M. Schrader, and G. Steinberg. 2015. Peroxisomes, lipid droplets, and endoplasmic reticulum "hitchhike" on motile early endosomes. *J Cell Biol*. 211:945-954.
- Gulyas, B.J., and L.C. Yuan. 1977. Association of microperoxisomes with the endoplasmic reticulum in the granulosa lutein cells of the Rhesus monkey (*Macaca mulatta*). *Cell Tissue Res*. 179:357-366.
- Hara, Y., F. Yuk, R. Puri, W.G. Janssen, P.R. Rapp, and J.H. Morrison. 2014. Presynaptic mitochondrial morphology in monkey prefrontal cortex correlates with working memory and is improved with estrogen treatment. *Proc Natl Acad Sci U S A*. 111:486-491.
- He, M., Z. Pei, A.W. Mohsen, P. Watkins, G. Murdoch, P.P. Van Veldhoven, R. Ensenauer, and J. Vockley. 2011. Identification and characterization of new long chain acyl-CoA dehydrogenases. *Mol Genet Metab*. 102:418-429.
- Hogenboom, S., J.J. Tuyp, M. Espeel, J. Koster, R.J. Wanders, and H.R. Waterham. 2004a. Human mevalonate pyrophosphate decarboxylase is localized in the cytosol. *Mol Genet Metab*. 81:216-224.
- Hogenboom, S., J.J. Tuyp, M. Espeel, J. Koster, R.J. Wanders, and H.R. Waterham. 2004b. Mevalonate kinase is a cytosolic enzyme in humans. *J Cell Sci*. 117:631-639.
- Holtzman, E. 1982. peroxisomes in nervous tissue. *Ann NY Acad*.
- Hosoi, K.I., N. Miyata, S. Mukai, S. Furuki, K. Okumoto, E.H. Cheng, and Y. Fujiki. 2017. The VDAC2-BAK axis regulates peroxisomal membrane permeability. *J Cell Biol*. 216:709-722.
- Houdou, S., H. Kuruta, M. Hasegawa, H. Konomi, S. Takashima, Y. Suzuki, and T. Hashimoto. 1991. Developmental immunohistochemistry of catalase in the human brain. *Brain Res*. 556:267-270.
- Hua, R., D. Cheng, E. Coyaud, S. Freeman, E. Di Pietro, Y. Wang, A. Vissa, C.M. Yip, G.D. Fairn, N. Braverman, J.H. Brumell, W.S. Trimble, B. Raught, and P.K. Kim. 2017. VAPs and ACBD5 tether peroxisomes to the ER for peroxisome maintenance and lipid homeostasis. *J Cell Biol*. 216:367-377.
- Hulshagen, L., O. Krysko, A. Bottelbergs, S. Huyghe, R. Klein, P.P. Van Veldhoven, P.P. De Deyn, R. D'Hooge, D. Hartmann, and M. Baes. 2008. Absence of functional peroxisomes from mouse CNS causes dysmyelination and axon degeneration. *J Neurosci*. 28:4015-4027.
- Huttlin, E.L., L. Ting, R.J. Bruckner, F. Gebreab, M.P. Gygi, J. Szpyt, S. Tam, G. Zarraga, G. Colby, K. Baltier, R. Dong, V. Guarani, L.P. Vaites, A. Ordureau, R. Rad, B.K. Erickson, M. Wuhr, J. Chick, B. Zhai, D. Kolippakkam, J. Mintseris, R.A. Obar, T. Harris, S. Artavanis-Tsakonas, M.E. Sowa, P. De Camilli, J.A. Paulo, J.W. Harper, and S.P. Gygi. 2015. The BioPlex Network: A Systematic Exploration of the Human Interactome. *Cell*. 162:425-440.

- Islinger, M., A. Abdolzade-Bavil, S. Liebler, G. Weber, and A. Volkl. 2012a. Assessing heterogeneity of peroxisomes: isolation of two subpopulations from rat liver. *Methods Mol Biol.* 909:83-96.
- Islinger, M., S. Grille, H.D. Fahimi, and M. Schrader. 2012b. The peroxisome: an update on mysteries. *Histochem Cell Biol.* 137:547-574.
- Islinger, M., J. Kirsch, S. Angermüller, R. Rotaru, A. Abdolzade-Bavil, and G. Weber. 2011. Sucellular Fractionation of Brain Tissue Using Free-Flow Electrophoresis. *In Neuroproteomics*. Vol. 57. K.W. Li, editor. Springer. 27-39.
- Islinger, M., K.W. Li, M. Loos, S. Liebler, S. Angermüller, C. Eckerskorn, G. Weber, A. Abdolzade, and A. Volkl. 2010. Peroxisomes from the heavy mitochondrial fraction: isolation by zonal free flow electrophoresis and quantitative mass spectrometrical characterization. *J Proteome Res.* 9:113-124.
- Islinger, M., G.H. Luers, H. Zischka, M. Ueffing, and A. Volkl. 2006. Insights into the membrane proteome of rat liver peroxisomes: microsomal glutathione-S-transferase is shared by both subcellular compartments. *Proteomics.* 6:804-816.
- Islinger, M., A. Voelkl, H.D. Fahimi, and M. Schrader. 2018. The peroxisome: an update on mysteries 2.0. *Histochem Cell Biol.* 150:443-471.
- Issemann, I., and S. Green. 1990. Activation of a member of the steroid hormone receptor superfamily by peroxisome proliferators. *Nature.* 347:645-650.
- Ivashchenko, O., P.P. Van Veldhoven, C. Brees, Y.S. Ho, S.R. Terlecky, and M. Fransen. 2011. Intraperoxisomal redox balance in mammalian cells: oxidative stress and interorganellar cross-talk. *Mol Biol Cell.* 22:1440-1451.
- Jansen, M., Y. Ohsaki, L.R. Rega, R. Bittman, V.M. Olkkonen, and E. Ikonen. 2011. Role of ORPs in sterol transport from plasma membrane to ER and lipid droplets in mammalian cells. *Traffic.* 12:218-231.
- Jo, D.S., N.Y. Park, and D.H. Cho. 2020. Peroxisome quality control and dysregulated lipid metabolism in neurodegenerative diseases. *Exp Mol Med.* 52:1486-1495.
- Joshi, A.S., and S. Cohen. 2019. Lipid Droplet and Peroxisome Biogenesis: Do They Go Hand-in-Hand? *Front Cell Dev Biol.* 7:92.
- Kanzawa, N., Y. Maeda, H. Ogiso, Y. Murakami, R. Taguchi, and T. Kinoshita. 2009. Peroxisome dependency of alkyl-containing GPI-anchor biosynthesis in the endoplasmic reticulum. *Proc Natl Acad Sci U S A.* 106:17711-17716.
- Kanzawa, N., N. Shimosawa, R.J. Wanders, K. Ikeda, Y. Murakami, H.R. Waterham, S. Mukai, M. Fujita, Y. Maeda, R. Taguchi, Y. Fujiki, and T. Kinoshita. 2012. Defective lipid remodeling of GPI anchors in peroxisomal disorders, Zellweger syndrome, and rhizomelic chondrodysplasia punctata. *J Lipid Res.* 53:653-663.
- Kawano, M., K. Kumagai, M. Nishijima, and K. Hanada. 2006. Efficient trafficking of ceramide from the endoplasmic reticulum to the Golgi apparatus requires a VAMP-associated protein-interacting FFAT motif of CERT. *J Biol Chem.* 281:30279-30288.
- Kemp, S., F.L. Theodoulou, and R.J. Wanders. 2011. Mammalian peroxisomal ABC transporters: from endogenous substrates to pathology and clinical significance. *Br J Pharmacol.* 164:1753-1766.
- Kihara, A. 2012. Very long-chain fatty acids: elongation, physiology and related disorders. *J Biochem.* 152:387-395.
- Kilwein, M.D., and M.A. Welte. 2019. Lipid droplet motility and organelle contacts. *Contact (Thousand Oaks).* 2.
- Kim, J.J., and R. Miura. 2004. Acyl-CoA dehydrogenases and acyl-CoA oxidases. Structural basis for mechanistic similarities and differences. *Eur J Biochem.* 271:483-493.

- Kirov, G., M.C. O'Donovan, and M.J. Owen. 2005. Finding schizophrenia genes. *J Clin Invest.* 115:1440-1448.
- Kou, J., G.G. Kovacs, R. Hoftberger, W. Kulik, A. Brodde, S. Forss-Petter, S. Honigschnabl, A. Gleiss, B. Brugger, R. Wanders, W. Just, H. Budka, S. Jungwirth, P. Fischer, and J. Berger. 2011. Peroxisomal alterations in Alzheimer's disease. *Acta Neuropathol.* 122:271-283.
- Kovacs, W.J., P.L. Faust, G.-A. Keller, and S.K. Krisans. 2001. Purification of brain peroxisomes and localization of 3-hydroxy-3-methylglutaryl coenzyme A reductase. *Eur. J. Biochem.*
- Kovacs, W.J., L.M. Olivier, and S.K. Krisans. 2002. Central role of peroxisomes in isoprenoid biosynthesis. *Prog Lipid Res.* 41:369-391.
- Kovacs, W.J., K.N. Tape, J.E. Shackelford, X. Duan, T. Kasumov, J.K. Kelleher, H. Brunengraber, and S.K. Krisans. 2007. Localization of the pre-squalene segment of the isoprenoid biosynthetic pathway in mammalian peroxisomes. *Histochem Cell Biol.* 127:273-290.
- Kovacs, W.J., K.N. Tape, J.E. Shackelford, T.M. Wikander, M.J. Richards, S.J. Fliesler, S.K. Krisans, and P.L. Faust. 2009. Peroxisome deficiency causes a complex phenotype because of hepatic SREBP/Insig dysregulation associated with endoplasmic reticulum stress. *J Biol Chem.* 284:7232-7245.
- Kragelund, B.B., K. Poulsen, K.V. Andersen, T. Baldursson, J.B. Kroll, T.B. Neergard, J. Jepsen, P. Roepstorff, K. Kristiansen, F.M. Poulsen, and J. Knudsen. 1999. Conserved residues and their role in the structure, function, and stability of acyl-coenzyme A binding protein. *Biochemistry.* 38:2386-2394.
- Lai, J.C., K.F. Sheu, Y.T. Kim, D.D. Clarke, and J.P. Blass. 1986. The subcellular localization of glutamate dehydrogenase (GDH): is GDH a marker for mitochondria in brain? *Neurochem Res.*
- Larocca, J.N., and W.T. Norton. 2007. Isolation of myelin. *Curr Protoc Cell Biol.* Chapter 3:Unit3 25.
- Lazarow, P.B., and C. De Duve. 1976. A fatty acyl-CoA oxidizing system in rat liver peroxisomes; enhancement by clofibrate, a hypolipidemic drug. *Proc Natl Acad Sci U S A.* 73:2043-2046.
- Lazo, O., A.K. Singh, and I. Singh. 1991. Postnatal development and isolation of peroxisomes from brain. *J Neurochem.* 56:1343-1353.
- Le Borgne, F., A. Ben Mohamed, M. Logerot, E. Garnier, and J. Demarquoy. 2011. Changes in carnitine octanoyltransferase activity induce alteration in fatty acid metabolism. *Biochem Biophys Res Commun.* 409:699-704.
- Lee, J.H., D.N. Garboczi, P.J. Thomas, and P.L. Pedersen. 1990. Mitochondrial ATP synthase. cDNA cloning, amino acid sequence, overexpression, and properties of the rat liver alpha subunit. *J Biol Chem.* 265:4664-4669.
- Lev, S., D.B. Halevy, D. Peretti, and N. Dahan. 2008. The VAP protein family: from cellular functions to motor neuron disease.
- Li, X., and S.J. Gould. 2002. PEX11 promotes peroxisome division independently of peroxisome metabolism. *J Cell Biol.* 156:643-651.
- Liu, X., and G. Hajnoczky. 2011. Altered fusion dynamics underlie unique morphological changes in mitochondria during hypoxia-reoxygenation stress. *Cell Death Differ.* 18:1561-1572.
- Lodhi, I.J., and C.F. Semenkovich. 2014. Peroxisomes: a nexus for lipid metabolism and cellular signaling. *Cell Metab.* 19:380-392.
- Loewen, C.J., A. Roy, and T.P. Levine. 2003. A conserved ER targeting motif in three families of lipid binding proteins and in Opi1p binds VAP. *EMBO J.* 22:2025-2035.

- Lohner, K. 1996. Is the high propensity of ethanolamine plasmalogens to form non-lamellar lipid structures manifested in the properties of biomembranes? *Chemistry and Physics of Lipids*. 81:167-184.
- Lopez-Terrada, D., S.W. Cheung, M.J. Finegold, and B.B. Knowles. 2009. Hep G2 is a hepatoblastoma-derived cell line. *Hum Pathol*. 40:1512-1515.
- Ma, C., and S. Reumann. 2008. Improved prediction of peroxisomal PTS1 proteins from genome sequences based on experimental subcellular targeting analyses as exemplified for protein kinases from Arabidopsis. *J Exp Bot*. 59:3767-3779.
- Ma, C., U. Schumann, N. Rayapuram, and S. Subramani. 2009. The peroxisomal matrix import of Pex8p requires only PTS receptors and Pex14p. *Mol Biol Cell*. 20:3680-3689.
- Manner, A., and M. Islinger. 2017. Isolation of Peroxisomes from Rat Liver and Cultured Hepatoma Cells by Density Gradient Centrifugation. *In Peroxisomes*. Vol. 1595. M. Schrader, editor. Humana Press, New York. 1-11.
- Marzec, M., D. Eletto, and Y. Argon. 2012. GRP94: An HSP90-like protein specialized for protein folding and quality control in the endoplasmic reticulum. *Biochim Biophys Acta*. 1823:774-787.
- Maynard, E.L., G.J. Gatto, Jr., and J.M. Berg. 2004. Pex5p binding affinities for canonical and noncanonical PTS1 peptides. *Proteins*. 55:856-861.
- McBride, H.M. 2018. Mitochondria and endomembrane origins. *Curr Biol*. 28:R367-R372.
- Mesmin, B., J. Bigay, J. Moser von Filseck, S. Lacas-Gervais, G. Drin, and B. Antony. 2013. A four-step cycle driven by PI(4)P hydrolysis directs sterol/PI(4)P exchange by the ER-Golgi tether OSBP. *Cell*. 155:830-843.
- Mindthoff, S., S. Grunau, L.L. Steinfort, W. Girzalsky, J.K. Hiltunen, R. Erdmann, and V.D. Antonenkov. 2016. Peroxisomal Pex11 is a pore-forming protein homologous to TRPM channels. *Biochim Biophys Acta*. 1863:271-283.
- Mohanty, A., and H.M. McBride. 2013. Emerging roles of mitochondria in the evolution, biogenesis, and function of peroxisomes. *Front Physiol*. 4:268.
- Montilla-Martinez, M., S. Beck, J. Klumper, M. Meinecke, W. Schliebs, R. Wagner, and R. Erdmann. 2015. Distinct Pores for Peroxisomal Import of PTS1 and PTS2 Proteins. *Cell Rep*. 13:2126-2134.
- Morell, P., and R.H. Quarles. 1999. Characteristic Composition of Myelin. *In Basic Neurochemistry: Molecular, Cellular and Medical Aspects*. G.J. Siegel, B.W. Agranoff, and R.W. Albers, editors. Lippincott-Raven, Philadelphia.
- Moser, H.W. 1999. Genotype-phenotype correlations in disorders of peroxisome biogenesis. *Mol Genet Metab*. 68:316-327.
- Murphy, S.E., and T.P. Levine. 2016. VAP, a Versatile Access Point for the Endoplasmic Reticulum: Review and analysis of FFAT-like motifs in the VAPome. *Biochim Biophys Acta*. 1861:952-961.
- Nagai, K. 2015. Phytanic acid induces Neuro2a cell death via histone deacetylase activation and mitochondrial dysfunction. *Neurotoxicol Teratol*. 48:33-39.
- Nagase, T., N. Shimosawa, Y. Takemoto, Y. Suzuki, M. Komori, and N. Kondo. 2004. Peroxisomal localization in the developing mouse cerebellum: implications for neuronal abnormalities related to deficiencies in peroxisomes. *Biochim Biophys Acta*. 1671:26-33.
- Nazarko, T.Y., K. Ozeki, A. Till, G. Ramakrishnan, P. Lotfi, M. Yan, and S. Subramani. 2014. Peroxisomal Atg37 binds Atg30 or palmitoyl-CoA to regulate phagophore formation during pexophagy. *J Cell Biol*. 204:541-557.

- Neuspiel, M., A.C. Schauss, E. Braschi, R. Zunino, P. Rippstein, R.A. Rachubinski, M.A. Andrade-Navarro, and H.M. McBride. 2008. Cargo-selected transport from the mitochondria to peroxisomes is mediated by vesicular carriers. *Curr Biol.* 18:102-108.
- Nguyen, S.D., M. Baes, and P.P. Van Veldhoven. 2008. Degradation of very long chain dicarboxylic polyunsaturated fatty acids in mouse hepatocytes, a peroxisomal process. *Biochim Biophys Acta.* 1781:400-405.
- Nikolaou, K.E., A. Malamitsi-Puchner, T. Boutsikou, E. Economou, M. Boutsikou, K.P. Puchner, S. Baka, and D. Hassiakos. 2006. The varying patterns of neurotrophin changes in the perinatal period. *Ann N Y Acad Sci.* 1092:426-433.
- Nishikawa, M., T. Hagishita, H. Yurimoto, N. Kato, Y. Sakai, and T. Hatanaka. 2000. Primary structure and expression of peroxisomal acylspermidine oxidase in the methylotrophic yeast *Candida boidinii*. *FEBS Lett.* 476:150-154.
- Novikoff, P.M., A.B. Novikoff, N. Quintana, and C. Davis. 1972. Studies on microperoxisomes III Observations on human and rat hepatocytes.
- Paltauf, F. 1994. Ether lipids in biomembranes. *Chem Phys Lipids.* 74:101-139.
- Peeters, A., P. Fraisl, S. van den Berg, E. Ver Loren van Themaat, A. Van Kampen, M.H. Rider, H. Takemori, K.W. van Dijk, P.P. Van Veldhoven, P. Carmeliet, and M. Baes. 2011. Carbohydrate metabolism is perturbed in peroxisome-deficient hepatocytes due to mitochondrial dysfunction, AMP-activated protein kinase (AMPK) activation, and peroxisome proliferator-activated receptor gamma coactivator 1alpha (PGC-1alpha) suppression. *J Biol Chem.* 286:42162-42179.
- Peng, T.I., M.J. Jou, S.S. Sheu, and J.T. Greenamyre. 1998. Visualization of NMDA receptor-induced mitochondrial calcium accumulation in striatal neurons. *Exp Neurol.* 149:1-12.
- Petroni, A., R. Paroni, A.M. Aloisi, M. Blasevich, N. Haman, and D. Fessas. 2019. Thermogenic flux induced by lignoceric acid in peroxisomes isolated from HepG2 cells and from X-adrenoleukodystrophy and control fibroblasts. *J Cell Physiol.* 234:18344-18348.
- Picard, M., and B.S. McEwen. 2014. Mitochondria impact brain function and cognition. *Proc Natl Acad Sci U S A.* 111:7-8.
- Pieringer, J., G.S. Rao, P. Mandel, and R.A. Pieringer. 1977. The association of the sulphogalactosylglycerolipid of rat brain with myelination. *Biochem J.* 166:421-428.
- Ponce-Ruiz, N., A.E. Rojas-Garcia, B.S. Barron-Vivanco, G. Elizondo, Y.Y. Bernal-Hernandez, A. Mejia-Garcia, and I.M. Medina-Diaz. 2015. Transcriptional regulation of human paraoxonase 1 by PXR and GR in human hepatoma cells. *Toxicol In Vitro.* 30:348-354.
- Posset, R., S. Opp, E.A. Struys, A. Volkl, H. Mohr, G.F. Hoffmann, S. Kolker, S.W. Sauer, and J.G. Okun. 2015. Understanding cerebral L-lysine metabolism: the role of L-pipecolate metabolism in Gcdh-deficient mice as a model for glutaric aciduria type I. *J Inherit Metab Dis.* 38:265-272.
- Power, J.M., and H.W. Moser. 1998. Peroxisomal Disorders: Genotype, Phenotype, Major Neuropathologic Lesions, and Pathogenesis. *Brain Pathology.*
- Rasouli, M. 2016. Basic concepts and practical equations on osmolality: Biochemical approach. *Clin Biochem.* 49:936-941.
- Raychaudhuri, S., and W.A. Prinz. 2008. Nonvesicular phospholipid transfer between peroxisomes and the endoplasmic reticulum. *Proc Natl Acad Sci U S A.* 105:15785-15790.

- Reddy, J.K., and T. Hashimoto. 2001. Peroxisomal beta-oxidation and peroxisome proliferator-activated receptor alpha: an adaptive metabolic system. *Annu Rev Nutr.* 21:193-230.
- Rickwood, D., T. Ford, and J. Graham. 1982. Nycodenz: a new nonionic iodinated gradient medium. *Anal Biochem.* 123:23-31.
- Rocha, N., C. Kuijl, R. van der Kant, L. Janssen, D. Houben, H. Janssen, W. Zwart, and J. Neefjes. 2009. Cholesterol sensor ORP1L contacts the ER protein VAP to control Rab7-RILP-p150 Glued and late endosome positioning. *J Cell Biol.* 185:1209-1225.
- Rokka, A., V.D. Antonenkov, R. Soininen, H.L. Immonen, P.L. Pirila, U. Bergmann, R.T. Sormunen, M. Weckstrom, R. Benz, and J.K. Hiltunen. 2009. Pxmp2 is a channel-forming protein in Mammalian peroxisomal membrane. *PLoS One.* 4:e5090.
- Rucktaschel, R., W. Girzalsky, and R. Erdmann. 2011. Protein import machineries of peroxisomes. *Biochim Biophys Acta.* 1808:892-900.
- Ruffin, V.A., A.I. Salameh, W.F. Boron, and M.D. Parker. 2014. Intracellular pH regulation by acid-base transporters in mammalian neurons. *Front Physiol.* 5:43.
- Sambasivarao, D., and V. Sitaramam. 1983. STUDIES ON THE NON-LINEAR OSMOTIC PRESSURE-VOLUME RELATIONSHIP IN MITOCHONDRIA AND ENTRY OF SUCROSE INTO THE MATRIX SPACE DURING CENTRIFUGATION. *Biochim Biophys Acta.*
- Sampath, D., and R. Perez-Polo. 1997. Regulation of antioxidant enzyme expression by NGF. *Neurochem Res.* 22:351-362.
- Santos, M.J., R.A. Quintanilla, A. Toro, R. Grandy, M.C. Dinamarca, J.A. Godoy, and N.C. Inestrosa. 2005. Peroxisomal proliferation protects from beta-amyloid neurodegeneration. *J Biol Chem.* 280:41057-41068.
- Sargsyan, E., M. Baryshev, L. Szekely, A. Sharipo, and S. Mkrtchian. 2002. Identification of ERp29, an endoplasmic reticulum lumenal protein, as a new member of the thyroglobulin folding complex. *J Biol Chem.* 277:17009-17015.
- Sasabe, J., Y. Miyoshi, M. Suzuki, M. Mita, R. Konno, M. Matsuoka, K. Hamase, and S. Aiso. 2012. D-amino acid oxidase controls motoneuron degeneration through D-serine. *Proc Natl Acad Sci U S A.* 109:627-632.
- Schonfeld, P., and G. Reiser. 2016. Brain Lipotoxicity of Phytanic Acid and Very Long-chain Fatty Acids. Harmful Cellular/Mitochondrial Activities in Refsum Disease and X-Linked Adrenoleukodystrophy. *Aging Dis.* 7:136-149.
- Schrader, M. 2006. Shared components of mitochondrial and peroxisomal division. *Biochim Biophys Acta.* 1763:531-541.
- Schrader, M., E. Baumgart, A. Völkl, and H.D. Fahimi. 1994. Heterogeneity of peroxisomes in human hepatoblastoma cell line HepG2. Evidence of distinct subpopulations. *European Journal of Cell Biology.* 64.
- Schrader, M., N.A. Bonekamp, and M. Islinger. 2012. Fission and proliferation of peroxisomes. *Biochim Biophys Acta.* 1822:1343-1357.
- Schrader, M., J. Costello, L.F. Godinho, and M. Islinger. 2015. Peroxisome-mitochondria interplay and disease. *J Inherit Metab Dis.* 38:681-702.
- Schrader, M., and H.D. Fahimi. 2008. The peroxisome: still a mysterious organelle. *Histochem Cell Biol.* 129:421-440.
- Schrader, M., S.J. King, T.A. Stroh, and T.A. Schroer. 2000. Real time imaging reveals a peroxisomal reticulum in living cells. *J Cell Sci.* 113 (Pt 20):3663-3671.

- Schrader, M., K. Krieglstein, and H.D. Fahimi. 1998. Tubular peroxisomes in HepG2 cells: selective induction by growth factors and arachidonic acid. *Eur J Cell Biol.* 75:87-96.
- Silvestre, D.C., H.J. Maccioni, and B.L. Caputto. 2009. Content of endoplasmic reticulum and Golgi complex membranes positively correlates with the proliferative status of brain cells. *J Neurosci Res.* 87:857-865.
- Singh, H., S. Usher, and A. Poulos. 1989. Mitochondrial and peroxisomal beta-oxidation of stearic and lignoceric acids by rat brain. *J Neurochem.* 53:1711-1718.
- Singh, I., O. Carillo, and A. Namboodiri. 2000. Isolation and biochemical characterization of peroxisomes from cultured rat glial cells. *Neurochem Res.* 25:197-203.
- Singh, I., O. Lazo, and K. Kremser. 1993. Purification of peroxisomes and subcellular distribution of enzyme activities for activation and oxidation of very-long-chain fatty acids in rat brain. *Biochim Biophys Acta.* 1170:44-52.
- Sitaramam, V., and M.K. Sarma. 1981. Gravitational field enhances permeability of biological membranes to sucrose: an experimental refutation of sucrose-space hypothesis. *Proc Natl Acad Sci U S A.* 78:3441-3445.
- Speijer, D. 2014. Reconsidering ideas regarding the evolution of peroxisomes: the case for a mitochondrial connection. *Cell Mol Life Sci.* 71:2377-2378.
- Sporn, M.B., T. Wanko, and W. Dingman. 1962. The isolation of cell nuclei from rat brain. *J Cell Biol.* 15:109-120.
- Steinberg, S.J., G. Dodt, G.V. Raymond, N.E. Braverman, A.B. Moser, and H.W. Moser. 2006. Peroxisome biogenesis disorders. *Biochim Biophys Acta.* 1763:1733-1748.
- Subramani, S. 2004. Peroxisomes. *Encyclopedia of Biological Chemistry.* 3.
- Sugiura, A., S. Mattie, J. Prudent, and H.M. McBride. 2017. Newly born peroxisomes are a hybrid of mitochondrial and ER-derived pre-peroxisomes. *Nature.* 542:251-254.
- Terman, A., and U.T. Brunk. 2004. Lipofuscin. *Int J Biochem Cell Biol.* 36:1400-1404.
- Towbin, H., T. Staehelin, and J. Gordon. 1979. Electrophoretic transfer of proteins from polyacrylamide gels to nitrocellulose sheets: Procedure and some applications. *Proceedings of the National Academy of Sciences of the United States of America.* 76:4350-4354.
- Trompier, D., A. Vejux, A. Zarrouk, C. Gondcaille, F. Geillon, T. Nury, S. Savary, and G. Lizard. 2014. Brain peroxisomes. *Biochimie.* 98:102-110.
- Tsay, H.J., P. Wang, S.L. Wang, and H.H. Ku. 2000. Age-associated changes of superoxide dismutase and catalase activities in the rat brain. *J Biomed Sci.* 7:466-474.
- Uzor, N.E., L.D. McCullough, and A.S. Tsvetkov. 2020. Peroxisomal Dysfunction in Neurological Diseases and Brain Aging. *Front Cell Neurosci.* 14:44.
- Visser, W.F. 2002. Identification of human PMP34 as a peroxisomal ATP transporter. *BBRC.*
- Volkl, A., and H.D. Fahimi. 1985. Isolation and characterization of peroxisomes from the liver of normal untreated rats. *Eur J Biochem.* 149:257-265.
- Vujcic, S., P. Liang, P. Diegelman, D.L. Kramer, and C.W. Porter. 2003. Genomic identification and biochemical characterization of the mammalian polyamine oxidase involved in polyamine back-conversion. *Biochem J.* 370:19-28.
- Wanders, R.J. 2014. Metabolic functions of peroxisomes in health and disease. *Biochimie.* 98:36-44.

- Wanders, R.J., and H.R. Waterham. 2006. Biochemistry of mammalian peroxisomes revisited. *Annu Rev Biochem.* 75:295-332.
- Wanders, R.J., H.R. Waterham, and S. Ferdinandusse. 2015. Metabolic Interplay between Peroxisomes and Other Subcellular Organelles Including Mitochondria and the Endoplasmic Reticulum. *Front Cell Dev Biol.* 3:83.
- Wang, Y., J. Metz, J.L. Costello, J. Passmore, M. Schrader, C. Schultz, and M. Islinger. 2018. Intracellular redistribution of neuronal peroxisomes in response to ACBD5 expression. *PLoS One.* 13:e0209507.
- Wang, Y.X. 2010. PPARs: diverse regulators in energy metabolism and metabolic diseases. *Cell Res.* 20:124-137.
- Waterham, H.R., S. Ferdinandusse, and R.J. Wanders. 2016. Human disorders of peroxisome metabolism and biogenesis. *Biochim Biophys Acta.* 1863:922-933.
- Whittaker, P.V. 1967. The Morphology of Fractions of Rat Forebrain Synaptosomes Separated on Continuous Sucrose Density Gradients. *The Biochemical Journal.*
- Williams, J.M., V.L. Thompson, S.E. Mason-Parker, W.C. Abraham, and W.P. Tate. 1998. Synaptic activity-dependent modulation of mitochondrial gene expression in the rat hippocampus. *Brain Res Mol Brain Res.* 60:50-56.
- Wolosker, H., E. Dumin, L. Balan, and V.N. Foltyn. 2008. D-amino acids in the brain: D-serine in neurotransmission and neurodegeneration. *FEBS J.* 275:3514-3526.
- Yagita, Y., K. Shinohara, Y. Abe, K. Nakagawa, M. Al-Owain, F.S. Alkuraya, and Y. Fujiki. 2017. Deficiency of a Retinal Dystrophy Protein, Acyl-CoA Binding Domain-containing 5 (ACBD5), Impairs Peroxisomal beta-Oxidation of Very-long-chain Fatty Acids. *J Biol Chem.* 292:691-705.
- Zaar, K., A. Volkl, and H.D. Fahimi. 1987. Association of isolated bovine kidney cortex peroxisomes with endoplasmic reticulum. *Biochim Biophys Acta.* 897:135-142.
- Zhou, M.T., Y. Qin, M. Li, C. Chen, X. Chen, H.B. Shu, and L. Guo. 2015. Quantitative Proteomics Reveals the Roles of Peroxisome-associated Proteins in Antiviral Innate Immune Responses. *Mol Cell Proteomics.* 14:2535-2549.

7 LEBENS LAUF

PERSONALIEN

Name und Vorname: Andreas Felix Manner
Geburtsdatum: 15.08.1989
Geburtsort: Mannheim
Familienstand: Ledig

SCHULISCHER WERDEGANG

1999 – 2008 Schönborn Gymnasium Bruchsal
16.06.2008 Abitur

UNIVERSITÄRER WERDEGANG

10/2009 – 06/2017 **Medizinstudium** an der Medizinischen Fakultät Mannheim
der Ruprecht-Karls-Universität Heidelberg
18.05.2017 3. Ärztliche Prüfung (2,0)
09.10.2014 2. Ärztliche Prüfung (3,0)
09.09.2011 1. Ärztliche Prüfung (2,0)
Gesamttote der ärztlichen Prüfung (2,33)
08/2012 – 02/2016 **Masterstudiengang** in Translational Medical Research
Medizinische Fakultät Mannheim der Ruprecht-Karls-
Universität Heidelberg
18.05.2017 Master of Science (M.Sc.) in Translational Medical Research
(final grade 1,1)
Masterthesis Source and connectivity analysis of EEG data: Methodic
aspects of the open-source tools LORETA and Brainstorm
(1,0)

8 DANKSAGUNG

Herrn PD Dr. Markus Islinger danke ich für die Überlassung des Themas dieser Arbeit, die Betreuung während der Experimente und die beratende Unterstützung beim Verfassen dieser Arbeit sowie der resultierenden Publikationen.

Besonderen Dank schulde ich Frau Dr. Sandra Kühl für die Einarbeitung im Labor sowie die Ratschläge bei der Durchführung der Experimente.

Dank sage ich auch dem Team des Instituts für Neuroanatomie um Herrn Prof. Dr. Christian Schultz für die Möglichkeit, die Experimente in den dort angegliederten Laboren durchzuführen.